DOCTORAL THESIS

"Design, Manufacture and Properties of Cr-Re Alloys for Application in Satellite Thrusters"

Lluís Gimeno-Fabra

Tutor: Marc Anglada i Gomila

Universitat Politècnica de Catalunya, UPC
Departament de Ciència dels Materials i Enginyeria Metal.lúrgica

European Aeronautic Defence and Space Company, EADS
Corporate Research Center, Germany. Department of Metallic Structures

Foreword

My education in Industrial Engineering started in 1996, in the Technical University of Catalonia in Barcelona. It was on my second year of training that Prof. Marc Anglada proposed a group of students a Socrates scholarship to complete a Materials Engineering specialisation in the European EEIGM programme that would take me through France and Aero Engines Germany. Three years later, with a Spanish and French Materials Engineering Diploma in the pocket, and finishing a French DEA in the Ecole des Mines in Nancy, I was off looking for a PhD Thesis.

I signed for a PhD. Thesis in the Technical University of Catalonia in cooperation with the Corporate Research Center of EADS in Ottobrunn, Germany. I started working in CRC on May 2nd 2001, in the department of Metallic Materials. For a young engineer the idea of working in the field of satellite propulsion was quite exciting and I took the position with full enthusiasm. It was a challenging environment, as the only study that had been done in the company in the field of satellite thruster materials was 10 years old and there was no real systematic approach to the problem. The PhD. Thesis would take me again abroad, this time to Kiev and Novosibirsk, where I carried out part of the experimental work.

Three years later, and with the experimental results for the Thesis accepted, I was offered the possibility of joining the newly founded EADS Russian Technology Office, linking the company to the Russian scientific networks. It has taken a while to complete this PhD since then and I have no excuse for the delay, but for my defence I will say that I was quite busy, getting used to a management position in EADS, travelling 2/3 of my time and getting married. Now with all information put together, it's a great satisfaction to see the work done.

Lluís Gimeno-Fabra

Acknowledgements

To my family: Aurélie, Carme, Josep-Miquel i Miquel.

To EEIGM staff: Prof. G. Metauer and J. M. Ricard for their friendship and assistance through the PhD.

To the staff of the Technical University of Catalonia (UPC), for their flexibility and understanding and particularly to Prof. Marc Anglada and Prof. Antonio Mateo.

To EADS staff: Achim Schoberth and Dr. Johannes Vlcek for their help during my Thesis and to Dr. Rolf Buetje and Dr. Marc Strechinsky for the trust afterwards.

To IPMS staff in Kiev, Ukraine: Prof. Yuri Milman, Dr. Nikolay Bronikovskyy and Dr. Nikolay Krapivka.

To IICH staff in Novosibirsk, Russia: Prof. Igor Igumenov, Dr. Nikolay Gelfond and Dr. Natalia Morozova.

To my friends: Llorenc Llopart-Prieto and again, Johannes Vlcek.

Abstract

The manufacturing and properties of various Cr-Re alloys have been investigated in this work with the aim of replacing Pt alloys used currently in the satellite thruster combustion chambers. This Thesis has been supported by the Corporate Research Center of EADS and tutored by the Technical University of Catalonia.

Studies carried out in the past on the Re effect on the mechanical properties of refractory alloys resulted in the industrial application of Mo-Re and W-Re alloys. Cr-Re alloys have been studied at a fundamental level indicating an improvement of the mechanical properties of the alloys containing Re. Other properties related to its potential application in satellite thrusters were not characterized and an industrial manufacturing process for Cr-Re alloys does not exist, hence the motivation for this PhD.

In this work Cr-Re alloys were manufactured initially by means of powder metallurgy. Their mechanical properties improved with increasing Re content verifying the results of the few literature references available. High purity Cr-18at%Re and Cr-35at%Re alloys were produced by melting and casting by a specific procedure. Heterogeneity problems in Cr-18Re alloys were reduced by inoculation of the melt with Ce, Pr and Sc.

Mechanical properties of the high purity Cr-Re alloys improve significantly over the powder metallurgical alloys. Compressive elastic limit of both Cr-18 and Cr-35Re alloys at room temperature is over 800 MPa and compressive deformation is possible up to 70% without formation of surface cracks. Elastic limit at 1400°C is over 140 MPa both under compression and tension. Fracture under tension is mixed transgranular and intergranular up to 1200°C. Above this fracture becomes intergranular, characterized by very little plasticity. Best ductility under tension is obtained between 600 and 1000°C with a deformation to fracture of about 10%.

Resistance of the alloys to oxidation and nitruration was characterized up to 1500 °C. Tests revealed that Cr-18Re alloys are not capable of building a stable protective layer during exposure to air or nitrogen at the test temperature. They also present a grain boundary instability caused by Cr segregation and evaporation during exposure. Cr-35Re alloys create a stable protective layer of Cr oxide that protects the substrate against light element diffusion. In nitrogen atmosphere Cr-35Re builds a stable layer that is not protective against diffusion of nitrogen. The investigation of the plasticity of the samples after exposure shows that diffused nitrogen does not affect significantly the plasticity of Cr-35Re however there is some scatter in the results due to the small sample cross section relative to grain size. Exposure to vacuum at 1700 °C verified that the grain boundary instability of Cr-18Re was not related to any reaction with the atmosphere as it also takes place in vacuum. Cr-35Re alloys did not present any significant sublimation at this temperature and no grain growth could be detected after exposure.

Additions of Re to Cr reduce the thermal and electric conductivity of the alloys as the symmetry of the lattice is distorted by the Re atoms. This, coupled to the improvement of the mechanical properties makes a prediction of the thermal shock resistance of the alloys difficult. For this reason it was decided to build an installation reproducing the thermal shocks and thermal gradients, of 500K/s and 500K/mm respectively, characteristic of the application. When cycled, Cr-18Re alloys suffered also from the grain boundary instability and fractured up to a depth of 200µm. Cr-35Re alloys showed minor cracks and accommodated the linear thermal gradient by means of twinning.

The mechanical, chemical and thermal cycling properties of the Cr-35Re alloys indicate that it is suitable for the application.

This work resulted in the construction of a 22N satellite thruster with Cr-35Re alloy that will be tested in EADS Space Transportation in Lampoldshausen.

TABLE OF CONTENTS

1. Introduction

1.1 Historical background, the concept of cost in space missions

On October the 4th 1957 the Soviet Union placed the first artificial satellite in orbit, Sputnik. This 90-kilogram device equipped with two high frequency transmitters remained in low earth orbit 21 days emitting binary signals that could be received from earth. Sputnik consisted of a small aluminium sphere containing transmitters (figure 1.1a) and had no independent propulsion system, so its controlled re-entry in the atmosphere was out of reach, but Sputnik descendents grew exponentially in size, weight and complexity and only one year after the original Sputnik flight, artificial satellites with a weight over 1000 Kg orbited earth.

By April 1961 the orbital flight of Yuri Gagarin in a Vostok rocket and his safe landing confirmed that it was possible to place a heavy charge in orbit and safely re-entry it. At a speed over 20.000Km/h, the re-entry of a capsule from space rendered useless all defence systems of the time. The space race between the USSR and the USA had begun.

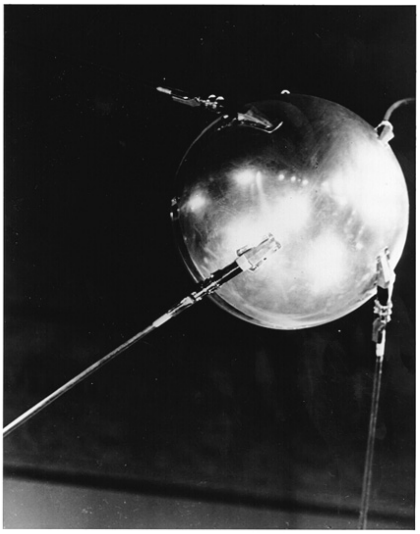

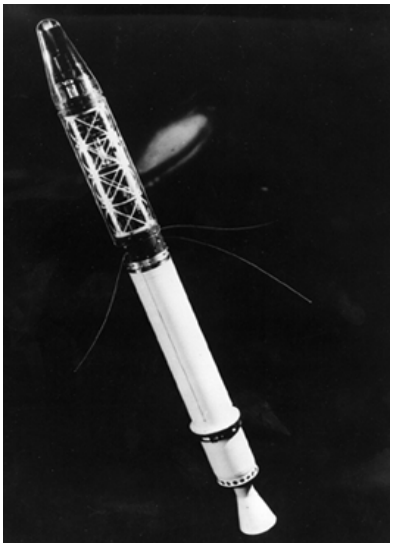

Figures 1.1a (left) and 1.1.b (right): The first artificial satellite, Sputnik (left) and the first American, satellite Explorer (right).

The space race triggered a 30 year long rivalry between the superpowers in which a cost-no-object philosophy became common in all space related activities. The cold war climate favoured this approach; American reaction to initial Soviet advantage was determined: the Explorer satellites orbited earth in January 31st 1958 (figure 1.1b) and the Mercury programme put an American in orbit in February 20th 1962, shortly after the first Orbital flight of a human, the Soviet Yuri Gagarin. The Apollo programme culminated in the first manned mission to the moon in 1969.

The crash of the Soviet Union in the 1980's and the absence of any technologically capable rivals to the USA had a direct consequence on space activities: space became free to be marketed for private commercial purposes. Space industry faced the challenge of making money out of the manufacturing, putting into orbit and operating of commercial satellites.

The boom of the satellite communication market in the 1980's and 1990's triggered fierce concurrence between American and European satellite manufacturers and operators. Today, with emerging operators besides the USA and Europe, satellite market has become even more competitive and following the trend of any commercial activity, the global mission cost is of great importance to the customer and is often the deciding factor when choosing a satellite manufacturer and operator.

The cost no object philosophy that accompanied aerospace industry during decades is reflected in particular on the materials used in rockets and satellites. As satellite price has become an increasingly important parameter in space industry, manufacturers investigate new cost effective materials offering high levels of performance and reliability. All satellite components are being investigated for potential cost reduction, including structure, energy systems, electronic systems and propulsion systems.

Cost of space missions in a commercial environment

Global mission cost is related to three main activities: satellite manufacturing, satellite launching and satellite operation. This work will focus on the reduction of the satellite launching costs which are basically a function of the satellite weight (roughly 20.000

€/Kg) [Astrium, 2001]. The weight of a satellite at take off consists approximately of 50% structure and components and 50% of fuel for the orbital engines.

Efficiency of satellite engines increases with the service temperature of their combustion chamber as described in section 1.2, establishing a direct relation between the resistance to high temperature exposure of the material from which the combustion chamber of the engine is built and its fuel consumption. For current engines service temperature of the combustion chamber is about 1500 °C, an increase of 200 °C in the service temperature would decrease the necessary propellant mass by about 500Kg, and therefore about 10 million € worth of reduction in launching cost [Tuffias, 1991].

Despite the potential in cost reduction, research in the field of high temperature materials for satellite applications is scarce due to the investment involved in the qualification of new materials for what is an extremely restrained market. This means that material manufacturers are usually not willing to finance research in this field, as potential profit is marginal. Research in this area often involves public funding and end user participation, it is for this reason that the European Aeronautic Defence and Space Company (EADS), itself an end user of high temperature materials, has been actively supporting research in this field. An important achievement of research in the past 15 years is the qualification at the beginning of the 1990's of the highly reliable platinum based satellite thrusters used widely in modern European satellites. These engines are able to operate at a highest continuous operation temperature of 1500°C, with peak temperatures attaining 1650 °C without the need of a protective coating.

Other companies with active in this field have qualified materials following different design philosophies, in particular the acceptance of the use of coated materials, American technology experienced a radical leap forward with the qualification in the mid-1990's of iridium coated rhenium combustion chambers with a highest operation temperature of 2000°C and a peak temperature of 2200°C by the California based company ULTRAMET [Tuffias, 1991], [Ultramet, 2001]. Despite the huge cost of these thrusters (300.000 €/combustion chamber in an apogee engine), increase in

engine efficiency adds up for a theoretical weight saving of over 1000Kg for a large satellite, the equivalent of 20 million € savings in launch costs.

The EADS Corporate Research Centre in Ottobrunn, Germany decided in 2001 to finance a research project in order to investigate the materials susceptible of increasing the service temperature of satellite thruster combustion chambers from the present values to 1800°C able to operate in uncoated form.

The project started as a clean sheet of paper and several materials including tantalum based alloys, iridium based alloys and chromium alloys were considered in a first screening that will not be presented in detail in this work. The present doctoral thesis is inscribed in this activity.

1.2 General background, satellite thrusters

Modern telecommunication satellites have a lifespan of about 15 years. To remain in orbit during this period of time, satellites need to keep a certain altitude, velocity and trajectory. Friction against the outer atmosphere of the earth, solar winds and impacts from space particles may change the satellite flight path to unwanted parameters causing catastrophic re-entry into the atmosphere. On the other side some satellites, and in particular space telescopes, need to change their observation position respective to earth or space. To carry out these movements, satellites are equipped with a propulsion system constituted of satellite thrusters and the ancillaries necessary for their operation.

The satellite shown in figure 1.2 corresponds to a typical telecommunications platform of about 3000 Kg of take off mass (including the telecommunication ancillaries not shown in the figure) [Astrium, 2001]. Such a platform is equipped with several **R**eaction **C**ontrol **T**hrusters (RCT) and a single or double apogee engine, both fuelled by a combination of liquid a propellant and an oxidiser. The apogee engine, which can be seen in the inferior part of the structure, produces a thrust of 400N and is in charge of the transfer of the satellite from the point where it is released by the transport rocket, at an altitude of about 250 Km, to its final geo stationary orbit, at approximately 39000 Km from the earth (figure 1.3). In geo

stationary position, normal acceleration of the satellite compensates gravity and allows the satellite to remain stationary to a reference on earth. Once in this position, and during the entire lifespan of the satellite, the RCT thrusters cater for satellite movements, such as orbit corrections, altitude regulation, rotation and velocity changes. During its operational life a satellite platform similar to the one shown in figure 1.2 consumes a total of 1500 Kg of fuel, of which the Apogee engine alone uses 800Kg to 1100 Kg in 4 mainly continuous operation hours during the first three days of satellite manoeuvring and the RCT thrusters between 150 Kg and 300Kg in about 700 operation cycles accounting for a total of 70 operation hours spread among the 16 years of the satellite service

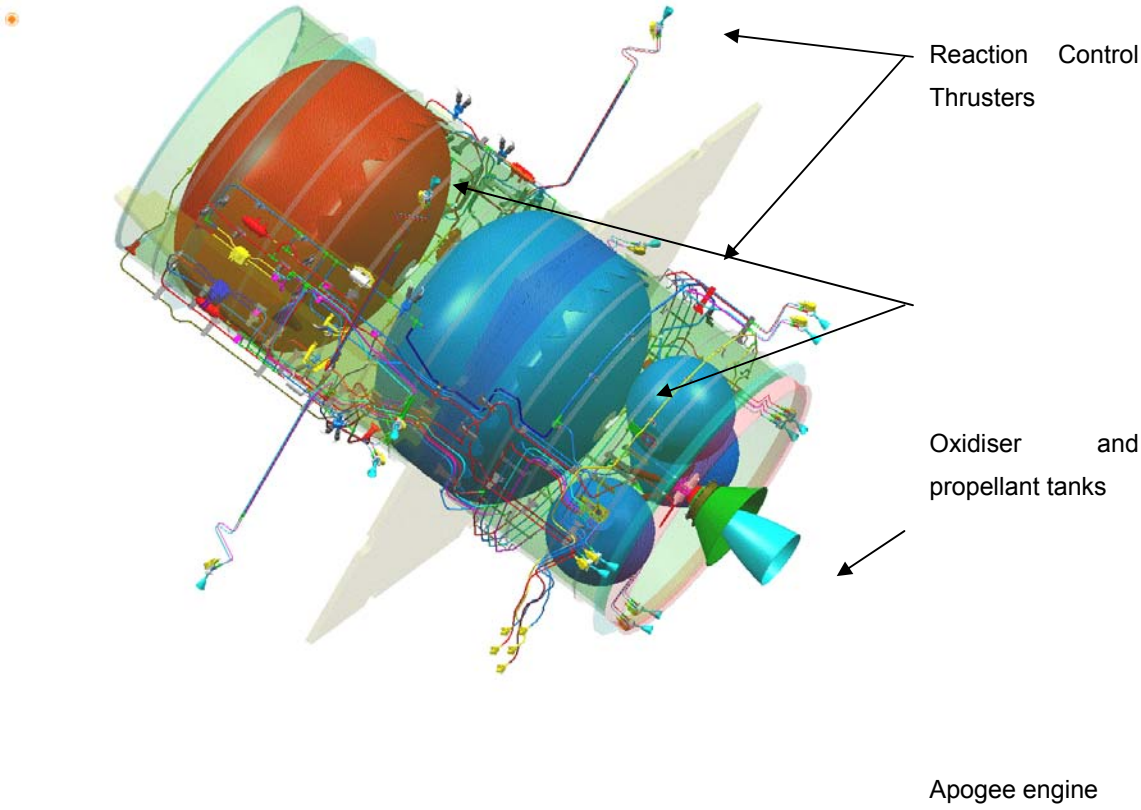

Figure 1.2: 3 ton communication satellite platform with 13 reaction control thrusters with a unitary thrust of 1 N and 1 apogee engine with 400N thrust. All thrusters are of the bipropellant type.

Chemical satellite thrusters and plasma satellite thrusters

The satellite represented in figure 1.2 is powered by chemical engines, as their thrust is obtained the expulsion at hypersonic velocity of the gasses resulting from the combustion of a propellant in the presence of an oxidiser (figure 1.4), this system is by far the most commonly used in satellites since the 1960's but it is not universal. Since the 1970's, some satellites are equipped with plasma engines, in which thrust is obtained by the expulsion of a plasma flow obtained by the ionisation of a gas in an electric field (figure 1.5).

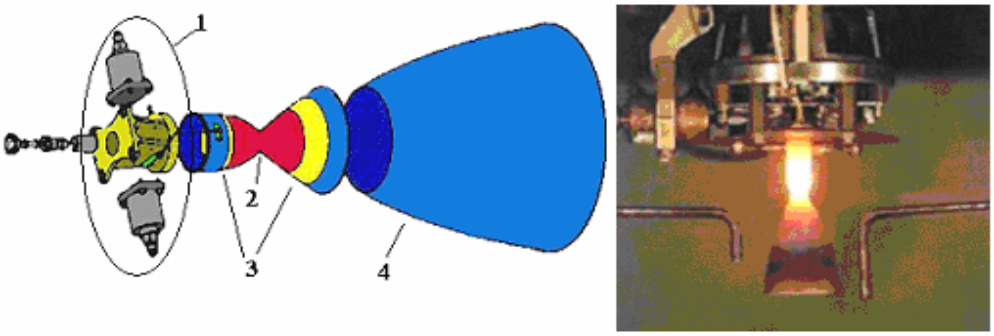

Figure 1.4: Exploded view of a chemical thruster:
1. Injector head with electro-valves (propellant and oxidizer)
2. Combustion chamber
3. Transition rings
4. Diffusion cone

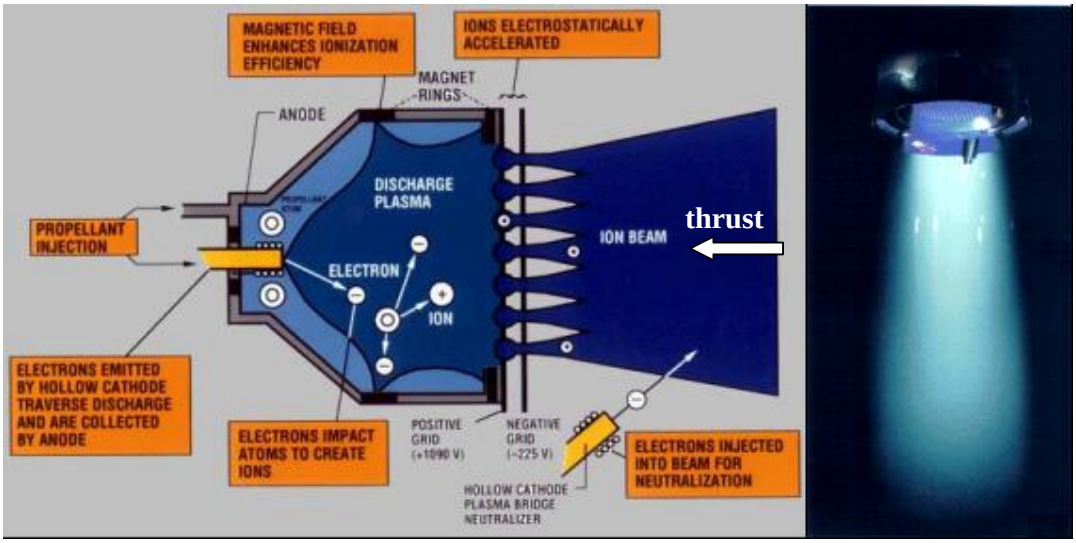

Figure 1.5: Schematic view of an electric thruster. Noble gas is ionised in a plasma discharge chamber. Ionised gas is then accelerated in the electrostatically loaded area between two grids generating the thrust.

Independently of the operation principle, performance of a satellite thruster is measured by two parameters: the thrust which corresponds to the uniaxial force that it generates expressed in Newton and the specific impulse, which is the period in seconds during which a 1-pound (0.45-kilogram) mass of propellant (total of fuel and oxidizer) produces a thrust of 1 pound (0.45- kilogram). Thrust represents therefore the power of the thruster while impulse represents its efficiency. Thrust of liquid chemical thrusters ranges between 0,1 and 400N and specific impulse between 2200 and 3200 s, while electric thrusters produce between 0,010 and 2 N of thrust with a specific impulse of about 30.000 s. Therefore electric thrusters are energetically more efficient than chemical thrusters but are restrained only to applications where a low power is necessary, for example interplanetary missions where long acceleration times are acceptable. On the other hand, due to their higher power of chemical thrusters, that allows them to produce strong accelerations, they are the most frequently used in earth orbiting and observation missions.

1.3 Operating conditions in liquid chemical satellite thrusters

A liquid chemical satellite thruster is actually a miniaturised rocket engine. Figure 1.6 shows the cross section of a typical 10N Astium thruster. It consists of an injection system, a combustion chamber and an exhaust nozzle represented. Several constructional parameters influence the performance of a satellite thruster, in particular the area ratio between the combustion chamber throat and the end section of the nozzle, the throat diameter, the nozzle length, the combustion chamber length and the convergence radiuses of the combustion chamber.

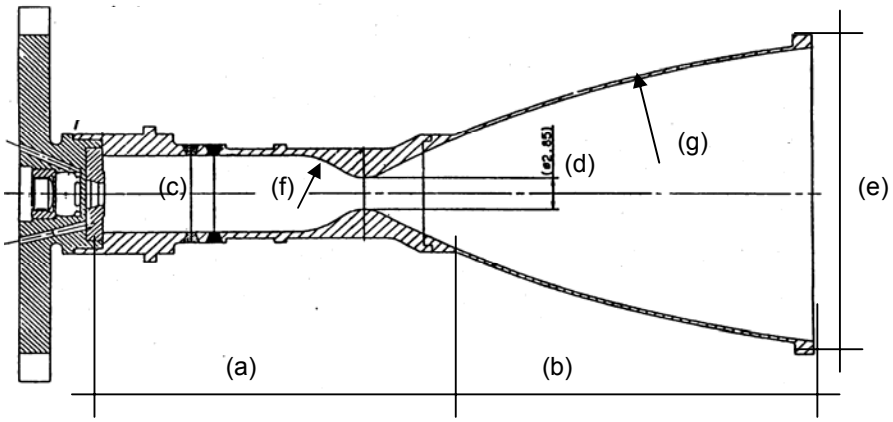

Figure 1.6: Characteristic dimensions of a satellite thruster. Figure is not to scale.	
(a) Combustion chamber length	~ 40 mm
(b) Nozzle length	~ 40 mm
(c) Combustion chamber diameter	~ 12 mm
(d) Throat diameter	~ 5 mm
(e) Nozzle diameter	~ 40 mm
(f) Chamber convergence radius	~ 20 mm
(g) Nozzle convergence radius	~ 100 mm

In the combustion chamber the propellant and the oxidiser are mixed to produce large amounts of combustion gasses that, after being accelerated in the Laval throat, are expelled through the nozzle producing a reaction force or thrust. High temperature operation of satellite thrusters in the aggressive combustion atmosphere and severe low temperature mechanical loading during launcher rocket take-off and thermal shock during pulse operation impose notable mechanical, chemical and thermal loads on their structure [DARA, 1991].

Chemical environment

Chemical solicitations in a satellite thruster are dependent on the type of propeller used. Large rocket engines, for example use environmentally safe propellants the combustion products of which are not aggressive. A modern example of propellant and oxidiser combination for a large rocket engine is liquid hydrogen and oxygen.

Satellite propellants need to fulfil very particular needs, in particular to have a very large stability range in liquid phase since heating by sun radiation of the satellite structure is very intensive and cryogenic temperatures can achieved in long

exposures to the dark. Other important properties are high flammability and high specific density to reduce their storage volume. Only a few chemicals fulfil the requirements to be used as satellite fuel, the most important of which are listed in table 1.1 [DARA, 1991]. Choice of propellant is related to the engine type and size: usually satellite engines with a thrust lower than 10N use single propellants that decompose in the presence of a catalyst whereas engines with thrust levels above 10N use combinations of an oxidiser and fuel. The oxidiser / propellant combinations may be self-igniting (hypergolic propellants) or non-self-igniting (non-hypergolic propellants). As the ignition system adds weight and may be sources of unreliability, manufacturers tend to use self-igniting propellants. Their handling is nevertheless complex since they are extremely toxic.

<table>
<tr><td>Single propellant</td><td colspan="3">Double propellant systems</td></tr>
<tr><td rowspan="3">Hydrazine,
Nitroglycerine,
Nitromethane,
H_2O_2</td><td colspan="2">Hypergolic combinations
(Self-igniting / Highly Toxic)</td><td>Non hypergolic combinations
(Non self igniting / Non toxic)</td></tr>
<tr><td>Oxidiser</td><td>Fuel</td><td rowspan="2">

$RP1/O_2$
CH_4/O_2</td></tr>
<tr><td>H_2O_2
N_2O_4</td><td>MMH, UDMH (*),
Nitroglycerine,
Nitromethane, H_2O_2.</td></tr>
</table>

Table 1.1: Propellants used in liquid chemical satellite thrusters. (*) MMH = Monomethylhidrazine, UDMH = Unsymmetrical Dymethylhydrazine. Source [DARA, 1991]

Amongst the propellants listed above, the most common are the combinations of hypergolic propellants known as: MON/MMH (MON = N_2O_4 + NO, MMH = $CH_3N_2H_3$) and MON/Hydrazine (Hydrazine = N_2H_4). Combustion of these compounds is highly exothermal, attaining a temperature of 2500°C. The main combustion products of satellite engines are listed in table 1.2. At the service temperature of the walls, which in some areas exceeds 1500°C oxidation and nitrogen and hydrogen embrittlement of the substrate is possible.

High temperature chemical resistance of the combustion chamber material largely determines the operation temperature of the combustion chamber in continuous

operation. Once stable service temperature has been achieved, mechanical resistance of the material, plays only a secondary role as internal pressure in the combustion chamber is low at about 2 Bar.

Element	*Atomic % in the combustion atmosphere at nominal point and wall temperature of the combustion chamber*			
	Interaction with substrate	*Satellite propellants (T 1600°C)*		*Rocket propellant (T 900°C)*
		Az-50 / N_2O_4	*MMH / N_2O_2*	*LH_2 / LO_2*
CO	Carburetion	6	7	0
CO_2		7,3	10	0
H	Hydrogen embrittlement	0,2	0,02	Traces
H_2		6	7,9	Traces
H_2O	Oxidation	44	41	100
NO	Nitruration	0,03	0	0
N_2	Nitruration	35	33	0
O	Oxidation	0,005	0	Traces
OH		0,25	0,008	Traces
O_2	Oxidation	0,02	0	Traces

Table 1.2: Concentration of the elements and compounds present in the exhaust gasses of a satellite thruster. MMH = Monomethylhydrazine, Az-50 = 50%MMH + 50%UDMH (Unsymmetrical Dymethylhydrazine)

Thermal gradient and thermal shock in combustion chambers

Besides chemical constraints, thermo-mechanical loads also play a major role in the deterioration of the combustion chamber structures. Geometrical thermal gradients in combustions chambers are related to the cooling system used in some parts of the structure. Heat generated by the combustion can also flow back to the injector head through the combustion chamber with dangerous consequences. Therefore satellite thrusters are equipped with a cooling system to effectively sink wall temperature in this area. Large rocket engines and old satellite thrusters achieved cooling by flowing fuel in channels inside the combustion chamber walls and injecting the hot fuel in the chamber to be burnt. This system minimised thermal gradients in the

combustion chamber but had negative effects on the combustion stability and thruster efficiency.

Modern satellite thrusters achieve cooling just by the vaporization of a film of liquid fuel on the surface of the walls adjacent to the injector head (figure 1.7), isolating it from the hottest part of the combustion atmosphere and preventing heat flow back to the combustion chamber.

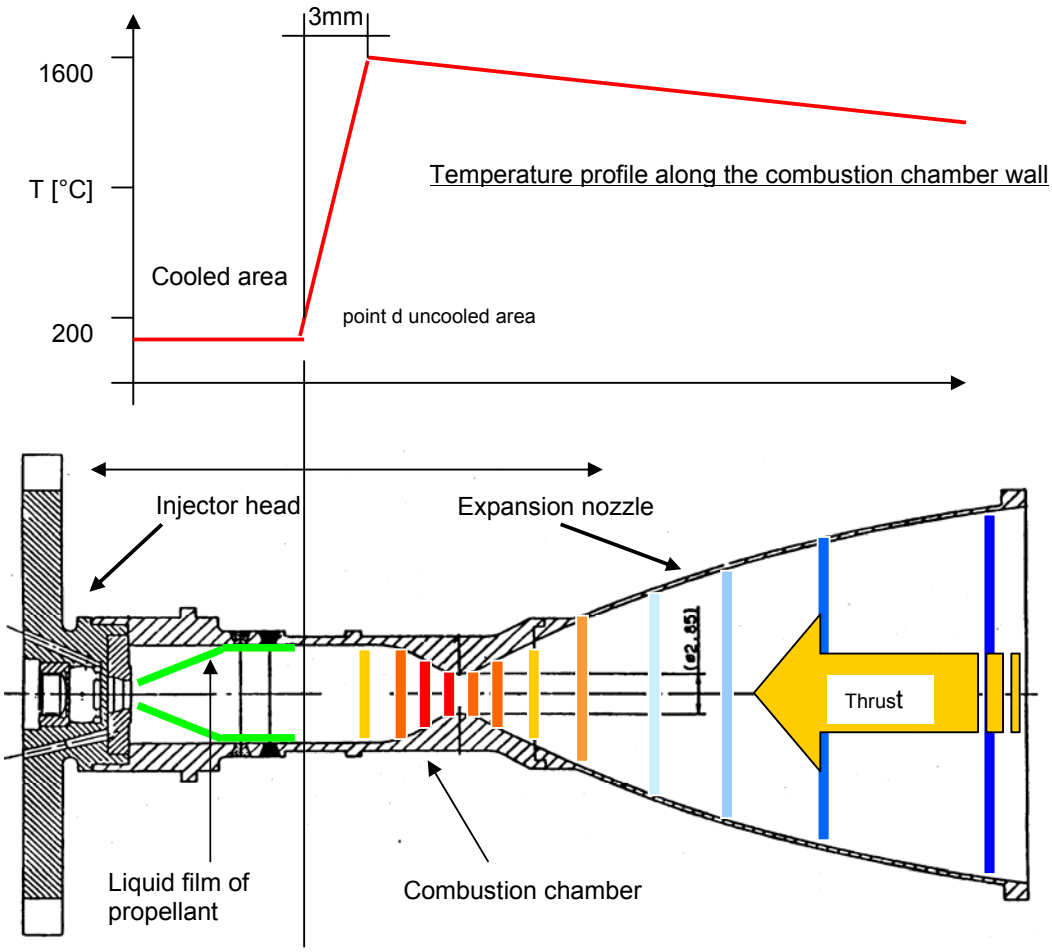

Figure 1.7: Schematic representation of a satellite thrusters and temperature profile along the longitudinal axis [DASA, 1999].

This type of cooling decreases the temperature of the walls to less than 300°C in this area. At the point C in figure 1.7, the fuel film looses its stability, fully evaporating and reacting with the oxidiser, thus exposing the dry combustion chamber walls to the

combustion gasses. In this area the wall temperature increases to 1600°C in less than 3mm. Geometrical thermal gradient in the longitudinal direction is in the region of 500°C/mm in this area [DASA, 1999].

Heating kinetic at the hottest spot of the structure, in point d in figure 1.7 is about 500 °C/sec (from –60°C to 1600°C) inducing a thermal shock in each of the 700 life cycles of the chamber. EADS Astrium performed a simulation to give an idea of the thermo-mechanical constraints in this area during operation in the framework of this work. The properties of Cr were used to perform the simulation. The geometric thermal gradient in the vicinity point C induces constraints of up to 300 MPa in the cooled area of the chamber [Rocflam, 1997]. This value indicates the minimum level of resistance required and the importance of having a ductile behaviour in this area.

The chemical resistance of the combustion chamber material and to some extend its thermal-shock resistance determine the amount of cooling which is necessary to protect it. A low material resistance involves strong cooling which decreases the efficiency of the thruster, as ideally all of the energy contained in the propellant should be transformed in mechanical thrust and not be dissipated. Figures 1.8-1.10 shows the evolution of the combustion chamber structural material and its influence on the cooling system and on the efficiency of the thruster.

Cobalt and nickel thrusters from the 1960's and 1970's had an active cooling system, in which a circuit of liquid propellant running inside the walls cooled the hottest zone of the chamber. This type of cooling necessitated cost intensive manufacturing and was gradually substituted in the 1980's by film cooling, as new generation Pt-based combustion chamber materials were qualified [DARA, 1991].

Besides the strength and chemical stability requirements of the combustion chamber material some other properties must also be taken in account, in particular the heat conductivity and surface emissivity [Tuffias, 1991].

1.3.1 Qualified materials for use in satellite thruster combustion chambers

Requirements for satellite thruster combustion chamber materials have changed much since the 1960's. In particular the need for higher efficiency has been translated in higher combustion temperatures and severer requirements on the structural materials. Only few materials are able to withstand the complex load profile imposed by the given application. A specific combination of mechanical thermal and chemical properties is necessary for the material to be appropriate.

The problem of increasingly higher service temperatures may be dealt with constructional solutions, such as high efficiency cooling systems or improved chamber geometry, the description of which is out of the scope of the present work. Nevertheless chamber geometry and even constructional solutions can only increase the efficiency of the thrusters to a certain extend. Despite the increase in efficiency that constructional changes have provided, it is not possible to foresee further increases in performance without considering materials able to withstand higher service temperatures. Therefore the development of alloys with increased high temperature properties has been an unavoidable topic of research. In this direction two tendencies have evolved since the 1960's, basically differentiated by the use of coated of uncoated alloys.

Coated materials

Coated materials have found great acceptance in the United States since the development of the Apollo project. Some Apollo generation materials for combustion chambers are still in use today. It is the case of the Boeing-Hughes quartz coated niobium chambers. These are made of Nb C103 alloy and coated with a Hitemco R512 Si-based coating deposited through slurry techniques (figure 1.8). This type of coating is based on the Si-Cr-Fe system and are self healing, providing chemical protection for Nb C103 alloys up to 1400°C.

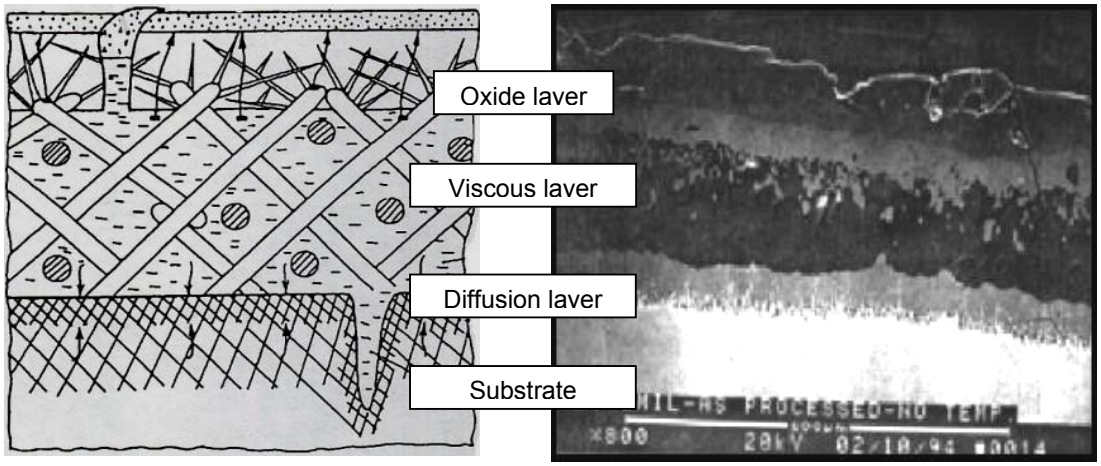

Figure 1.8: Si-Cr-Fe coating on a refractory metal substrate. This approach is standard for the Apollo generation C103 Nb alloy combustion chambers.

The most recent advance in coated metallic materials for satellite thrusters is the Ir-lined Re chamber qualified in 1990 by the American company Ultramet. This type of chamber is manufactured entirely by chemical vapour deposition of Ir and Re on a molybdenum mandrel that is later removed by chemical dissolution (figure 1.9). An excellent bonding between coating and substrate is achieved by modifying the process parameters during the deposition of the interface area between the Ir coating and the Re substrate. At 2200°C the operation temperature of Ir-lined Re combustion chambers is the highest which has ever been qualified [Tuffias, 1999].

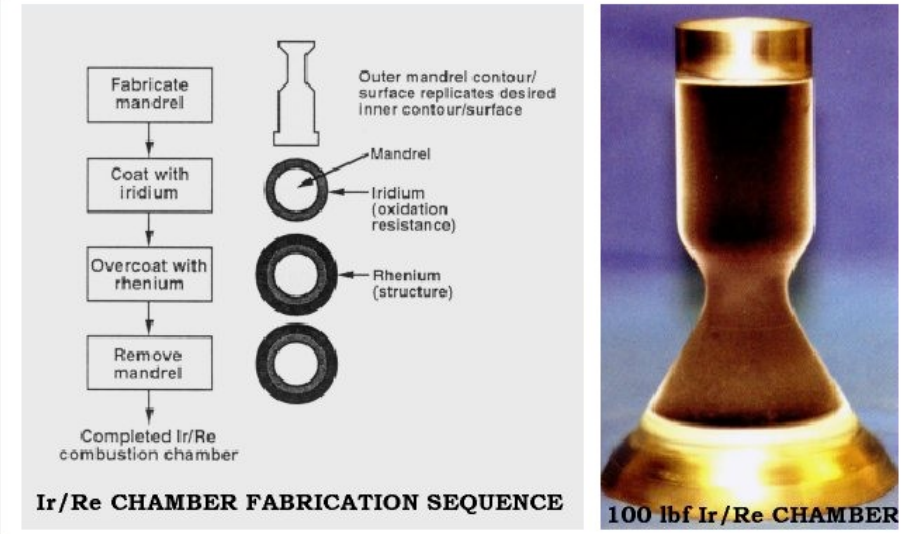

Figure 1.9: Fabrication sequence on an iridium coated rhenium chamber by chemical vapour deposition. Source [ULTRAMET 2001]

Uncoated materials

Coated satellite engines present the inconvenient of being dependent on their coating. Delaminating or erosion of the Ir liner is the typical failure mechanism of Ir lined Re chambers that failed under development. Often this dependence on coatings is not desired by satellite manufacturers, which are ready to sacrifice some engine efficiency in exchange for a higher reliability. In particular the European satellite manufacturers do not tolerate the use of coated engines. This has lead to a completely different approach to material development than in the USA where satellite manufacturers and operators are ready to accept coated engines.

Figure 1.10: Uncoated material technology for satellite thrusters [Hopmann, 1999].
a) Co basis alloy for a single propellant engine (1964)
b) Nimonic alloy (1972-1975)
c) Nimonic alloy, second generation (1975-1985)
d) Pt-Rh alloy, without regenerative cooling (1992→)

European satellite thrusters contemporary to the Apollo generation niobium thrusters were manufactured of Nimonic 90 alloys. Their maximum operation temperature was approximately 1100°C and they had a slightly lower efficiency than Nb thrusters. Nevertheless the fact that they were manufactured from an intrinsically oxidation resistant alloy made them very reliable and they gained good market acceptance. By the mid-1980's the efficiency of Nimonic chambers was unacceptably low and a research programme was started by DASA to investigate new materials with higher operation temperature. Amongst the researched materials were Cr, Ta-W and Pt-Rh.

The history of European satellite thruster materials is illustrated in figure 8 [Hopmann, 1999].

The result of the project was the qualification in 1992 of Pt-Rh alloys as structural materials for satellite thrusters operating up to 1650 °C. Since then, no failure in operation of this type of combustion chamber has ever been reported. Pt-Rh combustion chambers follow the same kind of engineering philosophy than Nimonic 90 offering a high degree of intrinsic chemical stability but present the inconvenient of a very high raw material cost of about 30 €/g representing about 2/3 of the total engine cost for satellites engines with integral nozzle.

With the increased competition and pressure to reduce costs in the satellite market this situation has become unacceptable. Additionally the call for higher efficiency of satellite engines will eventually only be satisfied with a new combustion chamber material capable of operating at a constant service temperature above the present limit of about 1600°C. An increase of 200°C in the operation temperature of these devices would be translated in a launch cost reduction of 10.000.000 € [Tuffias, 1991]. With this in mind, a research line to investigate new material candidates to substitute Pt-Rh alloys was opened in EADS in 2001. Amongst the material candidates C/SiC-based materials, Ta-W and Cr alloys were evaluated.

The two metallic candidates, Ta-W and Cr-based alloys, present melting points above that of Pt but are differentiated by the need of a coating system at least for Ta-W alloys. Alloying additions to Cr are necessary to increase its ductility and resistance to diffusion of light elements but the intrinsically good oxidation resistance of Cr may eventually allow its use in uncoated form. This characteristic, which is most appreciated by the satellite market in Europe, eventually raised enough interest to test a prototype combustion chamber manufactured from pure Cr and investigate its failure mechanisms. This investigation should lead to the definition of useful alloying additions and the design of a Cr-based alloy capable of withstanding the demanding atmosphere of this application. It was the design and manufacture of a Cr-based alloy to substitute the present Pt-Rh alloys, the study of its properties and the construction of a functional demonstrator that eventually led to this doctoral thesis.

1.4 Experience in the use of Cr as combustion chamber material

BCC refractory metals, Cr, Mo, and W present high melting points and a relatively low cost. From these, only Cr has a significant chemical resistance, related to its ability to built a stable Cr-oxide layer when in contact with high temperature oxidizing atmosphere. Table 1.3 shows that melting point and oxidation resistance properties of commercial Cr are similar to those of Pt-Rh alloys. This simplified selection criteria is nevertheless insufficient to judge the potential of Cr for the application. Even with a melting point 100 °C higher than that of Pt and a recrystallisation temperature that can attain 1500 °C when doped with ceramic micro particles, the potential of Cr as a combustion chamber material is severely limited because by its meagre mechanical properties, in particular the low plasticity of commercial Cr [Yoshikazu, 2002].

The yield stress of Cr at 1400 °C, about 40 MPa, is very similar to that of most commercial Pt-based alloys. Room temperature yield stress is about 500 MPa and high purity Cr alloys with Pr doping to remove oxygen traces have been reported to attain 8% deformation at room temperature [Trefilov, 1975], a value that is considered sufficient for the application. Unfortunately the mechanical properties of Cr and all other BCC refractory metals depend strongly on the level of interstitial impurities in the base material [Milman, 1997]. Solubility of light elements in BCC refractory metals is low and this, results in the precipitation of oxides and nitrides in grain boundaries and other crystal defects, where energetic conditions for precipitation are most favourable resulting in embrittlement.

Property	Pt-Rh	Ducropur	Ducrolloy-CRL	Cr-0.5La-Pr
T_m [°C]	1770	1850	1850	1850
T_r [°C]	1650	1250	1500	1500
DBTT [°C]	< - 60°C	150	300	< -60
$\sigma_{0,2}$ [MPa], room T	550	650	650	650
$\sigma_{0,2}$ [MPa], 1200 °C	37	40	40	37

Table 1.3: Properties of commercial Cr and Pt alloys.
Ducropur is a commercial Plansee powder metallurgical extruded alloy, 99.99 Cr [Plansee]
Ducrolloy is a commercial Plansee powder metallurgical extruded alloy.
Cr+0.5 La-Pr was developed in the Ukrainian Academy of Sciences in 1980-1985, results not published

The concentration of impurities depends on the initial level of impurities in the materials in as manufactured condition, which can be remarkably low for some manufacturing processes that will be examined in chapter 5, and on the diffusion of light elements into the material during operation which ultimately renders impossible the application of ultra-high purity ductile Cr alloys, since these are contaminated during operation.

Degradation mechanisms during operation

Cr forms a passive Cr_2O_3 surface oxide layer when exposed to oxygen. This layer prevents the material from oxidation theoretically up to 1100 °C in air. In the presence of Al in the alloy the protective layer remains stable up to 1300 °C, but this involves the formation of an Al_2O_3 layer. Since pure Cr is not usually used as a structural material, the maximum temperature in different atmospheric conditions at which the oxide layer is protective is not well known, and in the complex load profile found in combustion chambers, the behaviour of Cr is difficult to preview.

Based on literature data, the interaction of Cr with the combustion atmosphere described in table 1.2, may either be characterized by the formation a stable and protective oxide layer, at least in the colder areas of the chamber, impeaching the diffusion of light elements in the material, either by the diffusion of light elements in the material and their internal precipitation resulting in the embrittlement of the material.

The grain growth behaviour in is conditioned not only by its recrystallisation temperature in the delivery condition, but also by the appearance of stable precipitates at the grain boundaries that may decrease grain growth. The formation of such precipitates is also conditioned by the diffusion of light elements through the oxide layer, which is, with the available data, difficult to foresee.

A further property relevant to the application is the resistance to thermal shock loading and in particular to thermal gradients that may lead to structural failure. The high thermal conductivity of Cr and its low coefficient of thermal expansion [Trefilov, 1984], combined with high mechanical strength [Holzwarth, 2001] may compensate

for inherent material brittleness. The ductile to brittle transition temperature of commercial chromium is similar to the operation temperature of the cooled area of the combustion chamber, described in chapter 2. In this area thermo mechanical stress in maximum and may generate fracture in the brittle cold area. Simulations of thermo mechanical constraints carried out in EADS Astrium to preview the highest stresses in the cooled area of the combustion chamber [Rocflam, 1997], near the zone of maximum temperature gradient, indicate that a maximum stress of 320 MPa is attained near the breaking point of the cooling film. Theoretically this level of stress is below the ultimate tensile stress of Cr at the service temperature of this area.

The response of Cr to the complex load profile found in combustion chambers is difficult to preview based in the available data. In order to build an application relevant database of the degradation mechanisms of Cr in this particular application, it was considered to be convenient to adopt an experimental approach and perform a vacuum firing test with conventional propellant and oxidiser combinations on a pure Cr combustion chamber and characterise its failure mechanisms.

To evaluate the interaction of the combustion atmosphere with pure Cr, high purity Cr material manufactured by Plansee through powder metallurgy and commercialised under the designation Ducropur has been chosen instead of the Ducrolloy variants of the same manufacturer, which present the advantage of a higher recrystallisation temperature. The database of degradation mechanisms will be used to evaluate potential alloying solutions on Cr based alloys.

1.4.1 Vacuum Firing Test

The standard testing of satellite thruster combustion chambers reproducing the conditions of outer space is carried out in a vacuum chamber, where the combustion chamber is fired with a conventional mixture of oxidiser and propellant. The combustion chamber and the welded injector head assembly is vertically attached to a support equipped with gauges that monitor the thrust. Propellant and oxidiser are fed from external tanks to the satellite thruster injection system. In order to maintain vacuum, the chamber is continuously evacuated by means of vacuum pumps.

Temperature monitoring is carried out by thermocouples welded on the external surface of the combustion chamber figure 1.11a.

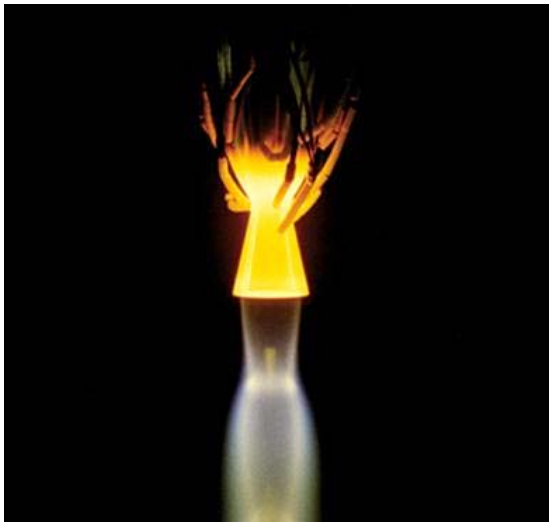

Figure 1.11b: Vacuum firing test of a 400N combustion chamber. Source Astrium.

The propellant and oxidiser combination selected for the test was the conventional used in EADS-Astrium satellites, monomethyhydrazine and nitrogen peroxide. Under nominal conditions in a combustion chamber with 400N of thrust, this propellant and oxidiser combination reacts at 2700 °C and at a pressure of 15 Bar. Firing time was set at 8 minutes, 15 pulses were performed of this duration were performed. After the test the combustion chamber was removed and inspected.

1.4.2 Degradation mechanisms of the Cr combustion chamber

After the firing session the combustion chamber was inspected for macroscopic and microscopic signs of failure. Optical microscopy, scanning electron microscopy, and TEM were used to characterise the microstructure of the combustion chamber before and after firing.

Characterization of the material is as-delivered condition

In order to have a reference microstructure, samples of the material in as manufactured condition were characterized by means of optical microscopy. Samples from the blocks from which the chambers were machined were cut in the longitudinal

and transversal directions. Samples were polished with sand paper and diamond paste with a final mean diameter of 1 µm.

Microstructure of the material is represented in figure 1.11b and consists of elongated grains, oriented in the extrusion direction. Mean grain diameter is approximately 50µm and mean grain length about 250µm.

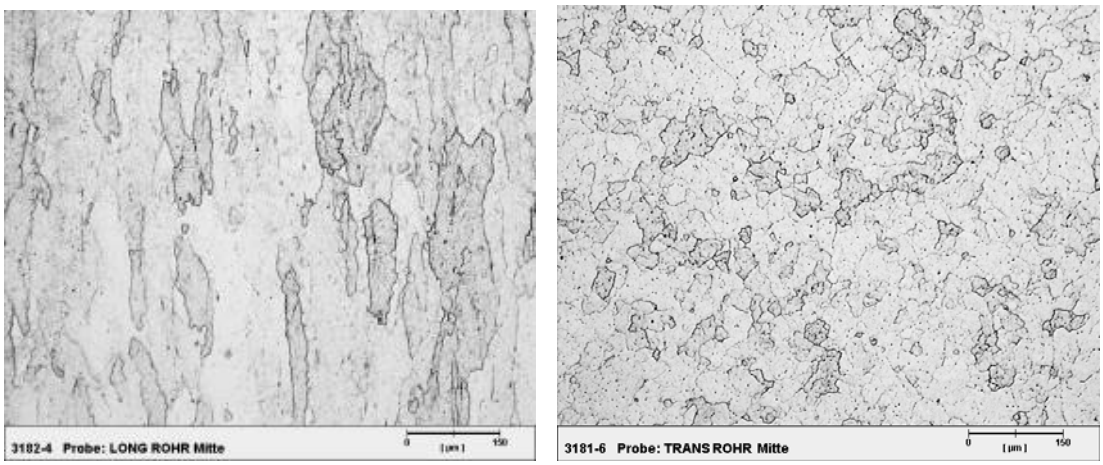

Figure 1.11b: Longitudinal and transversal microstructure of DUCROPUR Cr in as manufactured condition.

The microstructure is characteristic of the manufacturing process used to produce the material, which consists of two basic phases, sintering in inert atmosphere and extrusion at high temperature to break by shear the oxides formed in the grain boundaries and which are one of the key factors contribution to the low room temperature ductility of Cr [Milman, 1972]. The microstructure corresponds to a non-re-crystallised condition. Transmission electron microscopy revealed a low concentration of impurities in the material, which did not present any visible of oxides and nitrides near crystal lattice defects, as discussed in chapter 4.

Macroscopic observation of the combustion chamber after test

The cold and hot areas of the combustion chamber presented specific macroscopic degradation mechanisms:

The main macroscopic failure evidence in the cold section of the combustion chamber is the presence of transversal cracks that did not fully rupture the combustion chamber structure. The position of these cracks corresponds to the film break point, named point d in figure 1.7, where longitudinal temperature gradient attains its highest value. This indicates that transversal were produced by the thermo-mechanical constrains in this area.

The hot area of the combustion chamber presents a smooth layer of chromium oxide with a dark green appearance indicating that the low concentration of oxygen in the combustion atmosphere, approximately 3%, is enough to generate a stable oxide layer. Metal erosion is not evident in any area of the structure.

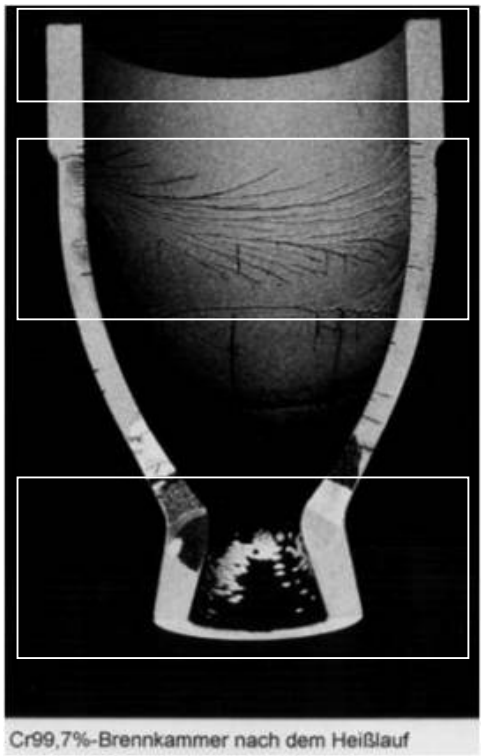

Injection area

Film breaking point, transversal cracks

Highest Temp. area, through cracks

Figure 1.12a: Cross cut of the Cr combustion chamber after vacuum firing and macroscopic damages observed in different areas.

The area adjacent to the throat of the combustion chamber fractured during disassembly of the combustion chamber from the rig (figures 1.12 and 1.13). The fractured area was shiny, but up to a depth of approximately 2mm oxidation was evident. This indicates that cracks started to propagate during service but did not completely fracture the combustion chamber structure. The position of the cracks is very close to the hottest area of the combustion chamber. Mechanical constraints in this area are minimum, explaining which the chamber did not fracture during operation.

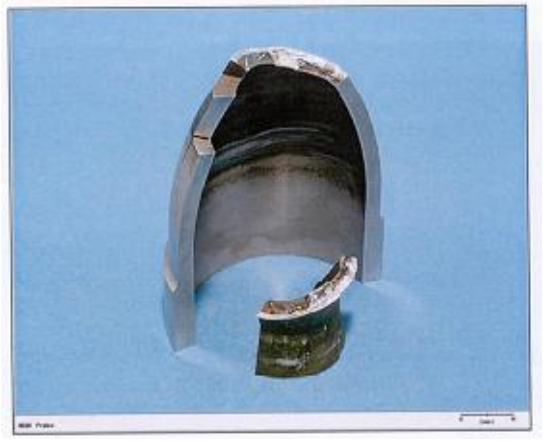

Fig 1.12: Global appearance of the combustion chamber. The green surface consists of chromium oxides. The fracture near the throat is the most evident failure point of the chamber.

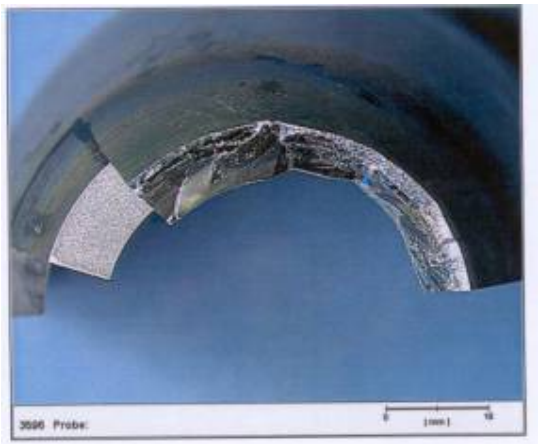

Fig 1.13: Through fracture near the throat of the combustion chamber. The fracture is fragile in appearance but the microstructure analyse has shown otherwise.

From the macroscopic point of view, the main failure mechanism of the combustion chamber is the decrease of the mechanical properties in the throat area that made disassembly from the test rig without damaging the structure impossible. In service conditions, where the mechanical loads in the throat are considerably higher because of the presence of the nozzle, it is certain that the throat would have fractured. Metal loss due to oxidation and erosion plays a negligible role. There is also no evidence of material melting in the structure.

Microscopic analysis of the combustion chamber

The hot area of the combustion chamber was inspected by means of SEM and optical microscopy.

Recrystallisation and grain growth are evident in the hot area of the combustion chamber. Grain size attains its highest value in the fractured area, as seen in figure 1.14, with dimensions of about one millimetre. The microstructure of the cross section of the hot area of the combustion chamber can be divided into three zones with distinct grain sizes and morphology:

- The outer zone of the combustion chamber, where for a given longitudinal point, the temperature is lower than in the inner wall, is in fully recrystallised condition, with polygonal grains of a mean size of 30 μm. Precipitation of a secondary phase in evident in the grain boundaries and to some extend inside the grains. Maximum temperature in this area was 1350 °C.

- The central zone of the cross section is occupied by grains with a mean size exceeding 2mm. The temperature in this area is higher than the temperature of the outer section therefore grain growth has taken place. Second phase precipitates are present inside the grains.

- The inner area of the combustion chamber, where temperature is highest is constituted of precipitate free grains. The maximum temperature in this area is approximately 1500°C. This area is subdivided in two distinct zones:

    - One layer of approximately 500 μm thickness with large elongated grains between 200-500 μm in length

    - One layer of approximately 100 μm thickness with polygonal grains with a mean size of approximately 50 μm

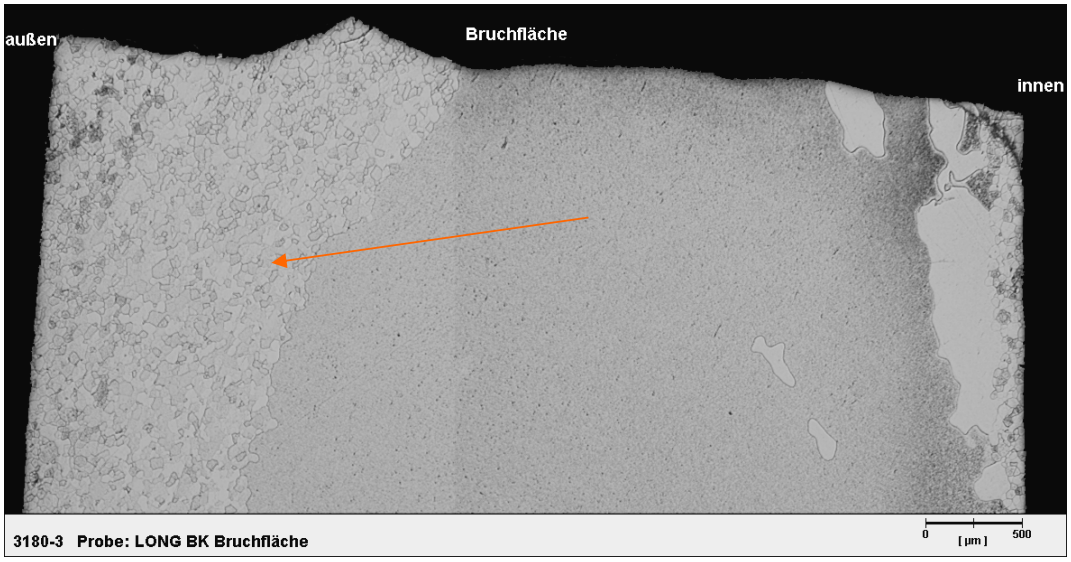

Figure 1.14: Section of the hot area of the combustion chamber. The arrow indicated heat flow direction. Material has completely recrystallised and grain growth exceeds largely millimetric dimensions

Figure 1.15 shows how the density of precipitates in the central zone increases in the vicinity of the inner zone, which is itself free of precipitates. This indicates that segregation of light elements may have taken place from the inner zone where high temperature does not allow for formation of stable precipitates to the central zone where temperature is lower.

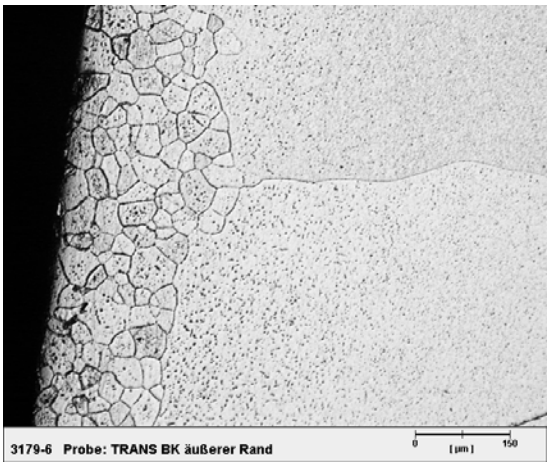

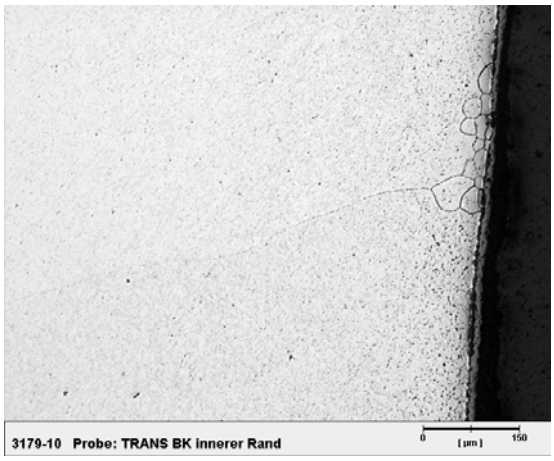

Figure 1.15a (left) and 1.15b (right): Grain growth in the hot area of the combustion chamber. Figure 1.15a a corresponds to the external wall and figure 1.15b to the internal wall adjacent to the combustion area.

Precipitation of intergranular and intragranular phases is rendered evident by optical microscopy in figures 1.16a and 1.16b. In order to obtain the chemical composition of the phases, local qualitative analysis and observations by TEM (figures 14 a and b) and quantitative analysis by hot gas extraction on the bulk material were carried out. Composition of the bulk material in as delivered condition and after firing is given in table 1.4.

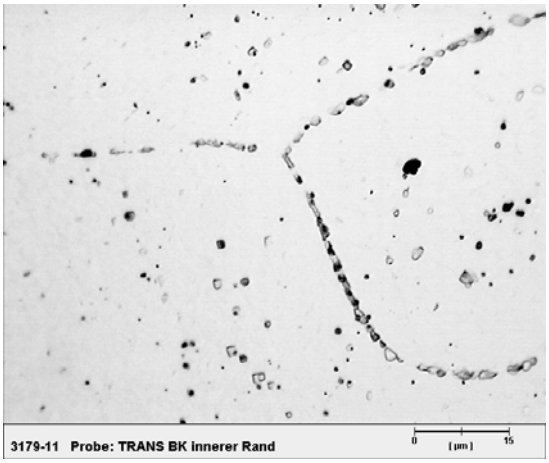

Figure 1.16a: Precipitation of carbides and nitrides at the grain boundaries and inside the grains in the hot section of the combustion chamber.

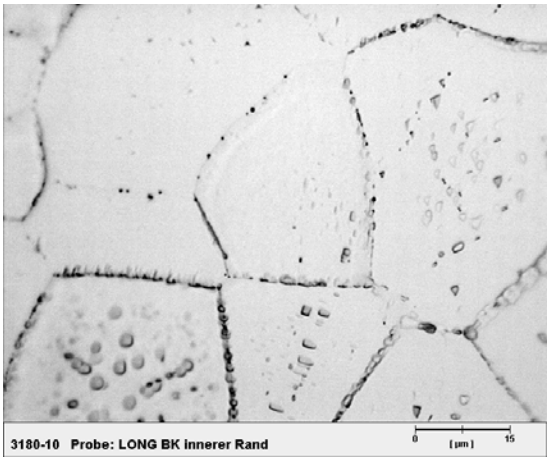

Figure 1.16b: Fracture path follows the grain boundaries when these phases have precipitated. Fracture happens at high temperature at extremely low stresses and is fragile at low temperature

The chemical analyses carried out in the hot area of the combustion chamber by means of chemical extraction indicate that the precipitates present in the alloy are basically chromium nitrides, carbides and oxides. Their precipitation is rendered possible by the diffusion of nitrogen through the otherwise stable layer of Cr_2O_3 (figure 1.17) during high temperature operation of the combustion chamber.

Table 1.4: Composition of Ducropur pure Cr in as delivered condition and after vacuum firing in the hot area (throat) and in the cold area adjacent to the injector head.

		After 120 min firing, 1500 °C	
Element	[ppm] as delivered	[ppm] in cold area	[ppm] in hot area
Hydrogen	7	7	9
Oxygen	35	34-38	87
Nitrogen	53	51-55	145
Carbon	1,7	1,7	2,5

Phase diagrams show that all Cr nitrides have melting points lower than the service temperature of the chamber causing intergranular high temperature fracture at very low stresses, as observed during service of the combustion chamber. This phenomenon is well known as the Cr high temperature brittleness and has been observed by several authors [Sully 1967], [Trefilov, 1975]. Cr nitride is also fragile at low temperature and liquefies at 1450°C, so its presence at grain boundaries further embrittles Cr and its traceability after test is meager.

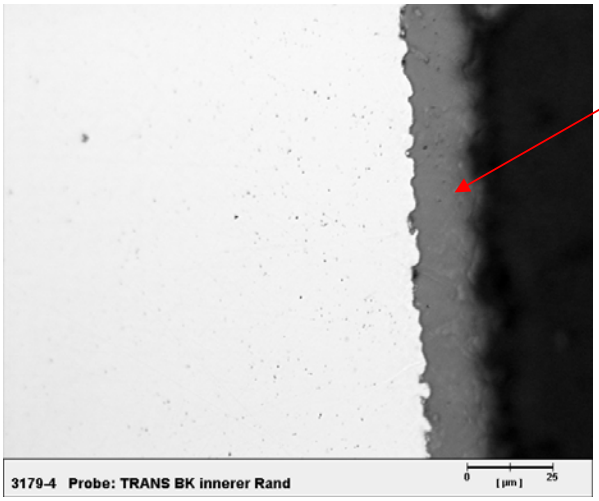

Figure 1.17:

Stable oxide layer in the inner wall of the hot zone of the combustion chamber. Oxide has a green, smooth surface and is not detached from the substrate in any point.

The remarkable absence of hydrogen in the material, despite its important concentration in the combustion atmosphere, is related to the passiveness of Cr to this element and is an interesting benefit considering the application.

Figure 1.18a: Transmission electron Microscope image of the microstructure of the as manufactured material. There is a relatively high dislocation density, indicating its non fully recrystalised condition but no precipitation at dislocation borders, generally in the form of dark shadows, indicating the high purity of the material.

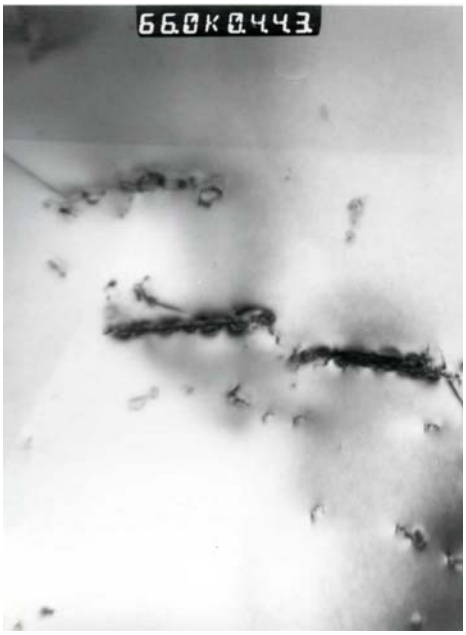

Figure 1.18b: Precipitation of nitrides at dislocation borders made evident by transmission electron microscopy (dark areas). The low dislocation density is a result of the high recrystallisation of the material. Nitrides and carbides surround remaining dislocations. These are the main responsible for the material brittleness.

1.4.3 Cr failure mechanisms and possible reinforcement methods

The tests and analyses carried on the pure Cr combustion have determined that under service conditions this material is degraded by the following mechanisms:

- Recrystallisation in the hot area
- Chemical instability in the presence of nitrogen (Cr_2O_3 layer not protective)
- Brittle fracture in the cold area under thermo-mechanical constraint.

Recrystallisation of the hot area was foreseeable from the available data. Brittle failure of the cold area contradicts simulations and may be related to mechanical property loss during service due to the diffusion of impurities into the alloy. Brittleness of Cr may be decreased and even eliminated by increasing its purity [Milman], nevertheless diffusion of light elements during service would inevitably embrittle the

material. The diffusion of nitrogen into the substrate, rendered evident by chemical analyses, indicates that the Cr_2O_3 layer on the surface is not protective against nitrogen diffusion. The precipitation of nitrides and oxides at grain boundaries and crystal lattice defects observed in figure 1.18 further embrittle the material at low temperature, offering preferential fracture paths. Besides being brittle, Cr nitrides have a melting point below the operation temperature of the chamber, originating inter-granular fracture during service.

Despite the failure of the combustion chamber, it is remarkable that the material did not suffer catastrophic oxidation during service and that hydrogen take up was insignificant. In these two application-relevant points, Cr outperforms all other uncoated metallic material alternatives, aside from precious metals. This renders interesting the investigation of possible solutions to the incompatibility problems of Cr with the application.

The recrystallisation temperature can be controlled by means of second phase particle dispersions impeaching grain growth. This is nevertheless done at the expense of the ductile to brittle transition temperature, which increases with the addition of ceramic particles in the material. Increase of the recrystallisation temperature of Cr can also be done by alloying it with higher melting point materials, such as Ta, Mo, W, Ir and Re, with unknown consequences on the other properties of the alloy, and in particular on the chemical stability and, exception given for Re, on the ductility.

The low temperature plasticity of Cr may be increased by eliminating the interstitial impurities dissolved in the metal. This option is nevertheless not relevant for this particular application; the chemical analyses have proved that nitrogen diffuses into the material during service, thus embritteling it independently of the original alloy purity, with this possibility ruled out, only the option of ductilisation by alloying remains. Some fundamental studies concerning the effect of second element additions on the deformation properties of Cr, and in general of Body Centred Cubic refractory metals have been carried out in the past. These works have been basically focussed on the effect of solid solution alloying of Mo and W with metals belonging to higher periods, such as Co, Fe and Re. Mo-Re and W-Re alloys are commercially

available from several manufacturers and show excellent ductility even at cryogenic temperature.

The problem of nitrogen compatibility of Cr at high temperature is many sided and considering the composition of the combustion atmosphere, it is most relevant for the application. BCC refractory metals present very low light element solubility. Nitrogen that cannot remain in solution in the Cr matrix segregates to crystal lattice defects and grain boundaries, causing the precipitation of nitrides. Some works have been done in the past dealing with this problem; they all have in common the use of light element traps to capture dissolved light elements and impeach their reaction with the matrix. Povarova (1997, 1-2) suggests that near solid solution alloying of Cr with Re may increase its resistance to nitrogen embrittlement. Unfortunately no experimental evidence of this effect has been found in the literature.

2. Existing data and objectives of this work

2.1 Previous works on the topic

The interest in very high temperature structural materials, and particularly refractory metals, grew considerably in the 1950's with the generalisation of the jet engine for aircraft and the need of radiation-resistant high temperature materials for nuclear reactors. The first systematic work on ductile refractory metals containing Re was published in 1956 by North-American scientists Hughes and Geach (1956). The works of these authors focussed on W-Re and Mo-Re alloys with potential to be used in the glass and aerospace industry. They identified the problem of their intrinsic brittleness as their main inconvenient for industrial use.

The alloys produced by Hughes and Geach were manufactured by means of electron arc melting in a cold crucible under vacuum. Figure 2.1 shows that they produced high purity W-Re and Mo-Re alloys showing excellent ductility. Results on Cr-Re alloys were not conclusive probably as high quality alloys could not be produced, due to technical difficulties that will be discussed in chapter 4.

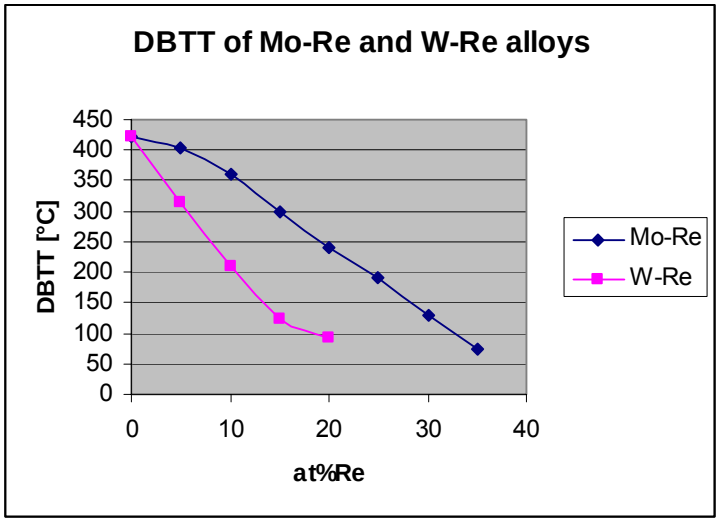

Figure 2.1: Effect of Rhenium in the ductile to brittle transition temperature of VIA refractory metals according to the observations of Hughes and Geach. Source [Hughes and Geach, 1956]

Most works related to Cr-Re alloys were published in the Soviet Union during the 1960's and 1970's by the team of Trefilov of the Kiev institute of Metallurgy. The activities of this team focussed in the ductilisation of BCC refractory metals by direct alloying and thermo mechanical treatment. In the same line of Hughes and Geach, the main research line of Trefilov was related to Mo and W based alloys, which present a high industrial application potential. Trefilov and his team published several works on the properties of W-Re and Mo-Re alloys, including detailed studies on their manufacturability, treatment and mechanical properties from cryogenic to very high temperature, [Trefilov 1969, 1975, 1984], [Milman 1981, 1995, 1997], just to name a few. Cr-Re alloys were not fully developed due to problems related to the low purity of available Cr and manufacturing difficulties which could be discussed directly with Milman during this PhD.

According to Trefilov and Milman [Trefilov, 1969, 1975, 1984], Milman [1995, 1997] BCC refractory metals present very oriented atomic bonds with a covalent character, for which a high Peierls stress is characteristic, hence difficulting dislocation motion and material plasticity. Any stable ductilisation in these alloys can only be produced by changing the directionality of their atomic bonds, reducing their covalent character. This hypothesis is further confirmed by other authors [Medvedeva, 2002]. For her, the highly directional bonds influence the parameters controlling deformation, basically the Peierls stress, the shear modulus and the stacking fault energy. Decreasing the directional character of the Cr atomic bonds by means of alloying or by introducing impurities like carbon increases the alloy plasticity. Medvedeva traces the breaking of the direction al bonds to changes in the electronic structure of the alloy by means of Monte-Carlo Simulation. When alloyed with Re the Density of States at Fermi level of the alloys is displaced from the minimum of the alloy in pure form, to higher values as the solid solution limit is achieved.

The results of the simulations of Medvedeva back up the theory of Trefilov who affirms that the ductilisation observed when alloying Cr, Mo and W with Re is related to the changes in the electronic structure in the solid solution produced as Re concentration increases. Re changes the electron density in the s and d bands which in turn changes the density of states of the alloy at Fermi level from its minimum when the base material is in pure form, to increasing densities as Re content

increases. A higher Density of States corresponds to less directional bonds, hence to a more plastic alloy [Milman, 1995].

Trefilov traced the relationships represented in figure 2.2 between the density of electrons in the s and d bands, proportional to the Re concentration in the alloy and the parameters controlling intrinsically the ductility, namely the Peierls stress, the stacking fault energy and the shear modulus. Notably there is an increase from 6 to 6.35 s+d electrons corresponding to 0 to 35 at% Re in the solid solution range of a BCC-Re alloy.

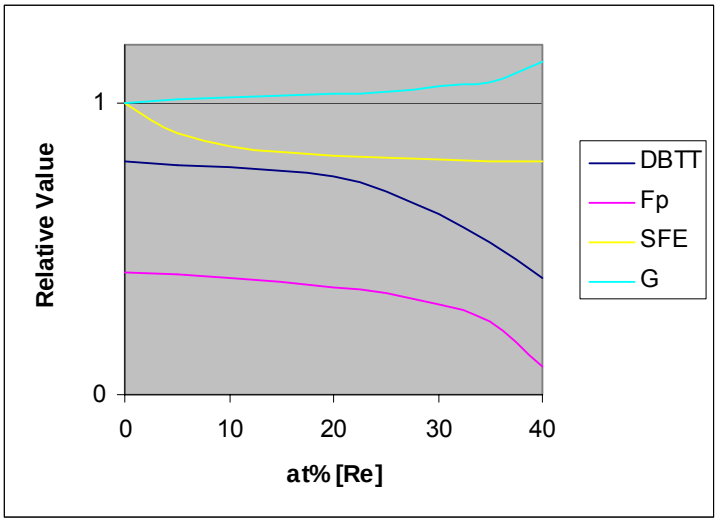

Figure 2.2: Qualitative dependence of the Peierls Stress (Tp), the Stacking Fault Energy (SFE) and the Shear Modulus (G) on the at % of Re and their influence on the Ductile to Brittle Transition Temperature of a the Mo-Re alloy

Other works state that not only rhenium, but also iron and cobalt are able to increase, at very high alloying percentages, the ductility of chromium and that osmium and carbon amplify the effect of rhenium in the ductility enhancement [Milman, 1997], [Buckman, 1997], [Holzwarth, 2001], [Yoshikazu, 2002]. This theory and that of Sully are in fact complimentary as relationships may be traced between the electronic structure the interstitial solubility.

The most recent works concerning Cr-Re alloys were published by Medvedeva, of the Institute of Solid State Chemistry of Ekaterinburg. Medvedeva proved the affirmations of Trefilov, Firstov and Milman by means of Monte-Carlo simulations,

concluding that the low density of states at Fermi level and the directional bonding of BCC refractory metals are linked and responsible for their brittleness. Medvedeva proved that alloying additions of Re and C decrease the directionality of the bonds, while oxygen had the inverse effect [Medvedeva, 2002]. Medvedeva states that a metastable A15 structured phase precipitated near the solid solution limit of Cr and Re. This phase would have a very high affinity for O, thus purifying the matrix and contributing to the decrease of directionality of bonds in the alloy. This phase has not been observed experimentally.

Besides the intrinsic properties of their atomic bonds, other elements also contribute to the brittleness of Cr, Mo, and W: In 1965, Sully and Brendes related the brittleness of BCC refractory metals to the low solubility of a number of elements in them. They observed that light elements, basically nitrogen and oxygen precipitate at crystal defects impeaching the dislocation mobility and therefore plastic deformation. This can be observed in figure 2.3, taken by TEM from a high purity Cr alloy exposed to air at 1200 °C during 3h. The explanation of Sully is in accordance with the classic theory of deformation, which links plasticity to dislocation mobility. This experimental observation, added to the intrinsically elevated Peierls stress of the materials, is generally accepted to contribute strongly to the brittleness of VIA group metals.

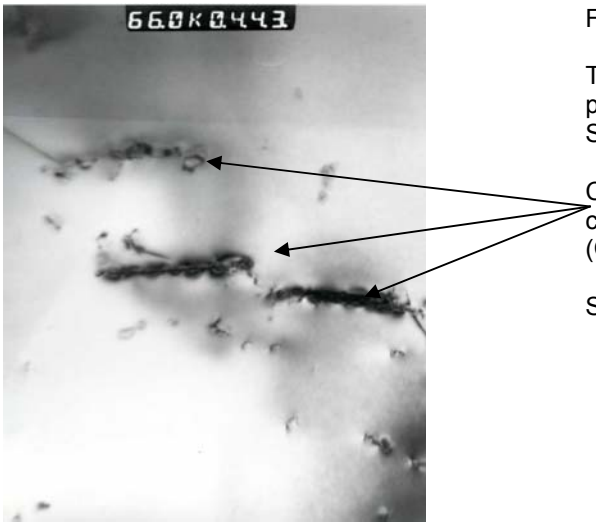

Figure 2.3:

Transmission Electron Microscopy image of phase precipitation at dislocations as observed by Sully and Brendes.

Chemical analysis showed that precipitate was chromium nitride. Composition not yet identified (CrN or CrN_2)

Source EADS / LSGS Nancy

Also in the 1980's, team team of Kira B. Povarova, of the Moscow Baikov Institute of Metallurgy published overview works of the manufacturing of W-Re and Mo-Re alloys

by means of powder metallurgy and mechanical activation of powders [Povarova, 1997 1-2]. Studies on Cr-Re alloys were not published by this author.

In the USA, studies on the Re effect on BCC refractory were published by Wukusick (1966) who obtained cryogenic ductility in W-Re and Mo-Re alloys but who did not study extensively Cr-Re alloys. Work on the effect of Re on BCC refractory metals stopped in the mid 1970's, after negative experiences using these type of alloys in jet engines, [Klopp, 1975]. Interest in the Re effect effect on BCC refractory metals was revived in the 1980's for their application in space nuclear systems, results were published by [Klopp, 1987], these do not include Cr-Re alloys. A review of American works in the field of Refractory metals alloyed with Re was published by [Buckmann, 1997].

Besides the discussed research works, other publications listed in the bibliography on this chapter have been used for this work, basically [Neumann, 1987], [Huang, 1998] and [Gritsiv, 1999] for the phase diagrams of the Cr-Re system used in this work.

2.2 Objectives of this work

Firing experiences of Cr combustion chambers with conventional satellite propellants proved that this material is unable to provide the mechanical and chemical stability required for the application. This study was done as an introduction to this PhD. The failure analysis described in section 1.4.3 revealed that the main problem areas of Cr are:

- Low ductility below 200 °C
- Recrystallisation and grain growth under 1500 °C
- Embrittlement by diffusion of light elements into the alloy at high temperature and the subsequent precipitation of nitrides and oxides at crystal lattice defects.

Some studies indicate that solid solution alloying of BCC refractory metals with Re may improve chemical resistance, ductility and in the particular case of Cr, also the recrystallisation temperature [Milman, 1997], [Buckman, 1997], [Medvedeva, 2002].

The effect of Re has been investigated in detail for Mo-Re and W-Re alloys and the research work has given place to industrial products, in particular thermocouples and other high temperature components. Despite that the ductilising effect of Re on Cr is generally reported in the literature, the properties of Cr-Re alloys have not been characterized in detail and a manufacturing process for Cr-Re alloys in a semi-industrial scale does not exist, this PhD has been aimed at obtaining a better understanding of the properties of solid solution Cr-Re alloys and defining a manufacturing process for them. The goal application of the alloys is satellite thruster engines.

The objective of this work may be summarised in the next points:

- To design a manufacturing process for Cr-Re alloys
- To characterize the influence of Re and other alloying additions on the microstructure of the alloys
- To determine the influence of Re on the properties of the alloys relevant to the application
    - Mechanical properties from ambient temperature to 1400°C
    - Chemical properties
        - High temperature resistance to oxygen and nitrogen
        - Stability in cold hydrazine
        - Influence of oxygen and nitrogen contamination on the mechanical properties
    - Influence of Re on the thermal-shock resistance of the alloy
    - Influence of Re on the temperature gradient resistance of the alloy
    - Influence of Re on the thermal conductivity and capacity of the alloy

The properties that will be investigated in the present work are listed in table 2.1

Table 2.1: Main parameters to be investigated during this work

Property	Solicitation range
Mechanical strength ($\sigma_{0,2}$, E, UTS)	20 °C-1400 °C in compression and tension
Resistance to air	1200 °C-1600 °C up to 4 hours
Resistance to pure nitrogen	1500 °C up to 4 hours
Thermal shock resistance	500 K/s; from 20°C to 1890 °C
Thermal gradient resistance	500 k/mm; combined with thermal shock
Thermal capacity	20 °C-1200°C
Thermal conductivity	20 °C-1200°C

3. General experimental techniques

3.1 Experimental techniques specific to each chapter

Manufacturing process and the application-related properties of Cr-Re alloys have been studied in this work. This means that a wide variety of specific experimental techniques have been used. In this chapter only the general experimental techniques that are used in this work are described, basically Scanning Electron Microscopy, Transmission Electron Microscopy and Optical Microscopy. The experimental techniques specific to each chapter of the work have been treated individually according to table 3.1.

Table 3.1: Experimental techniques described specifically in the chapters where they have been used.

Experimental technique	Chapter where described
Alloy processing	
Powder metallurgical processing of Cr-Re alloys	4
Melting and Casting of Cr-Re alloys	4
X-ray diffraction	4
Measurement of alloy properties	
Compression tests to ASTM E9-81 standard	5
Tension tests	5
Micro indentation	5
Chemical stability of Cr-Re alloys in air and nitrogen	6
Stability of Cr-Re alloys in vacuum at high temperature	7
Thermal capacity Cr-Re alloys	8
Thermal conductivity of Cr-Re alloys	8
Electric conductivity of Cr-Re alloys	8
Coefficient of thermal expansion	8

3.2 Optical Microscopy

Optical microscopes use visible light, typically coming from an artificial light source, to amplify the features of the surface of a sample. A beam of light is focused onto a tiny,

bright spot of the specimen by means of a system of lenses called the condenser. The image of the object is brought into focus through the microscope's tube using spherical objective lens. This is then magnified by a second lens, called an ocular lens or eyepiece. The increase on the magnification of the analysed area occurs by changing the objective lenses: relatively flat lenses produce low-magnification compared to rounder lenses. The quality of the image is controlled by the brightness, the focus, the resolution and the contrast [Techniques 1, 3].

Brightness is related to the illumination system and can be adapted, changing the voltage of the lamp (rheostat), adjusting the condenser and/or the diaphragm apertures. Moreover, brightness is related to the numerical aperture of the objective lens. Brighter images are obtained with larger numerical apertures.

The focus is associated to the focal length and it is controlled with the focus switches. The capacity to difference two neighbour points is the resolution. This is related to the numerical aperture of the objective lens and the wavelength of light passing through the lens. Better resolution is attained with higher numerical aperture and shorter wavelength. The minimal appreciable distance, d_{min}, can be calculated using next equation.

$$d_{\min} = \frac{0.6\lambda}{n \sin \alpha} \quad (4.2)$$

where α is the overture angle, λ the wave length and n the refractive index. Optical microscopy can then distinguish objects separated by down to *0.2* µm.

The contrast is related to the illumination system and can be adjusted by changing the intensity of the light and the diaphragm aperture. Chemical stains applied to the specimen can also enhance contrast. Furthermore, contrast can be improved by closing the condenser aperture, but this tends to reduce the resolution. Other contrast techniques are based into splitting the light beam into two pathways. Light waves that pass through dense structures slow down compared to those passed through less dense structures. These light waves are then collected and transmitted to the eyepiece, where they interfere. The contrast is then produced by means of the

interference patterns, which forms a false 3D image [Techniques]. During this work a light microscope Leica Polyvar SC was used.

3.3 Transmission Electron Microscopy (TEM)

TEM's are patterned after Transmission Light Microscopes and yield similar information. In this work TEM microscopy has been basically used to study the alloy microstructure after deformation at different temperatures. [Techniques, 3] The main characteristics of a specimen that can be investigated by means of TEM are:

- Morphology: The size, shape and arrangement of the particles which make up the specimen as well as their relationship to each other on the scale of atomic diameters.

- Crystallographic Information: The arrangement of atoms in the specimen and their degree of order, detection of atomic-scale defects in areas a few nanometers in diameter

- Compositional Information: The elements and compounds the sample is composed of and their relative ratios, in areas a few nanometers in diameter

TEMs shine a beam of electrons through a thin specimen. Whatever part is transmitted is projected onto a phosphor screen. Figure 3.1 shows the main components of a TEM.

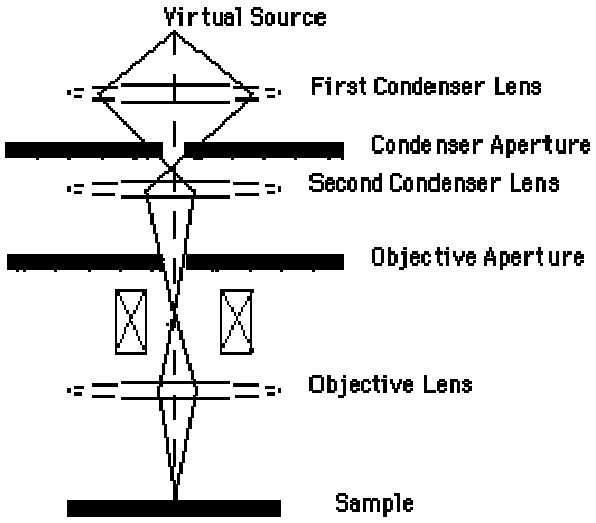

Figure 3.1: Main elements of a transmission electron microscope, TEM

The "Virtual Source" at the top represents the electron gun, producing a stream of monochromatic electrons. TEM and scanning electron microscopes described in the next section, use an electron source of some kind with the majority using a Thermionic Gun represented in figure 3.2.

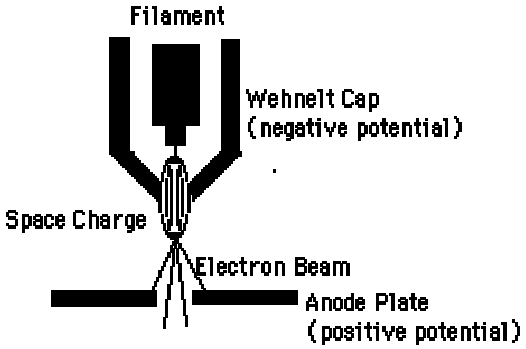

Figure 3.2: Main components of an electron gun

A Thermionic Electron Gun functions in the following manner

1. An positive electrical potential is applied to the anode
2. The filament (cathode) is heated until a stream of electrons is produced
3. The electrons are then accelerated by the positive potential down the column
4. A negative electrical potential of approximately 500 V is applied to the Whenelt Cap

5. As the electrons move toward the anode anyones emitted from the filament's side are repelled by the Whenelt Cap toward the optic axis horizontal centre
6. A collection of electrons occurs in the space between the filament tip and Whenelt Cap. This collection is called a space charge
7. Those electrons at the bottom of the space charge nearest to the anode can exit the gun area through the orifice of less than 1mm in the Whenelt Cap
8. These electrons then move down the column to be later used in imaging

For reliable operation of the electron microscope, the electron gun must comply with the following points:

- That the electrons later used for imaging will be emitted from a nearly perfect point source or space charge
- The electrons used for imaging are monochromatic, this means that they have similar energies
- Only electrons nearly parallel to the optic axis will be allowed out of the gun area

This stream is focused to a small, thin, coherent beam by the use of condenser lenses 1 and 2. The first lens, usually controlled by the spot size knob, determines the spot size; the general size range of the final spot that strikes the sample. The second lens (usually controlled by the "intensity or brightness knob" actually changes the size of the spot on the sample; changing it from a wide dispersed spot to a pinpoint beam.

The beam is restricted by the condenser aperture, which is usually user selectable, knocking out high angle electrons, those far from the optic axis, the dotted line down the centre.

The beam strikes the specimen and parts of it are transmitted

This transmitted portion is focused by the objective lens into an image

Optional Objective and Selected Area metal apertures can restrict the beam.

The image is passed down the column through the intermediate and projector lenses, being enlarged all the way

The image strikes the phosphor image screen and light is generated, allowing the user to see the image. The darker areas of the image represent those areas of the sample that fewer electrons were transmitted through (they are thicker or denser). The lighter areas of the image represent those areas of the sample that more electrons were transmitted through (they are thinner or less dense)

Interactions of electron beam with thin specimen

Electron beam interactions with thin sample can be used to determine different sample characteristics. Figure 3.3 represents the main electron beam solid interactions present in TEM.

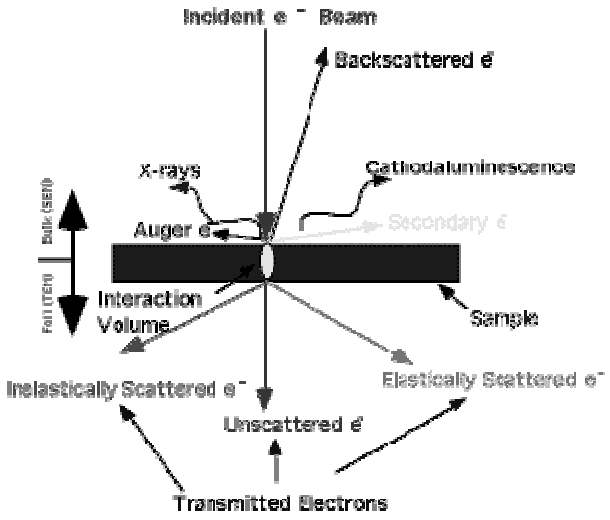

Figure 3.3: Main interactions between electron beam and thin sample in TEM

The main interactions between the electron beam and the specimen, their source and their use for sample characterization are described below.

- Unscattered Electrons

  Source: Incident electrons which are transmitted through the thin specimen without any interaction occurring inside the specimen.

Utilization: The transmission of unscattered electrons is inversely proportional to the specimen thickness. Areas of the specimen that are thicker will have fewer transmitted unscattered electrons and so will appear darker, conversely the thinner areas will have more transmitted and thus will appear lighter. This allows for a morphologic characterization of the specimen.

- Elastically Scattered electrons

Source: Incident electrons that are scattered (deflected from their original path) by atoms in the specimen in an elastic fashion (no loss of energy). These scattered electrons are then transmitted through the remaining portions of the specimen.

Utilization: All electrons follow Bragg's Law and thus are scattered according to Wavelength=2*Space between the atoms in the specimen*sin(angle of scattering). All incident electrons have the same energy(thus wavelength) and enter the specimen normal to its surface. All incidents that are scattered by the same atomic spacing will be scattered by the same angle. These "similar angle" scattered electrons can be collated using magnetic lenses to form a pattern of spots; each spot corresponding to a specific atomic spacing (a plane). This pattern can then yield information about the orientation, atomic arrangements and phases present in the area being examined.

- Inelastically Scattered Electrons

Source: Incident electrons that interact with specimen atoms in a inelastic fashion, loosing energy during the interaction. These electrons are then transmitted trough the rest of the specimen

Utilization: Inelasticaly scattered electrons can be utilized two ways
Electron Energy Loss Spectroscopy: The inelastic loss of energy by the incident electrons is characteristic of the elements that were interacted with. These energies are unique to each bonding state of each element and thus

can be used to extract both compositional and bonding (i.e. oxidation state) information on the specimen region being examined.

- Kikuchi Bands:

  Source: Bands of alternating light and dark lines that are formed by inelastic scattering interactions that are related to atomic spacing in the specimen.

  Utilization: The width of the Kikuchi bands is inversely proportional to atomic spacing and can be used to measure it.

3.4 Scanning electron Microscopy-SEM

The Scanning electron microscope (SEM) is based on the analysis of the signals emitted by the electron-solid interaction. It is used to characterize solid topography, chemical links, atomic distance, features of polarization and relaxation of dielectrics. In this work SEM has been used to study the microstructure and composition of Cr and Cr-Re alloys and for the fractography investigations [Techniques 2, 3].

In combination with other experimental techniques, basically XRD and TEM, it constitutes a fundamental investigation technique in the field of metallurgy, semiconductors, geology and biology.

The resolution capability of SEM is much higher than that of optical microscopy since the minimum distance to difference 2 points, d_{min}, is described by equation (1):

$$\boxed{d_{\min} = \frac{0{,}6\lambda}{n \sin \alpha}} \qquad (1)$$

where α is the overture angle, λ the wave length and n the refractive index.

By the wave-particle dualism, this relation is not exclusively reserved to the optic, but also it can be applicable on electron beam and so becomes also the basis for electron microscopy. Wave length of the electron beam used in SEM is around 10^5

times smaller than that of light, making the resolution limit 10^5 than that of an optical microscope.

SEM equipment description

A scanning electron microscope is built from a vacuum chamber, the electron microscope body and the sample carrier. The body parts are:

- Cannon of electrons, described in the TEM section
- Lenses to focus the ray and scanning the specimen surface
- Detector of the signals released on the specimen

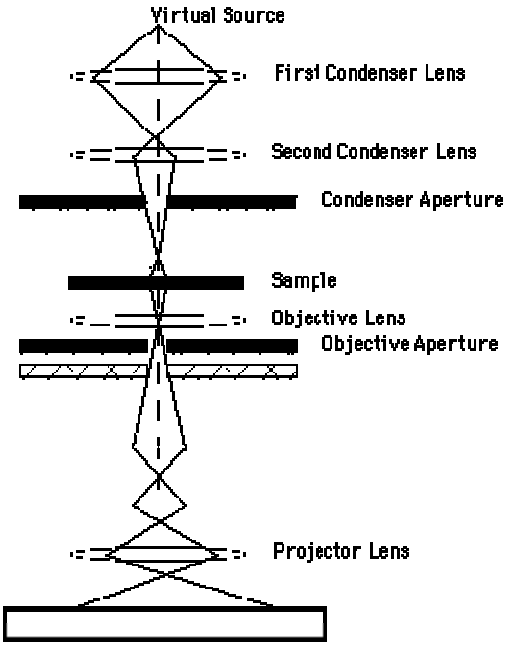

Figure 3.4: Main components of a SEM

In many microscopes, the pressure in the body is of the order of 10^{-7} Pa. It is reached after heating the installation in approximately 250°C during several hours.

The electron canon allows obtaining a beam of accelerated electrons in the wished potential. The emission is produced either by thermo-electric effect (law of Dusham-Richardson), or by field effect (law of Fowler-Nordheim).

The thermo-electrical guns can be actually from two materials: W or LaB_6 (hexa-bore of lanthanum). For the classic applications, a standard wire of tungsten is enough (resolution of 5 µm). If a high resolution is necessary, it is used a mono-crystal tip of hexa-bore of lanthanum (resolution 3,5 µm), but the constraints are then more important, < 10^{-7} Torr (1 Torr = 133,3 Pa). Normal used thermal cathode is the tungsten capillary-cathode. A bent tungsten wire, filament, fastened on a ceramics base, can be stimulated applying a heating tension to thermal emission of electrons. To get over the work function of 4,5 electron volts, temperatures between 2700 °C and 2800 °C are required; only then, the electrons build a space charge before the cathode.

A SEM with tungsten capillary-cathode requires as an additional assembly a Wehnelt-cylinder between cathode and anode, also known as cathode-ray tube grid or shield, which lies on a higher negative tension 0-500V than the cathode. This Bias-tension determines together with the cathode temperature the number of the emitted electrons and it bundles, by overlay with the electric field between anode and cathode, the electrons to a small spot about 20-50 µm of diameter, the Crossover.

For the electron generation using a field emittance, an electric field is put on to the cathode, which reduces the potential threshold for the electrons and makes possible its discharge in the vacuum.

Afterwards the electron beam passes through a system of magnetic condenser and objective lenses, which allow focusing the beam on the target. Diaphragms limit the opening of the beam. The diameter of the beam d_{ce} results from the reduction of the crossover by means of the lenses system. It reduces the ray diameter about to 3-20 nm.

The task of the beam generator system is to form a very small Crossover before the entry of the electron beam in the lenses system. However, problems appear from the decreasing beam current, which should not remain under a minimum value of 10^{-12}A to produce a low-noise image.

The hitting primary electrons of the beam produce different interactions with the specimen, which would be used to generate the picture: released secondary electrons and back scatter electrons (material contrast). A hitting electron can get up to four secondary electrons out of the surface with an energy of approximately 5 eV or it would be thrown back for the specimen and thereby to back scattered electron.

The specimen can be scanned by means of deflection coils on the optical path point to point; it arises, dependent on the surface state, different intensities in the detector, which are represented on the screen as brightness values. There appears a very plastic picture of the specimen.

A resolution power of 30 times higher compared to light microscope (4 nm with tungsten capillary-cathode) and a much higher depth of sharpness are the big merits of the scanning electron microscope. Limitations appear only from the required vacuum and the conductivity of the specimens, without it is impossible to create an image, therefore, a specimen preparation by vaporizing is required.

The different optical components present aberrations, which produce an extension of the electronic sensor. The different types of aberration are: Opening aberration, chromatic aberration, electronic diffraction and astigmatism aberration.

The carry-sample device is one of the most important pieces of the installation. It is characterized by several degrees of freedom: translation, rotation, sample inclination and movement of the object on the optical axe of the column. It has to be able to tilt the sample without moving its position on the optical axis.

The emitted electrons by the sample reach an electron multiplier or fall on a light-sensitive layer (ZnS), which produce photons. These photons are then guided towards a photo-multiplier by mans of a guide of light. The images generated using secondary electrons are essentially formed by electrons of low energies because of the most important part of the emission occur in energy of some eV. These secondary electrons are generally post-accelerated to increase the solid angle of collection. The images are obtained with primary intensities of the order of 10-11 A.

The images generated using backscattered electrons are formed by the electrons with more high energy of the distribution n(E). The detector is either a photo-multiplier, or a semiconductor detector.

Interaction of electron beam with specimen

The volume inside the bulk specimen in which interactions with electron beam take place is called the specimen interaction volume and it is responsible for a number of interactions with the electron beam. This volume depends on several factors, basically:

- Atomic number of the material being examined; higher atomic number materials absorb or stop more electrons and so have a smaller interaction volume.
- Accelerating voltage being used; higher voltages penetrate farther into the sample and generate larger interaction volumes
- Angle of incidence for the electron beam; the greater the angle (further from normal) the smaller the volume

Figure 3.5 represents the interaction for and specimen of main element with an atomic number 28 when scanned with a beam of an accelerating voltage of 20 kV with 0 degrees tilt.

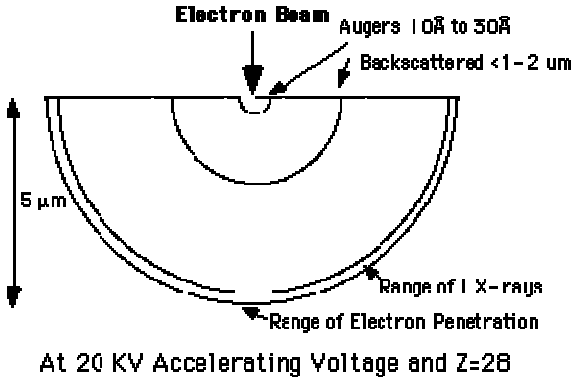

Figure 3.5: Specimen interaction volume in a SEM

A number of interactions between the material and the electron beam take place in the interaction volume. The following points describe those which are used for the characterization of the material in SEM.

Backscattered Electrons

Formation: Caused by an incident electron colliding with an atom nearly normal to the incident's path in the specimen. The incident electron is then scattered "backward" 180 degrees.

Utilization: The production of backscattered electrons varies directly with the specimen's atomic number. This differing production rates causes higher atomic number elements to appear brighter than lower atomic number elements. This interaction is utilized to differentiate parts of the specimen that have different average atomic number.

Secondary Electrons:

Source: Caused by an incident electron passing "near" an atom in the specimen, near enough to impart some of its energy to a lower energy electron (usually in the K-shell). This causes a slight energy loss and path change in the incident electron and the ionization of the electron in the specimen atom. This ionized electron then leaves the atom with a very small kinetic energy (5eV) and is then termed a "secondary electron". Each incident electron can produce several secondary electrons.

Utilization: Production of secondary electrons is very topography related. Due to their low energy, 5eV, only secondary electrons that are up to 10nm near the surface can exit the sample and be examined. Any changes in topography in the sample that are larger than this sampling depth will change the yield of only secondary electrons due to collection efficiencies. Collection of these electrons is aided by using a collector in conjunction with the secondary electron detector. The collector is a grid or mesh with a +100V potential applied to it which is placed in

front of the detector, attracting the negatively charged secondary electrons to it which then pass through the grid-holes and into the detector to be counted.

Auger Electrons

Source: Caused by the de-energization of the specimen atom after a secondary electron is produced. Since a lower (usually K-shell) electron was emitted from the atom during the secondary electron process an inner (lower energy) shell now has a vacancy. A higher energy electron from the same atom can "fall" to a lower energy, filling the vacancy. This creates and energy surplus in the atom which can be corrected by emitting an outer (lower energy) electron; an Auger Electron.

Utilization: Auger Electrons have a characteristic energy, unique to each element from which it was emitted from. These electrons are collected and sorted according to energy to give compositional information about the specimen. Since Auger Electrons have a relatively low energy they are only emitted from the bulk specimen from a depth of less than 3nm.

X-rays

Source: Caused by the de-energisation of the specimen atom after a secondary electron is produced. Since a lower electron, usually from the K-shell was emitted from the atom during the secondary electron process an inner (lower energy) shell now has a vacancy. A higher energy electron can fall into the lower energy shell, filling the vacancy. As the electron falls it emits energy, usually X-rays to balance the total energy of the atom so it.

Utilization: X-rays or Light emitted from the atom will have a characteristic energy which is unique to the element from which it originated. These signals are collected and sorted according to energy to yield micrometer diameter of bulk specimens limiting the point-to-point comparisons available.

Table 3.2: Main analytical possibilities of a scanning electron microscope

Physical phenomenon	**Measured signal**	**Type of image detector**	**Resolution**	**Voltage of acceleration for the analysis**	**Data**
Atomic ionisation	Secondary emission	Multiplier of electrons	5-10 nm	Any voltages: 100-50 x 10^3 V	Topography
	Characteristic losses of energy	Analyser of electrons	1-5 µm	Low voltage lower than 500 V	Densities of states
	Phenomena of threshold			Variables continuously from 100 V to some kilovolts	Distances between close neighbours
Atomic relaxation	Emission of electrons Auger	Analyser of electrons	50 nm	Variables between some kilovolts and 20-30 kV	Elementary analysis
	Emission of X-rays Cathodeluminescence UV and visible	Detector of photons and monochromatic	1 µm		
Diffraction and electronic canalisation	Electrons	Screen of diffraction	20 x 0,5 µm² (low-angled incidence)	Between some kilovolts and 50 kV	Crystallography, internal constraints defects
		Multiplier and analyser of electrons	< 10 µm (diagrams of Kikuchi)		
Load and unload of the insulators	Potential	Multiplier of electrons	Determined by the diameter of the sensor on the working voltage		Spatial distribution of the defects and relative primitive
	C_p variation Energy exchanges in the course of dielectric relaxation	Calorimeter in which is placed the insulator	100 nm-10 µm	Variable between 100 V and 30 kV	Energy of polarization and conditions of relaxation while break of links

SEM presents several advantages over optical microscopy that are not only related to the higher resolution but to the information that can be obtained with this technique, listed in table 3.1.

A scanning electron microscope presents several advantages over an optical microscope. SEM is cable of magnifications of 150000 in photo format, equivalent to 600000 on a screen and crosscheck with the optical microscope, rendering it very useful for microstructure evaluation.

A very important depth of focus: approximately hundred times that of the optical microscope from the same magnification, which is used to produce images on 3D samples not planes. This feature is very useful for fractography, where rugged surfaces are studied.

The possibility to carry on the spot measurements of concentration by means of X-ray electron diffraction described above is a further advantage of SEM. TEM can also produce these data, but specimen preparation is very complex. Measurement of composition by means of X-ray diffraction is well suited to detect the presence of heavy elements. Light elements, and in particular oxygen and nitrogen cannot be quantified by means of X-ray diffraction and other methods have been used in this work. SEM can also be used to study alloy textures, these feature has not been used in this work.

4. Manufacture of Cr-Re alloys

4.1 Introduction

For the manufacture of Cr-Re alloys two basic technologies have been considered: melting and casting and powder metallurgy. Each of them presents advantages and inconveniences when considering the production of Cr-Re alloys. In this work both techniques have been used to produce samples at different stages of the work, depending on the required degree of alloy refinement. Table 4.1 represents the available manufacturing methods for high temperature alloys with some of their most important advantages and inconveniences.

Melting in cold or hot crucibles is widely used to produce alloys in industry. The high melting point of the refractory metals object of this study may limit the applicability of this manufacturing technique, since alloy-crucible reactions and strong vaporization of Cr may take place.

Powder metallurgy is usually employed for the production of near net shape components, eliminating the need for machining processes after manufacture. Powder metallurgy consists in the mixing of powders in pre-alloyed form or in elementary form and their densification by solid-state diffusion. Some powder metallurgical variants also employ liquid phase diffusion. The main inconvenient related to PM is the risk of powder oxidation due its high specific surface; this is specially marked in refractory metals [Povarova, 1997, 2].

Chemical vapour deposition, a method used to produce massive Re alloys in the US is an onerous process used for very specific applications [Tuffias 1991, 1999]. An example of an industrial application of CVD to produce structural materials is the Re-Ir combustion chambers of Ultramet described in chapter 1. EADS is not equipped for this technology, and in general there are no installations in Europe, so it was not considered for this thesis.

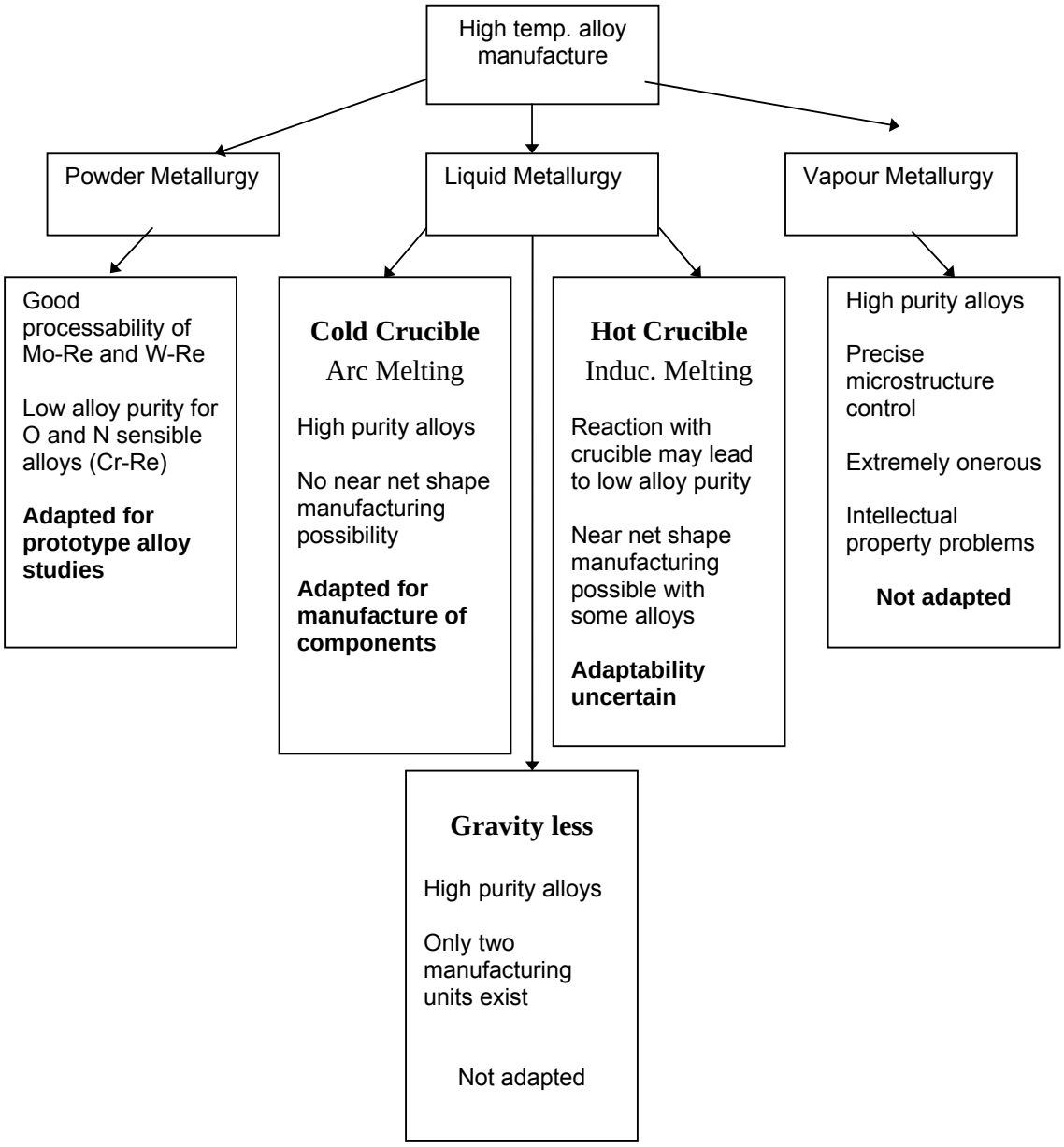

Table 4.1: Manufacturing methods considered for Cr-Re alloys and their advantages and inconveniences.

4.2 Potential manufacturing process for Cr-Re alloys

Powder Metallurgy

Refractory alloys with a high Re content, like Mo-Re and W-Re alloys, are produced at an industrial scale by powder metallurgical methods since the 1960's. However neither W nor Mo presents the reactivity of Cr to oxygen or its high vapour pressure; the protective Cr_2O_3 layer built on the surface of Cr powders when exposed to

oxygen can potentially contaminate the sintered bulk material and difficult diffusion and the high vapour pressure may render vacuum sintering or melting impossible.

The production of high purity pre-alloys Cr-Re powders is also troublesome as it is practically impossible to avoid contact with oxygen during the whole life cycle of the powder. High purity massive Cr can be produced through sintering in a reducing atmosphere containing partial pressure of hydrogen, however EADS is not equipped for this technology and the hydrogen compatibility problems of some potential alloying elements renders the production of many Cr-based alloys by this method uncertain.

Melting and Casting

Melting and casting processing which has important advantages in terms of purity, presents the technical problems due to the high melting point of the both Cr and Re and the potential high temperature reactions between the melt and the crucible. Hot crucible induction melt methods were investigated in the 1970's for Cr-Re alloys, with the conclusion that reaction with ceramic crucibles was inevitable, as liquid chromium is capable of reducing both zirconia and yttria, leading to contamination of the alloys with light elements from the crucible material [Trefilov, 1975].

Crucible compatibility with refractory metals was investigated in the 1970's and 1980's in the former Soviet Union, basically in the Institute of Materials Sciences of Kiev, with contradictory results. Trefilov affirms that compatibility of Cr-Re alloys with monocristalline Y_2O_3 crucibles was good enough to produce high purity alloys [Trefilov, 1975] while other teams of the same institution considered that only gravity less melting with no contact with the crucible could be used to produce high purity alloys. A melting process was designed in the Soviet Union in the 1980's and consisted in the crucible-less melting of the alloys. This was achieved under the combination of electric arc and induction currents that permitted the liquid metal sample to levitate. Research in this field was stopped in 1986 with the reduction of research activities in the Soviet Union [Milman, 1995]. An industrial scale installation still exists in the Institute for Problems in Material Sciences in Kiev.

The level of electromagnetic stir necessary to overcome the density difference between Cr and Re, 7.19 g/cm³ for Cr and 20.9 g/cm³ for Re is not obtainable through the induction currents usually present in a hot crucible furnace, as discussed by Trefilov (1975). The same author affirms that necessary level of agitation may be obtained by combined induction and arc melting techniques, but this kind of installations are not available in Western Europe. Additionally the difference of 1300°C between the melting points of the base materials, Cr melts at 1880 °C while Re melts at 3180 °C, coupled to the high vapour pressure of Cr , may induce strong evaporation of Cr during melting.

Arc-melting techniques in a cold crucible have been used since the 60's to produce high purity Cr-Re alloys. This method involves several re-melting processes to improve homogeneity of the alloy and is capable of producing very high quality alloys. Unfortunately arc melt techniques with refractory metals are only possible for batch laboratory scale alloy manufacturing, and are usually restrained to small dimensions (figure 4.1).

Figure 4.1 : Representation of an arc melt furnace and arc melting of an alloy in a cooled crucible

Manufacturing Strategy

As there are no Cr-Re alloys commercially available, it has been necessary to design a manufacturing process from scratch and upscale it to a small industrial level. Given the relatively small dimensions of the final product represented in figure 4.2 and the relatively low production volumes that the application requires, a relative wide range of manufacturing methods may be used.

Due to the lack of information on the properties of Cr-Re alloys, a screening of various compositions has been necessary to determine the adequate composition range for the application and therefore for the refining of the alloy.

The strategy that was chosen to determine the optimum alloy composition and manufacturing process has been to make a first screening of the alloys with the most flexible and economic process possible and to produce refined higher purity alloys by means of more onerous manufacturing processes only after a group of alloys has been identified and the effect of Re on the alloy properties been proved to some extent.

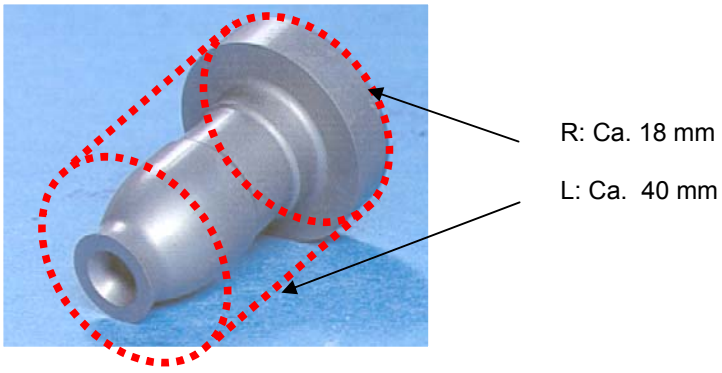

Figure 4.2: Combustion chamber of a positioning satellite thruster and minimum dimensions of the metal part from which to machine it.

Powder Metallurgy was selected for alloy screening and for the initial characterization of the effect of Re additions on the mechanical properties of Cr-Re alloys since this manufacturing process offers a high degree of flexibility. Powder Metallurgical

prototype alloys have been used to detect any increase in ductility induced by Re and to make a basic study on the influence of Re on other properties of the material. As discussed in the previous section, the difficulties in obtaining high purity Cr-based alloys through powder metallurgy mean that properties of these alloys will not be optimum, but the effect of Re may potentially be strong enough to select a composition range for detailed study.

4.3 Manufacture of prototype Cr-Re alloys by PM

A PM process was designed to produce samples to be tested under compression to ASTM E9-81 standard for a basic determination of the influence of Re on the mechanical properties of the alloys. The results on the testing of the samples are discussed in chapter 5. The process was designed with flexibility in mind and had the goal of obtaining a final sample with a relative density of over 98% without the need of densification in capsule. This was made to speed up as much as possible corrections to sample composition and manufacturing process. The process that has been designed may be summarised in the steps below and is based on the recommendations of [Laptev, 1994, 2001] for Cr alloys and [Povarova, 1997, 1,2] for BCC alloys containing Re and of [German, 1996] for general powder metallurgical processing.

- High energy milling of the Cr-Re powders to provide a homogeneous mixture.
- Characterisation of powders to determined the level of contamination.
- Uniaxial cold compaction to manufacture a green body with a density over 60%
- Low pressure sintering to over 92 % density to produce a green with closed porosity.
- Hot Isostatic Pressing to final density

The composition of the samples was selected to have representative points of the solid solution of Cr and Re: pure Cr, Cr-2at%Re, Cr-at%5Re, Cr-10at-Re, Cr-15at-Re and Cr-30at%Re (atomic percentages).

Process description

The first part of the process is the high energy milling of the Cr and Re powders and their characterisation. The goal is to produce a well-mixed powder mixture of the elements (almost at atomic level) and to create a very fine grained structure in the powders to aid the inter diffusion of Cr and Re while sintering. This part of the process is critical as it grossly determines the purity of the raw materials to be used for the manufacture of the samples. There exists little literature describing the ideal milling parameters for refractory alloys. Thus, for example [Povarova, 1997, 1,2] suggests the use of very high-energy milling and long milling times but does not give exact data on how to process the alloys.

A minimum particle size distribution under 40 µm was selected based on general powder metallurgy know-how, smaller particle size would have rendered the handling of powders very complex [German, 1996]. Milling parameters were empirically determined to obtain this minimum average particle size. Laser diffraction of the powder on a water suspension coupled to data decoding software was used to obtain the particle size distribution shown in figure 4.2b.

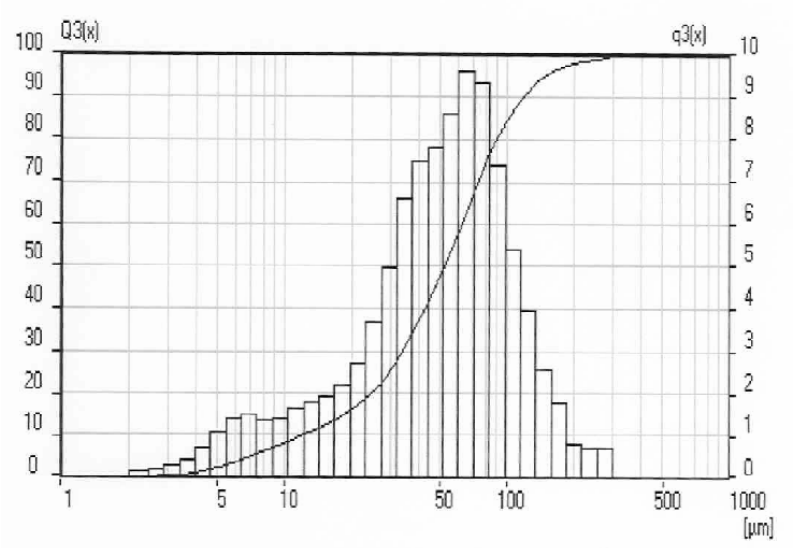

Figure 4.2b: Typical particle size distribution of a Cr-Re powder mix used for the production of prototype samples The figure represents a Cr-10Re mixture.

As particle size distribution alone is insufficient to guarantee the quality of the powders, morphological and chemical analyses were carried out to fully characterise the powders. Scanning Electron Microscopy was used for the morphological analysis and gas extraction chemical analysis was used to determine the content of oxygen and nitrogen of the powders. Element distribution on the powders was carried out by photoluminescence spectroscopy and it is shown in figure 4.3. X-ray diffraction was used for the study of the crystal structure of the alloys obtained. Figure 4.4 shows that the peaks of Cr and of Re are clearly distinguishable so that no alloy has been formed during milling.

Table 4.2: Process approach for the manufacture of the prototype alloys tested in chapter 5

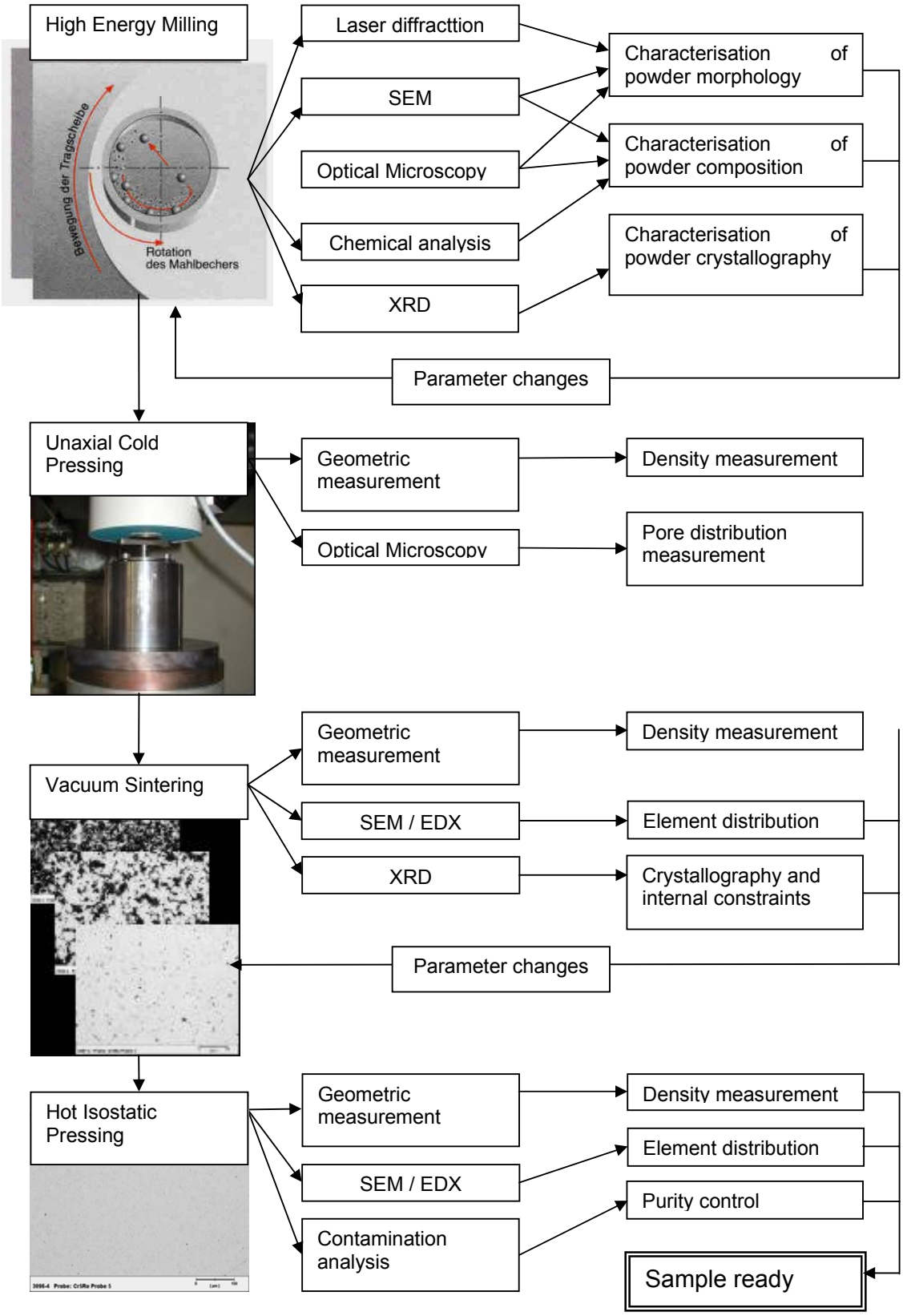

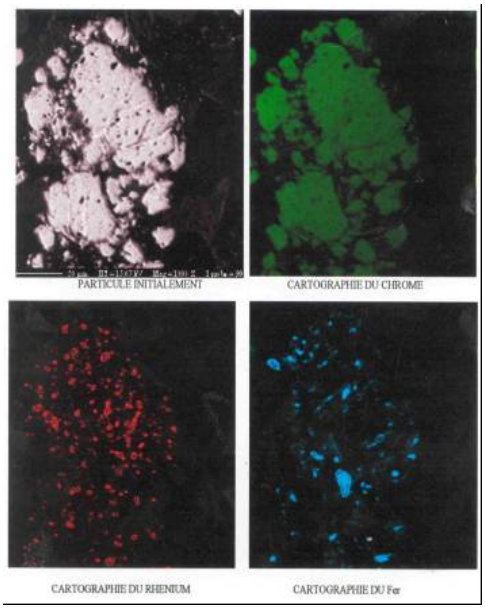

Figure 4.3: Photospectroscopy image of a particle of Cr-10Re powder after high energy milling. Re is on the particle surface (red) and iron (blue) is an impurity from milling.

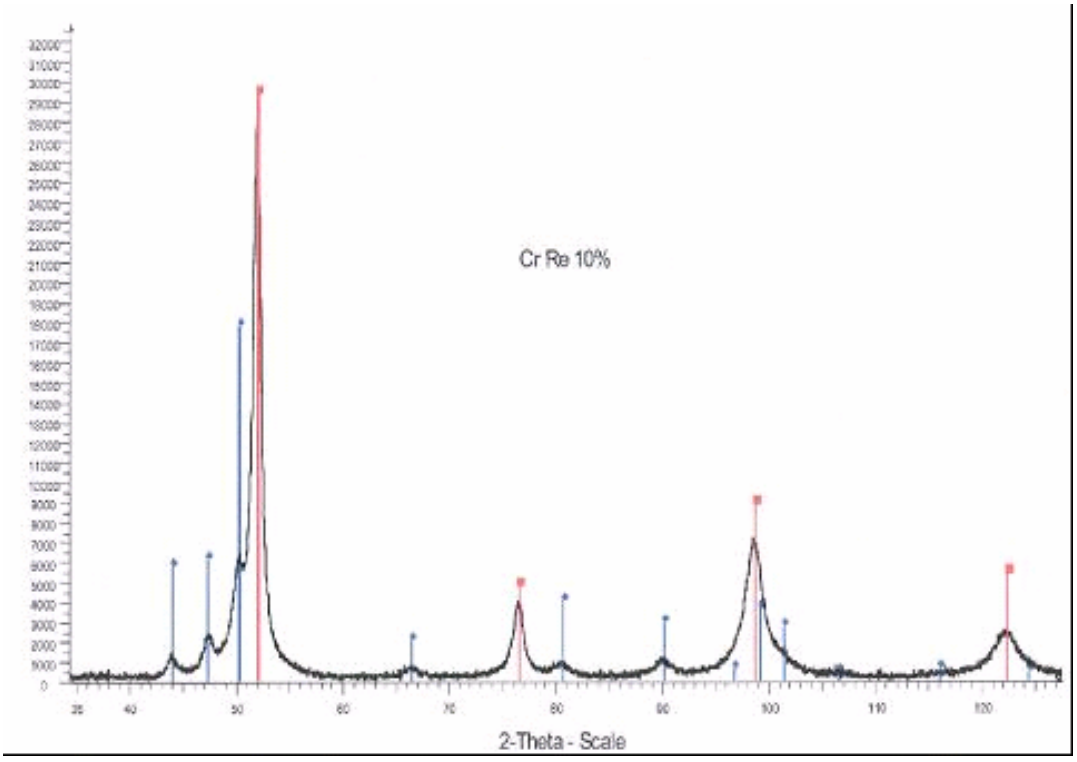

Figure 4.4: XRD spectrum of a Cr-10Re powder after high energy milling. Lattice distortion is as much as 15 % (compression). The peaks of Cr (red) and Re (blue) are clearly distinguishable, showing that no alloy has been formed.

Cold, single-axe pressing (figure 4.5) was used to obtain a sinter green of the powders. 5 g Cr-18Re and 7,5 g pure Cr greens were produced. A purpose built twin-matrix press, seen in figure 4.5a, was used to manufacture the greens.

The pressure-density relationship for different alloys is shown in figure 4.5a. Press parameters were determined according to the data of Laptev, 2001 for Cr-Fe alloys. For Cr-Re alloys, dimensions of the specimens compared satisfactorily with the determination of the density by means of optical microscopy and an image decoding software as represented in figure 4.5b.

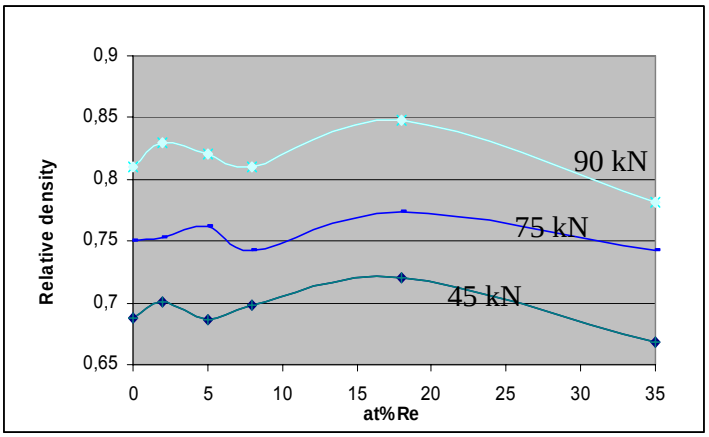

Figure 4.5a: Relative density of different Cr-Re alloys after compaction at 45 75 and 90 kN.

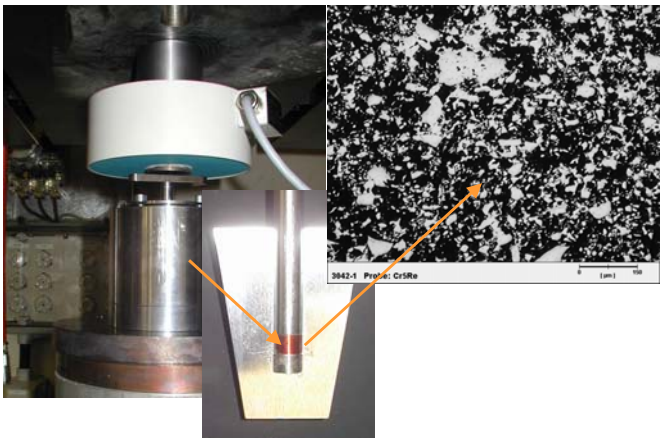

Figure 4.5b: Cold pressing to produce a sinter green with density ranging from 60 % to 70 % depending on compacting pressure

After extraction from the press, greens were sintered in a vacuum furnace at 10^{-5} Bar. Sintering temperature was set at 0.6-0.75 T_m (1300-1600 °C), sintering time was

empirically determined to provide a sample with completely closed porosity able to be fully sintered by hot isostatic pressure without encapsulation. Closed porosity was calculated by the Archimedes law or by optical and scanning electron microscopy. Figure 4.6 shows the typical behaviour of a Cr-35Re alloy at different stages of the process. Hot Isostatic Pressure at 0.85 T_m at 2000 bar during 3h was used to achieve near 100 % density, (figure 4.7).

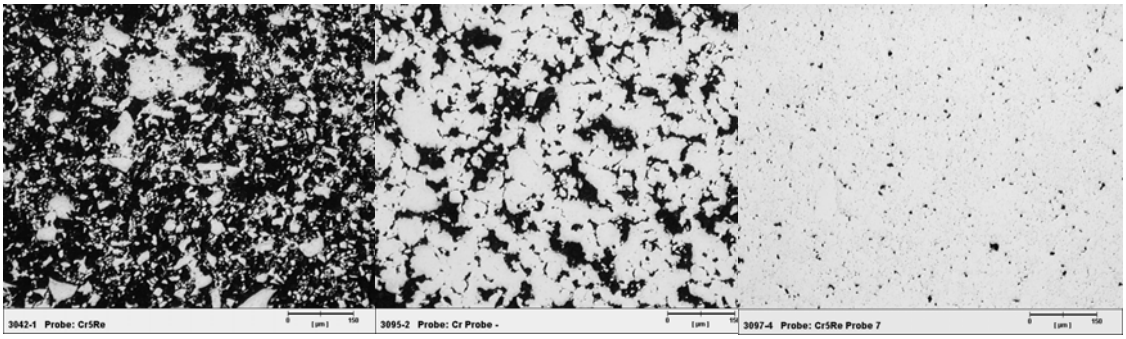

Initial porosity (55 %) 1 hour at 1250 °C (62%) 3 hours at 1250 °C (95%)

Figure 4.6: Evolution of the porosity during sintering in a Cr 35Re alloy. From left to right, after single axe pressing, after 1h sintering at 1250°C and after 3h at 1250°C.

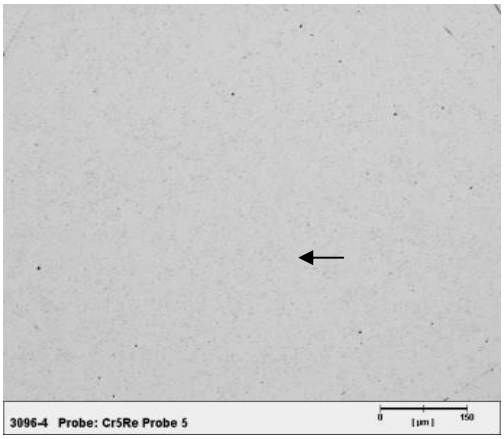

Figure 4.7: Near 100 % dense Cr 35Re sample after HIP at 1700 °C and 2000Bar during 3 hours. Arrows indicate micro porosity

Representative samples from each batch were characterised by optical and electron microscopy to determine their grain size, residual porosity and impurities. Figures 4.7a-c show the XRD spectra of Cr, Cr-18Re and Cr-35Re final samples. Spectra are typical of a BCC refractory metal containing no second phases. Peak displacement corresponds to lattice distortion due to cumulated stress and presence of impurities in Cr and the distortion caused by Re in the central lattice position in Cr-Re alloys. A more detailed investigation of lattice distortion is carried out in section 4.4.1.

Figures 4.8 to 4.11 represent some of the problems faced during the development of the powder metallurgical process development, basically related to impurities related to the milling process itself and to oxidation during high temperature processing. Problems were solved by changing the milling parameters, basically reducing the milling speed and using hardened stainless steel milling balls and by increasing the evacuation time of the furnace.

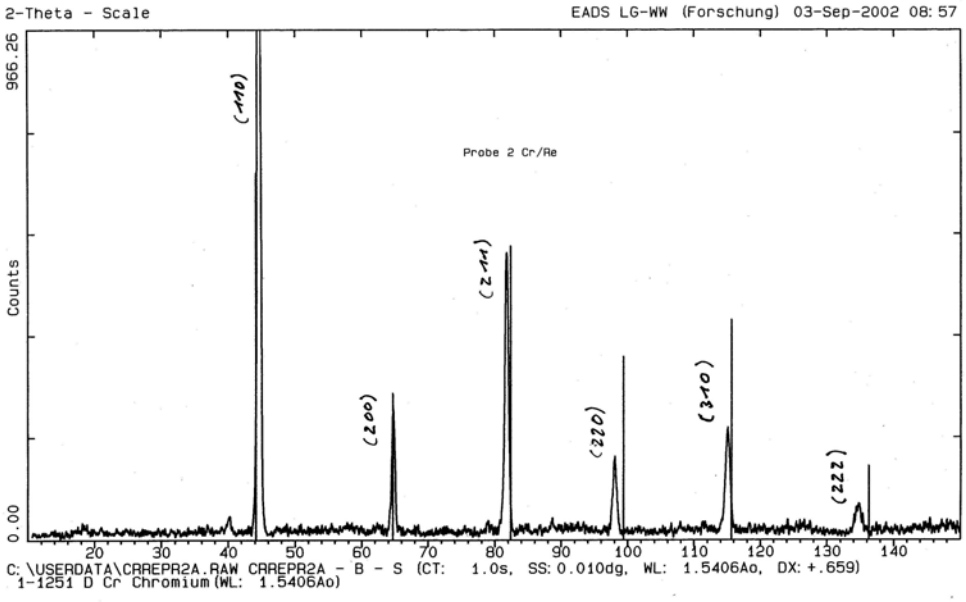

Figure 4.7a: XRD spectrum of pure Cr produced by means of Powder Metallurgy.

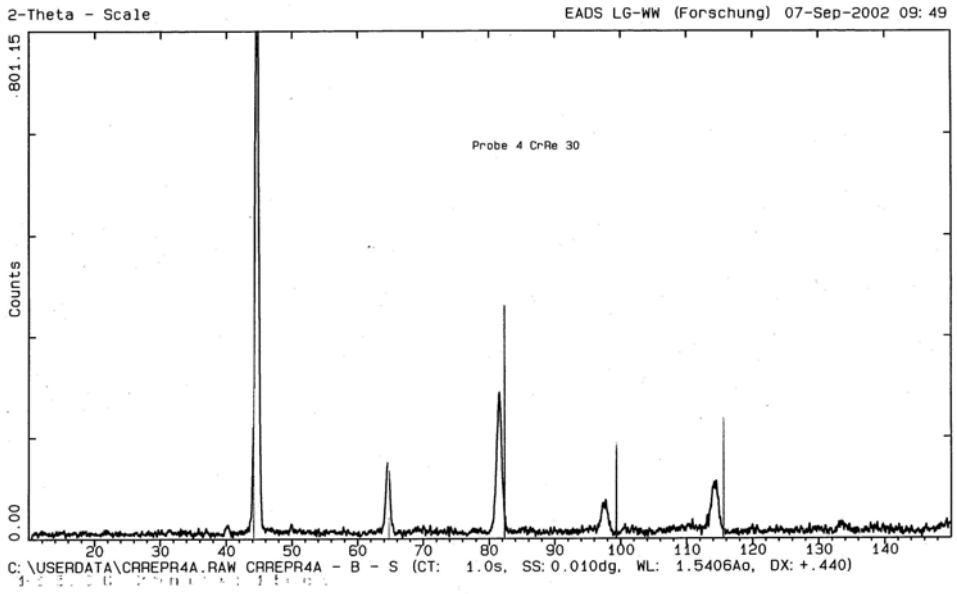

Figure 4.7b: XRD spectrum of Cr-18Re produced by means of Powder Metallurgy. Lattice distortion is due to the presence of Re is central position in the BCC matrix.

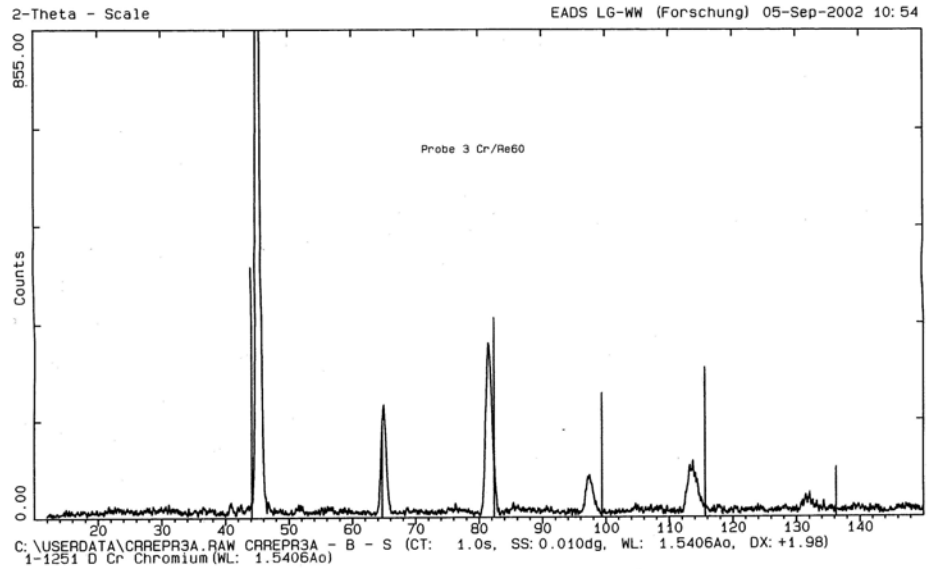

Figure 4.7b: XRD spectrum of Cr-35Re produced by means of Powder Metallurgy. Lattice distortion is due to the presence of Re is central position in the BCC matrix.

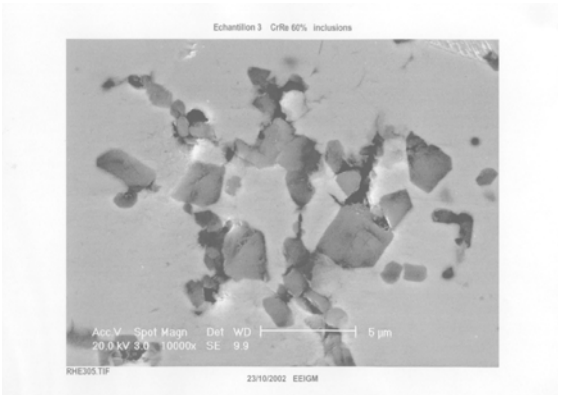

Figure 4.8: Oxides in a Cr-30Re alloy.

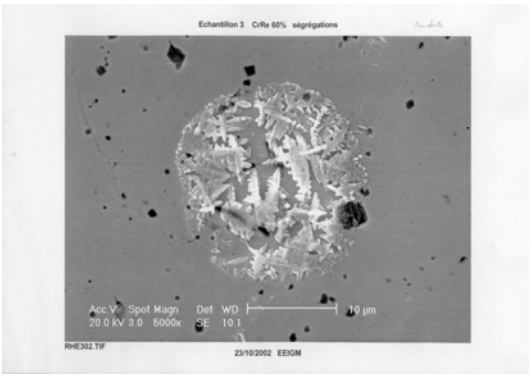

Figure 4.9: Local melting evidenced by the presence of dendrites due to Fe impurities (determined by EDX).

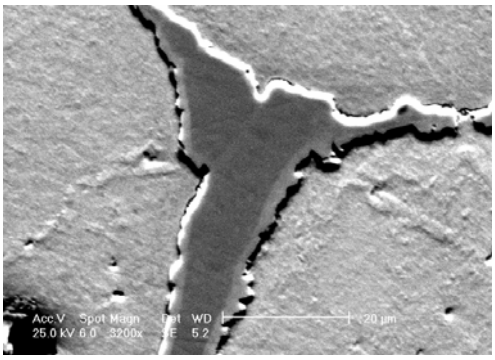

Figure 4.10: Precipitation of impurities at grain boundaries in Cr-18Re after 3h HIP at 1700 °C.

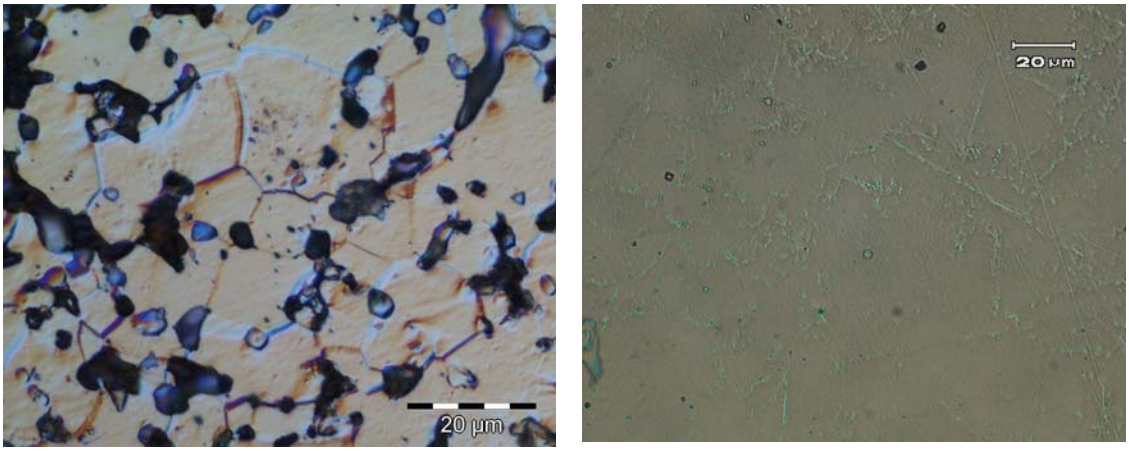

Figure 4.11: Process optimisation: Microstructure of the first sample produced and of the samples manufactured with high purity powders and reactive sintering.

After manufacture, samples were machined by electric arc discharge for the further phases of the study.

4.4 Melting and casting manufacture of Cr-Re alloys

The study of the mechanical properties of PM Cr-Re alloys discussed in chapter 5 concluded that Re additions improved substantially the behaviour of the alloy. For the subsequent phases of the work, high purity alloys were produced by means of melting and casting metallurgy. Since liquid metallurgy is less flexible than powder metallurgy, it was decided to focus the production in the following alloys:

- Pure Cr: for reference purposes.
- Cr18Re: due its low density of the alloy and singular properties observed.
- Cr35Re: due to the high level of mechanical properties observed.

The advantages and inconveniences of hot and cold crucible ingot metallurgical processing have been exposed in section 4.1. The low alloy volume demanded by the application makes it possible to carry out the manufacturing means of both arc-melt metallurgy and hot crucible casting. Cold crucible arc melting avoids reaction of the melt with the crucible and this method also has a greater flexibility than hot crucible melting since very small quantities of material can be produced. Since EADS is not equipped with arc melt furnaces, the melting and casting was carried out in the

Institute for Problems of Material Science, IPMS, of the Ukrainian Academy of Sciences. Part of this PhD thesis was carried out in the facilities of this institute.

Arc melting of Cr-Re alloys

For the melting of the high purity Cr-Re prototype samples a triple mould water-cooled copper crucible was used. Non consumable tungsten electrodes were employed for the arc generation. Pellets of 99.99% pure Cr and 99.99 percent Re produced by Heraeus were used to the manufacture of all samples. Melting took place in low pressure, high purity Argon atmosphere of 200 mBar in three phases:

- Cr pellets weighting 17.5 g were molten in the presence of 17.5 g of Re, Cr dissolved well the Re, making an alloy with a melting temperature of approximately 2500 °C.
- The rest of the Cr was added and the mixture re- melted to achieve the target composition.
- Sample was let to cool down and re-melted 5 times.
- Finally the arc intensity was lowered and the sample was heated on each side to approximately 1800°C in spiral from the inside to the outside to improve alloy homogeneity and eliminate surface porosity.

The observations made on the prototype samples concluded that the alloy is already formed after the first two melting processes. The remaining three melting series were carried out at decreasing intensities to eliminate porosity and increase the alloy homogeneity. After the last melting series the samples were allowed to cool down in the copper crucible to room temperature. Cooling velocity of this phase was approximately 20 °C per second. This process was recommended by the Institute of Problems in Materials Science of Kiev for the manufacturing of the prototype samples.

One of the problems faced during the manufacture of Cr-Re alloys was the vaporization of Cr. To keep it down to acceptable levels, a minimum level of Ar pressure was applied. according to Trefilov (1975).

Considering that Cr and Re start to react at a temperature considerably lower than the melting point of Re, the minimum vapour pressure to avoid Cr boiling has been estimated to be 150 Torr. In order to increase the purity of the atmosphere, 50 g of Cr pellets were molten in a separate crucible before the processing of the main alloy. The liquid Cr produced when melting of these pellets, called getters, reacts with the residual light elements present in the atmosphere forming inert Cr oxides.

Microstructural characterization of the arc molten samples

Arc-melt Cr, Cr-18Re and Cr-35Re alloys were characterized by means of optical microscopy, scanning electron microscopy and transmission electron microscopy. In parallel hot gas extraction chemical analysis and hardness were carried out on some samples.

The high vapour pressure of Cr is responsible for the presence of micro pores in the external layer of the alloy, seen in figure 4.13, as Cr boils in the sample surface. Cr-18Re alloys have significantly less porosity than pure C;, this is related to a decrease in the vapour pressure of the alloy that reduces its tendency to boil during processing and forming less pores in the ingot. Figure 4.15 shows that Cr-35Re alloys prepared with multiple melting passes present very little porosity, meaning that the vapour pressure of the alloys is quite low.

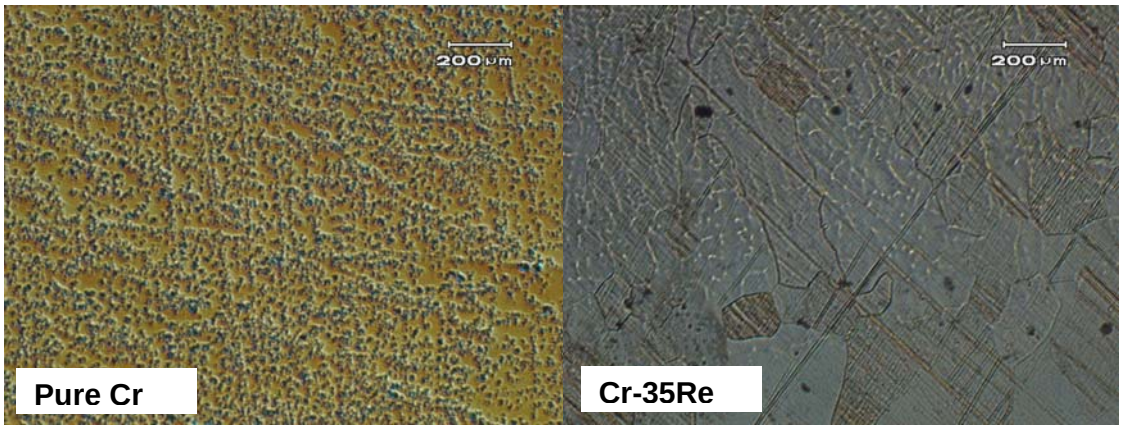

Figure 4.13 and 4.14: Porosity due to Cr evaporation in arc molten Cr and Cr-35Re samples.

All alloys present relatively large elongated grains. This feature is characteristic of the directional heat flow and temperature gradients during solidification and cooling of the sample in cold crucible melting. A slightly higher tendency to equiaxiality is evident on the pure Cr samples; this is due to the fact that the recrystallisation temperature of pure Cr is lower than that of Cr-Re alloys allowing more time for grain growth. Optical microscopy revealed a dendritic structure formed during solidification on Cr-18Re and Cr-35Re alloys. Dendritic solidification is characteristic of high cooling velocity processes such as arc melting. The relative large difference between the solidus and the liquidus of Cr-18Re alloys is responsible for the strong tendency of this alloy to micro microsegregation, evidenced by backscattering scanning electron microscopy in as shown in figure 4.17. Cr-35Re samples, with a much smaller solidification range, are characterized by a dendritic surface layer up to a depth of 200 µm this is due to the high cooling velocity in this area. Figure 4.15 shows the evolution of the dendritic structure to a columnar microstructure and finally to an equiaxed microstructure structure in the interior of the sample where the cooling velocity is lower than on the surface of the sample.

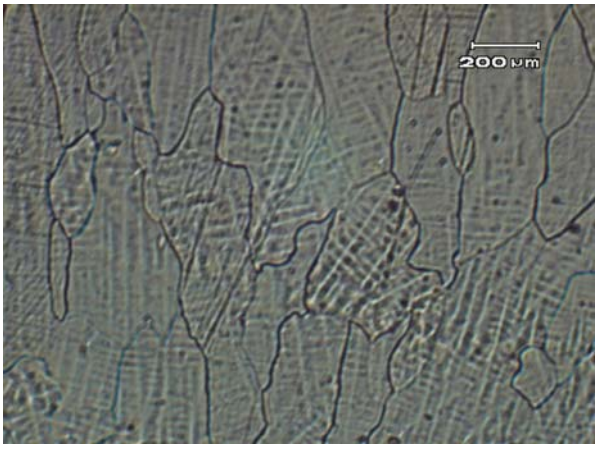

Figure 4.15: Microstructure of a Cr 18Re sample (outer layer). Note the dendritic structure and the relatively large grain size. Grain boundaries are free of second phases or impurities.

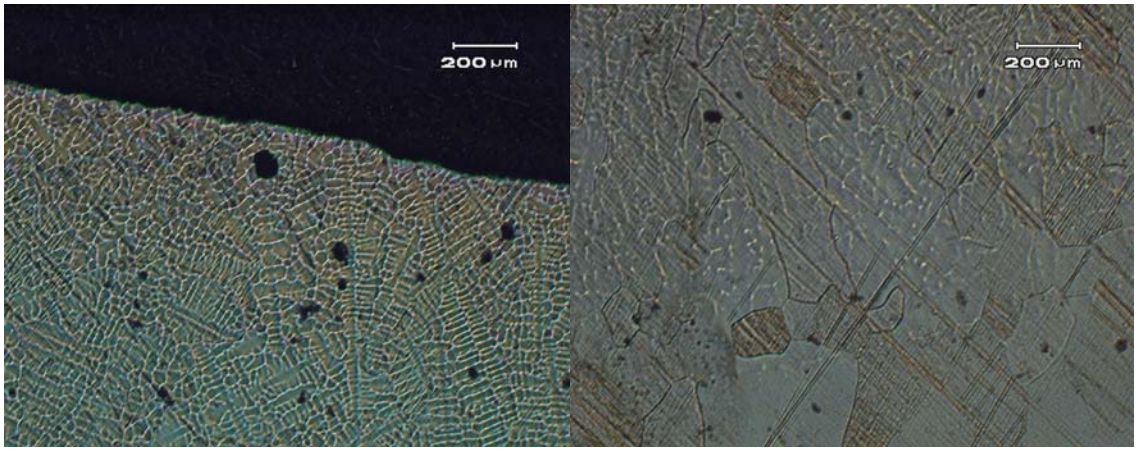

Figure 4.16: Surface microstructure of a Cr-35Re alloy produced by arc melting. Note the evolution of the dendritic microstructure at the surface (left) to an equiaxed microstructure in the interior part of the sample (right) and the presence of some porosity

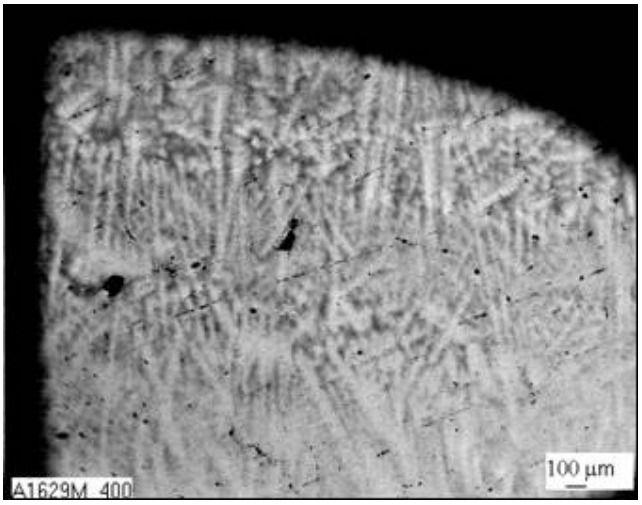

Figure 4.17: Dendritic structure of a Cr-18Re sample produced by arc melting observed by SEM

Homogenisation of the alloys

Properties of Cr-Re alloys depend greatly on the homogeneity of the solid solution. The dendritic microstructure of the alloys must therefore be eliminated through a homogenisation treatment in order to optimise the properties of the alloys. Homogenisation treatment suggested by [Povarova, 1997, 2] consists in a maintenance of two hours 200 °C below the melting point of the alloy. This would mean a treatment temperature in Cr-35Re of about 2100 °C.

Technical limitations related to the elevated temperature required carrying out the homogenisation treated proposed by Povarova and the risk of strong grain growth motivated the evaluation of other homogenisation treatments. [Trefilov, 1975] suggest a homogenisation treatment for W-Re and Mo-Re just below the recrystallisation temperature, considered to be around 0,8 T_m. Assuming that Cr-Re alloys present the same behaviour, the limit for the high temperature homogenisation treatment of Cr-35Re is around 1700 °C. Still technical difficulties rendered this method difficult and it was decided to examine the possibility of improving the alloy homogeneity without the requirement of high temperature maintenances. This was carried out by means of the inoculation of the melt with ceramic particles capable of nucleating solidification process, hence improving the alloy homogeneity in as cast condition.

Active metal additions in Arc-Melt Cr-Re alloys

Inoculation processes are based on the creation of nucleation sites for solidification in the melt by the addition of particles of high melting point materials. This reduces the under cooling which is necessary to start the solidification process and an increased density of solidification nuclei resulting in a refined grain size.

In industrial production and in particular for steel, nickel and titanium and alloys, ceramic particles, such as TiN as ZrO are used as inoculators. An inoculation process would be of much interest to refine the dendritic microstructure of Cr-Re alloys. Unfortunately, the ceramic particles most commonly used in inoculation processes are reactive with liquid refractory metals. An interesting variant to the inoculation process of refractory metals is reported by [Trefilov, 1975] who designed a process to purify commercial Cr from oxygen and nitrogen. His goal was to fabricate ductile Cr by eliminating interstitial impurities impending dislocation slip. The process was based on the addition of metals with a high oxygen affinity to molten Cr. These highly reactive metals should be inert in Cr and be capable of reacting with the dissolved light elements in the melt to produce extremely fine and stable ceramic particles. It was found that only Pr was capable of absorbing light elements in liquid refractory melt without interacting with the liquid metal. Excess of Pr not reacting with the light elements in the melt floats to the surface and may be removed from the

ingot. A secondary effect reported by Trefilov of Pr is that the very fine ceramic particles formed in the melt acted as nucleation sites, effectively reducing the grain size of the metal. Therefore, the inoculation method developed by the team of Trefilov, presented a double effect on the alloys: the increase on the metal purity and the active generation of solidification nuclei.

Besides Pr, other elements could have a similar effect on the alloy microstructure without its inherent cost and handling complexity. It is the case of Sc and Ce. It is nevertheless unclear whether these active elements would have the same purifying and refining effect on Cr-Re alloys as on pure Cr and whether excess active elements would float to the surface of the molten alloy.

Manufacturing Cr-Re alloys with active elements

In order to study the influence of active metals on the microstructure of Cr-Re alloys, Cr-18Re and Cr-35Re alloys containing Pr, Ce and Sc were prepared using arc melting techniques. The process described in section 5.4.1 was altered to permit the introduction of active metal in the samples. Master alloys containing 95 wt% of Cr and 0.8-1 wt% of one of the active elements were prepared and then added to the rest of the Cr and Re to have a final concentration of active element of approximately 0,5 wt%. This method, inspired from Trefilov, permits to increase the homogeneity of the concentration of the active element in the alloy. After manufacturing, the influence of additions of 0,5 wt% of Sc, Pr and Ce on the microstructure of Cr-Re alloys was investigated by means of back-scattering SEM.

Influence of doping elements on the microstructure of Cr-Re alloys

The effect of Ce and Sc on the microstructure of all alloys is very strong. Cr-18Re, that has a large solidification interval and that shows a very strong tendency to dendritization can be homogeneously solidified without any trace of dendritic microstructure.

Figure 4.19 shows the influence of Ce, and Sc on the dendritic structure of Cr-18Re alloys. Addition of any of the active elements has a strong influence in the contrast

obtained by BSSEM representing the segregation. A probable further effect of Ce and Sc is the reduction of melt surface tension, which could explain in part the different solidification behaviour observed during manufacturing. Another effect represented in figure 4.18 is the decrease of grain size related to the increased density of solidification nuclei. The effect of Sc on the alloys microstructure differs to that of Pr and Ce. Sc completely eliminates the dendritic structure of the alloys and forms a microscopic ScO dispersion that is visible by means of SEM.

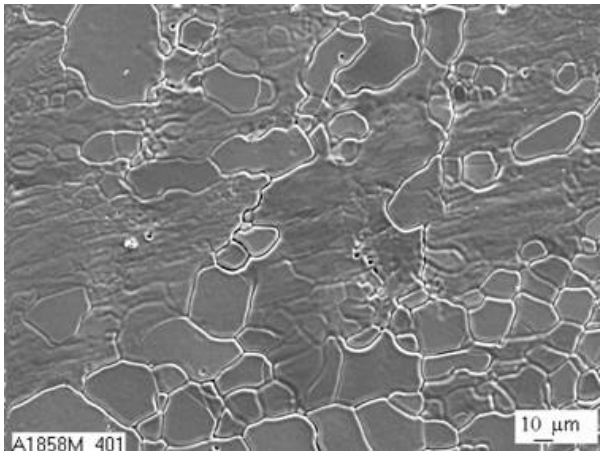

Figure 4.19: SEM image of the microstructure of a Arc-Melt Cr-35Re-0,5Ce alloy

Active metal additions in Cr-35Re alloys create a fine sub-grain structure. Non-doped Cr-35Re alloys did not present the strong dendritic solidification behaviour of Cr-18Re alloys so the effect of doping is less visible than in Cr-18Re. The fine sub-grain structure of Sc-doped Cr-35Re alloys is shown in figure 4.19

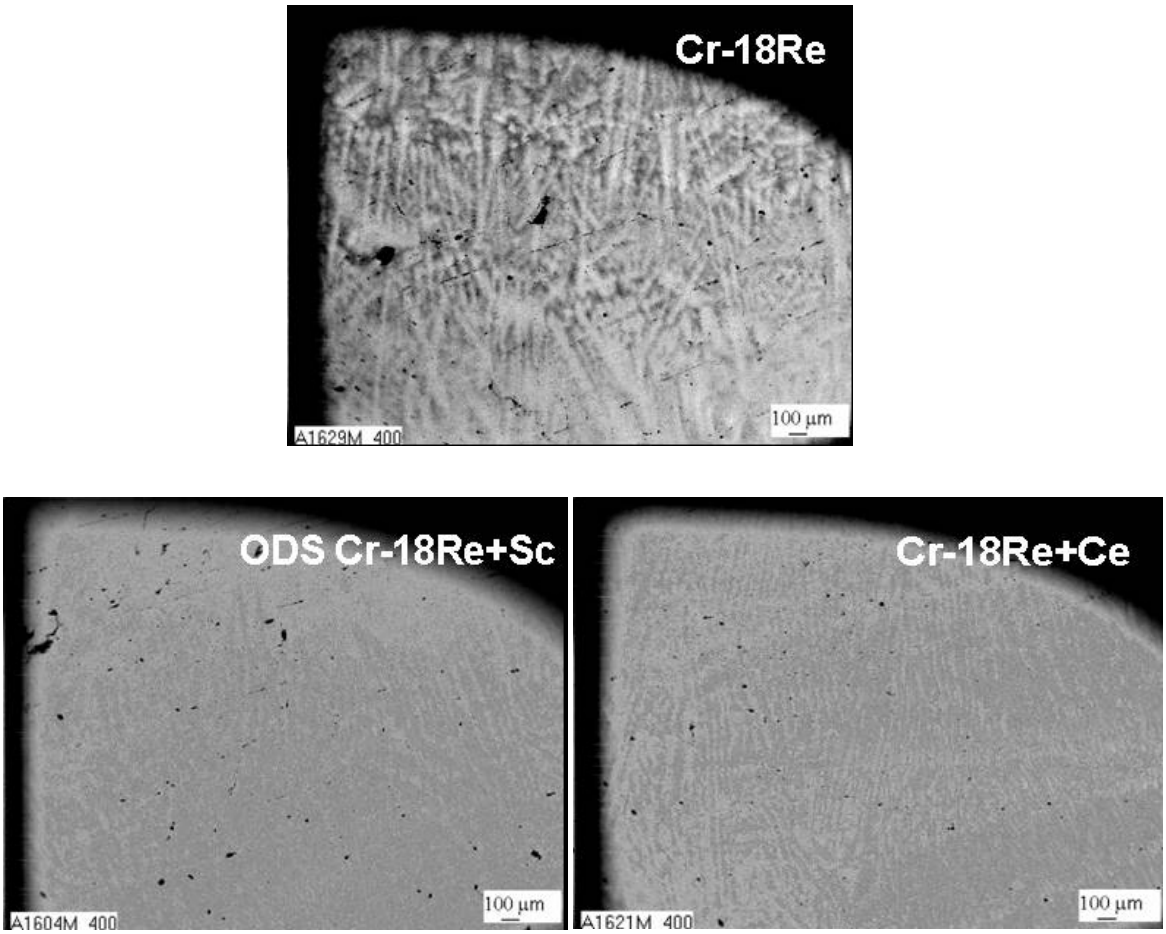

Figure 4.19: Effect of active element additions of the microstructure of Cr-18Re

Phase composition and crystal structure of arc-melt Cr-Re alloys

After homogenisation during 3 hours at 1700 °C alloys were characterized by means of XRD to determine their crystallography and phase content.

The XRD spectra show that Cr-18Re and Cr-35 Re alloys are constituted of a single solid solution BCC phase. No second phases could be detected by means of XRD in the alloy, taking into account its limitation of 3 vol% sensitivity. Optical and scanning electron microscopy could not reveal any second phases either.

Figure 4.20 represents the XRD spectrum of arc-melt Cr, Cr-18Re and Cr-35Re. The peak displacement to the left with increasing concentrations of Re is created by

distortion in the lattice caused by the large Re atoms, this phenomenon has already been observed in powder metallurgical alloys. Peak displacement has been used to calculate the lattice parameters of the alloys and compare it to the theoretically calculated lattice parameter. This was used to make a qualitative estimation of the alloy homogeneity.

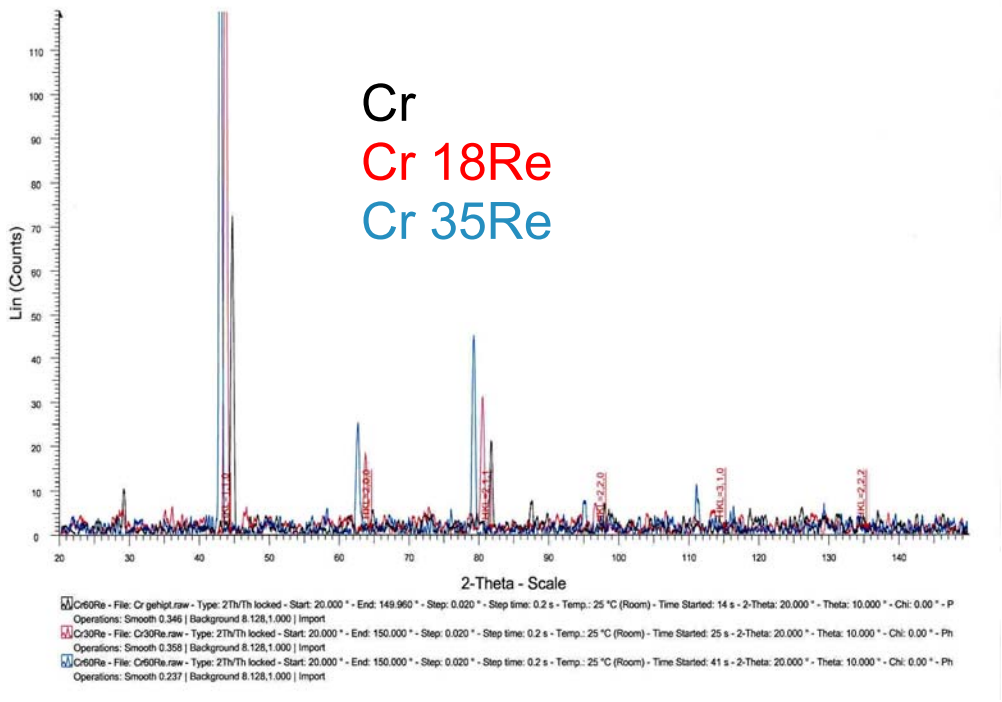

Figure 4.20: XRD spectra of a Cr, Cr -18R and Cr-35Re alloys

It can be calculated mathematically that a decreasing sin (θ) at constant λ represents an increase in the plane distance, d.

$$2d \cdot \sin(\theta) = n \cdot \lambda \qquad n \in N^{+}$$

Figure 4.21 shows that in BCC lattices which are characteristic of Cr-35Re alloys, the large Re atoms in the central positions create a uniform distortion in the lattice. The difference between the experimental values and the theoretical values in the distance of known planes allows calculating the homogeneity of the alloy. Phases with a volume percentage lower than 2% cannot be taken into account by this analysis.

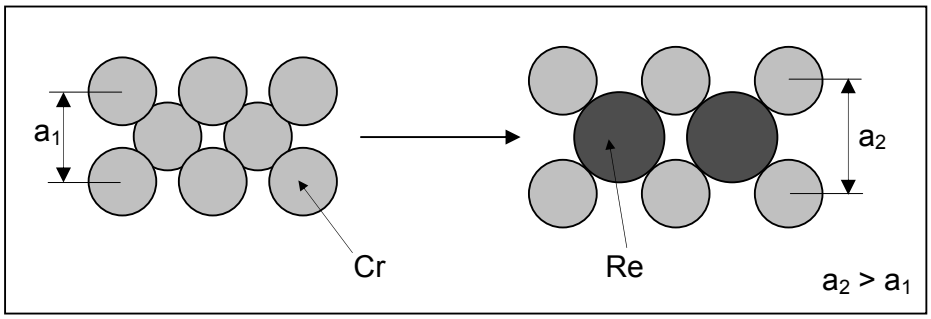

Figure 4.21: Illustration of the lattice distortion cause by Re.

Table 4.3 shows the calculated lattice parameter of Cr, Cr-18Re and Cr-35Re alloys produced though this process.

Re[at%]	A [Å]	Theoretical	Mismatch [%]
0	2,84	2.88	1,3
18	2,92	2.95	1
35	2,99	3,01	0,6

Table 4.3: Experimental lattice parameters of Cr, Cr-18Re and Cr-35Re alloys produced with active doping and theoretical lattice parameters of the alloys.

The theoretical lattice parameter of these alloys can be calculated with expression (4.2).

$$2 \cdot r_{Cr} + 2 \cdot r_{\mathrm{Re}} = \sqrt{3} \cdot a \qquad (4.2)$$

where r_{Re}=1,38 Å und r_{Cr}= 1,28 Å

This calculation gives a lattice parameter of 3,07 Å corresponding to a perfect solid solution of 50 at%Re where 100% of all cells would have a Re atom in central position. The alloys under study have a composition of Cr-35Re and Cr-18Re corresponding to 70% and 36% of all cells with a central atom. The theoretical average lattice parameter can be then calculated by:

$$a_{th} = 0.36 \cdot 3.07 + 0.64 \cdot 2.884 = 2.951 \text{ Å for Cr-18Re}$$

$$a_{th} = 0,7 \cdot 3,07 + 0,3 \cdot 2,884 = 3,014 \text{ Å for Cr-35Re}$$

This corresponds closely to the measured parameter meaning that the alloys produced by this method are very homogeneous and that the problem of heterogeneous solidification has been solved by the addition of active elements.

5. Mechanical properties of Cr-Re alloys

5.1 Introduction

The influence of the content of Re on the mechanical properties of Cr-Re alloys has been investigated by means of compression and tension tests. In chapter six, the study of the influence of high temperature exposure to air and nitrogen on the mechanical properties of the alloys has been investigated by means of three point bending. This methodology was used to determine the resistance of the alloys to embrittlement by measuring their ability to bend and mechanical properties were not measured. The Young's Modulus, hardness and coefficient of Poison of the alloys was determined by means of nano-indentation.

According to the work plan discussed in chapter 4, powder metallurgical samples were tested under compression to evaluate the gross effect that Re has on the mechanical properties of Cr-Re alloys. The powder metallurgical manufacturing method was used to manufacture economically samples with a wide range of compositions. Compression tests allow determination of the elastic limit and elastic modulus of the alloy and a characterization of the plastic deformation mechanisms involved and samples of smaller size can be used, which was an advantage during the alloy prototyping phase.

The characterization of the mechanical properties of the final alloys produced by arc melting was carried out by all the methods exposed above. Additionally fractography was carried out to determine the fracture mechanisms in these alloys.

5.2 Experimental techniques

Compression and tension tests

Tests were carried out with ASTM E9-81 standard. The specimens were cylindrical with an L/D ratio of 2 and with a 3mm diameter. Tests were conducted on an electromechanical testing machine INSTRON 8562, with an environmental chamber which allowed to change the temperature of the test. Cell loads of the testing

machines had been previously calibrated by INSTRON. The machine was controled by a software developed using LabView 6.1.

The dimensions of specimens (diameter, length) were measured by a micrometer along the gage section.The specimen was placed in the test fixture and concentric loading was ensured. Tests were carried out with position control with an amplitude of 1 mm and a rate of displacement of 0,01 mm/s. After the specimen had been installed and aligned, the recording devices were activated and the test was initiated at the prescribed displacement rate.

Tensions tests were carried out on flat samples with a section of 4x2mm using a servo-hydraulic machine. The dimensions of specimens (diameter, length) were measured by a micrometer along the gage section..

Tests were carried out with position control at the same displacement rate as in the compresion tests.

5.3 Mechanical properties of PM alloys

Room and intermediate temperature compression tests

The results of the compression tests on Cr, Cr2Re, Cr8Re, Cr18Re and Cr-35Re alloys are shown in figures 5.3 to 5.5. Figure 5.3 shows that very small additions of Re produce a significant increase in the elastic limit of the alloy. This effect has already been observed with other IVA group metals when alloyed with Re [Wadsworth, 1993]. The increase in the elastic limit of the alloy may be related to solution hardening of the material.

In figure 5.4 a significant softening of the alloy is appreciated as the Re content is increased from 2% to 8% and 18%. This softening could be related to a ductilization of the material. Observation of the Cr-18Re alloy deformed 12% under compression showed the apperance of of twining bands, this observation will be discussed in more detail in the section dedicated to the mechanical properties of the alloys fabricated by means of melting and casting. This is in accordance with some references, which

state that twining occurs very locally at even lower Re percentages, however this could not be observed in this study, since it was decided not to carry out any transmission electron microscopy in the prototype samples. [Milman, 1995] states that Cr-18Re alloys present a maximmum in DBTT and that twinning is not present in these alloys up to much higher temperature. This is may be due to the low purity of the alloys manufactured by Trefilov and Milman, this topic was dicussed with Milman during this work.

Figure 5.5 indicates that after alloy softening observed in the Cr-18Re alloys, increasing the Re content to 35% improves the mechanical properties of the alloy significantly, up to an elastic limit of 725 MPa. After pre-straining to 5% the elastic limit attains a maximum value of 975 MPa. Figure 5.6 shows the presence of twinning bands in the deformed alloy.

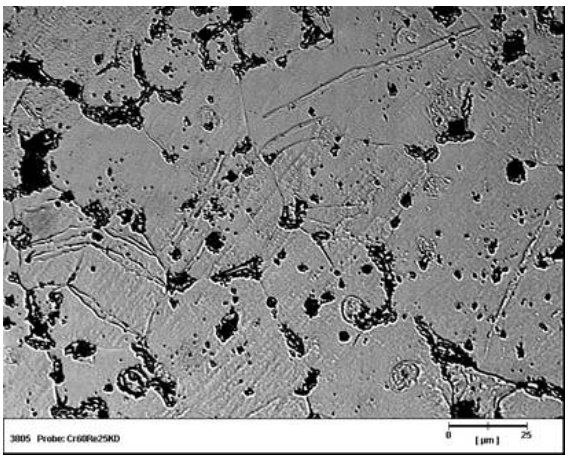

Figure 5.6: Cross section of Cr-35Re alloy showing the existance of twinning bands after 20% compression deformation at room temperature.

Identification	Yield Point (MPa)	Maximum Stress (MPa)
Cr	623	634
Cr-2Re	870	1102
Cr-8Re	851	1176
Cr-18Re	671	994
Cr-35Re	725	972
Cr-35Re(pre-strained)	975	1127

Table 5.1: Compression mechanical strength of PM alloys at room temperature.

High temperature compression tests

The addition of Re to Cr increases the high temperature compression mechanical resistance of the alloys significantly. Figures 5.8 to 5. show that Cr-18Re and Cr-35Re alloys have a strength that doubles that of pure Cr.

Optical microscopy revealed that, at high temperature, an intergranular phase precipitates. BSSEM observations revealed that this phase is qualitatively composed by Cr, N and C. According to the phase diagrams, some Cr nitrides have melting points lower than 1500°C and at the test temperature may show viscous behaviour, which could mean that the measured elastic limit is a combination of the elastic limit of the matrix and the elastic limit of these phases at the test temperature. Precipitation of these elements may be originated by the segregation of light elements already present in the alloys or by diffusion of light elements from the atmosphere to grain boundaries. The last option is less feasible due to the presence of carbon in the phase, which is the element used in the heating elements of the hot isostatic pressure furnace and not present in high percentages in air. Chemical analysis of the main alloy revealed that the samples contained above 1500 ppm of impurities, which is a problem typical of powder metallurgical samples of Cr.

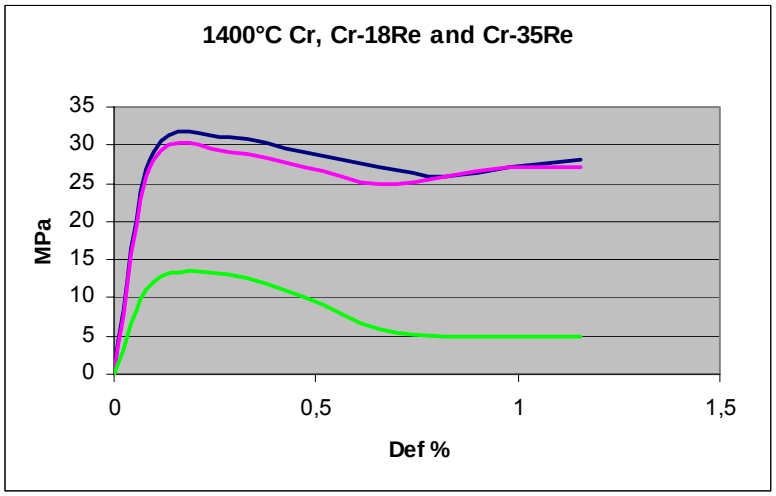

Figure 5.7: SD plots of Powder metallurgical Cr, Cr-18Re and Cr-35Re under compression

5.3.1 Mechanical properties of arc melt alloys

Room and intermediate temperature compression tests

Mechanical properties of Cr-18Re and Cr-35Re alloys were determined under tension and compression. Figure 5.7 shows the compression stress-strain plots of Cr and Cr-Re alloys at room temperature. The elastic limit of arc melt alloys at room temperature is similar to that of the alloys produced by means of powder metallurgy.

Deformation of over 5% without the detection of surface cracks is possible in Cr-18Re and Cr-35Re alloys. An increase of the elastic limit of over 40% is observed in Cr-18Re over pure Cr. increasing the Re content to 35 at% Re further increases the elastic limit of the alloy by approximately 20%.

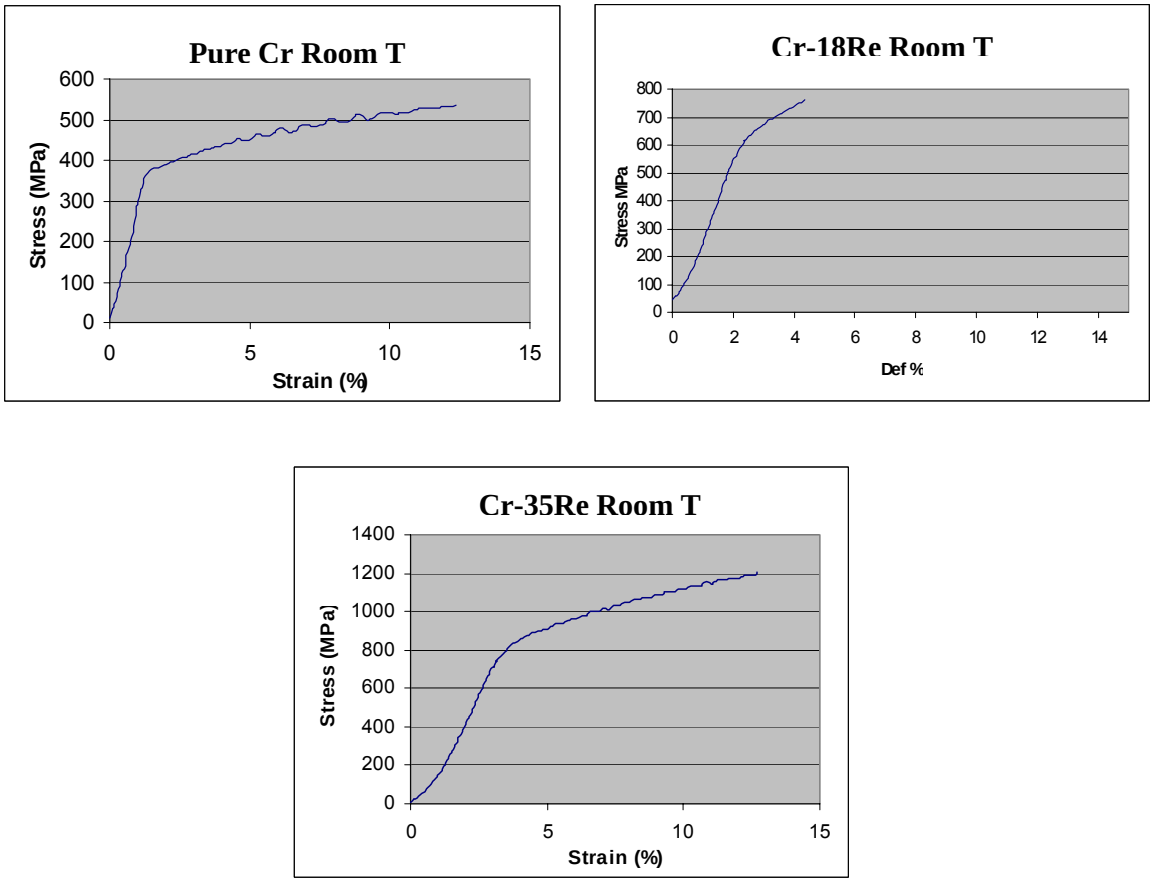

Figure 5.7: Stress Strain plots of Cr and Cr-Re arc-melt alloys under compression at room temperature.

The elastic limit of the alloys under compression is higher in all cases than the elastic limit of the alloys under tension. Under tension pure Cr did not show any ductility at room temperature while Cr-18Re alloys and Cr-35Re alloys presented all some plastic deformation r at room temperature. Ductility in BCC refractory metals is restrained to very low deformation; in the case of Cr-35Re deformation to rupture at room temperature was 5%. Figure 5.8 shows that twinning has an important contribution to deformation at room temperature in both Cr-18Re and Cr-35Re alloys. The contribution of twinning in the deformation of pure Cr is negligible, as discussed in chapter 2 and observed in figure 5.8. At 600 °C all alloys present a ductile behaviour under compression and tension. The elastic limit of Cr at 600°C is about 50% lower than at room temperature which is characteristic for pure metals. The presence of some plasticity reflects that the ductile to brittle temperature, DBTT, has been surpassed and dislocation motion is possible.

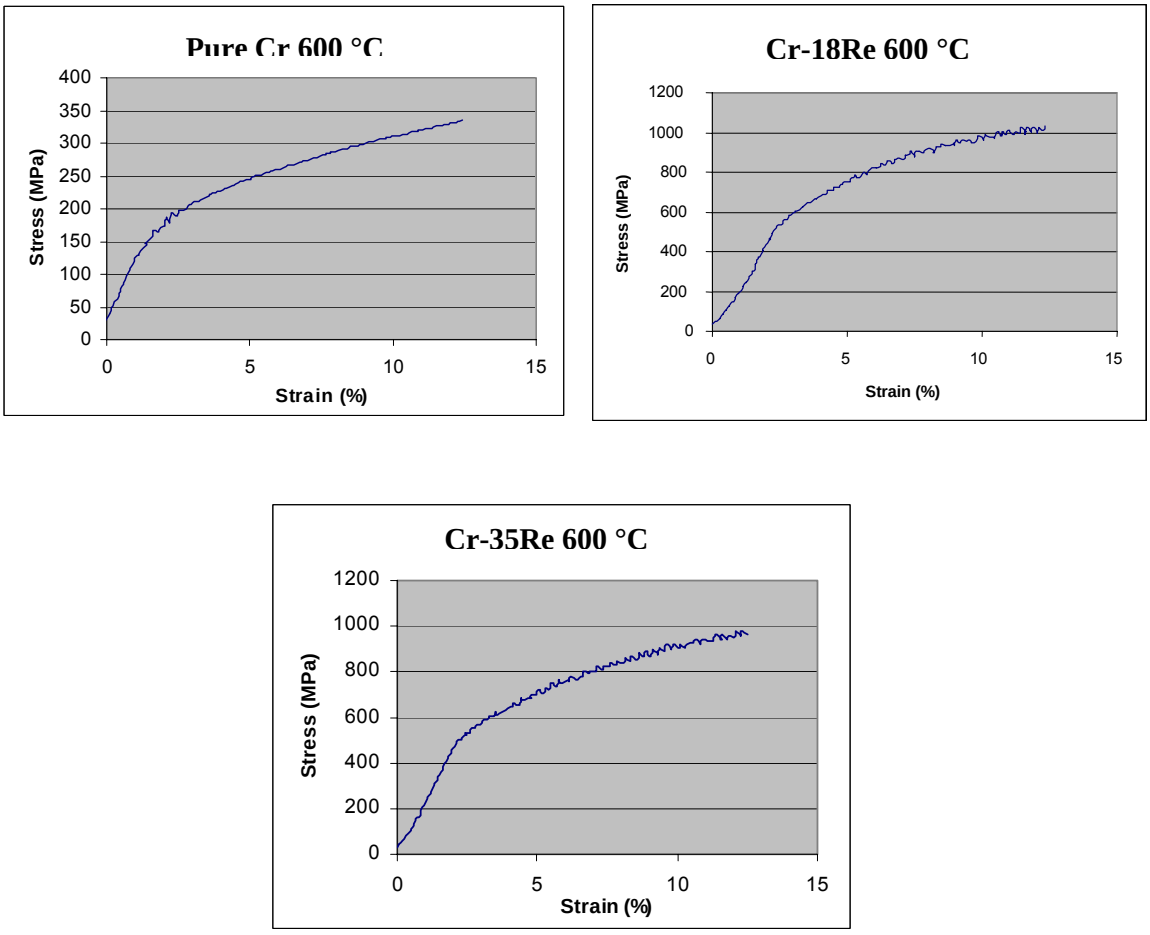

Figure 5.8: Stress-Strain plots of Cr and Cr-Re arc-melt alloys under compression at 600 °C.

The decrease in elastic limit of Cr-18Re and Cr-35 Re when increasing temperature to 600°C is remarkably low, of about 15%, with a value of 550 MPa. Small loss of strength with temperature is characteristic of solid solution alloys where the alloying element has a higher atomic radius than the matrix element, producing a resistance to dislocation motion and increasing strength. In the case of Cr-18Re and Cr-35Re alloys, the increase strength is not associated to a decrease in ductility, as with most solid solutions. Ductility increases also at 600°C with increasing Re content, this is particularly remarkable under tension, where Cr-35Re alloys show a deformation to fracture of over 8%.

At at 600 °C dislocation slip and twinning also contribute to deformation in both Cr-18Re and Cr-35Re alloys. Figure 5.8 shows that some twin bands are present, but their contribution to deformation can only be minor since their density is very low. TEM investigations revealed that Cr-18Re and Cr-35Re alloys produce a cellular dislocation structure when deformed in this temperature range, indicating strong dislocation mobility as observed in figure 5.11. Trefilov and Milman [Trefilov, 1981, 1984] predicted the formation of a cellular dislocation structure at this temperature. This dislocation structure is formed in both Cr-18Re and Cr-35Re deformed over 70%. The elongated diffraction points observed by means of TEM indicate that there is a high degree of mis-orientation between the cells.

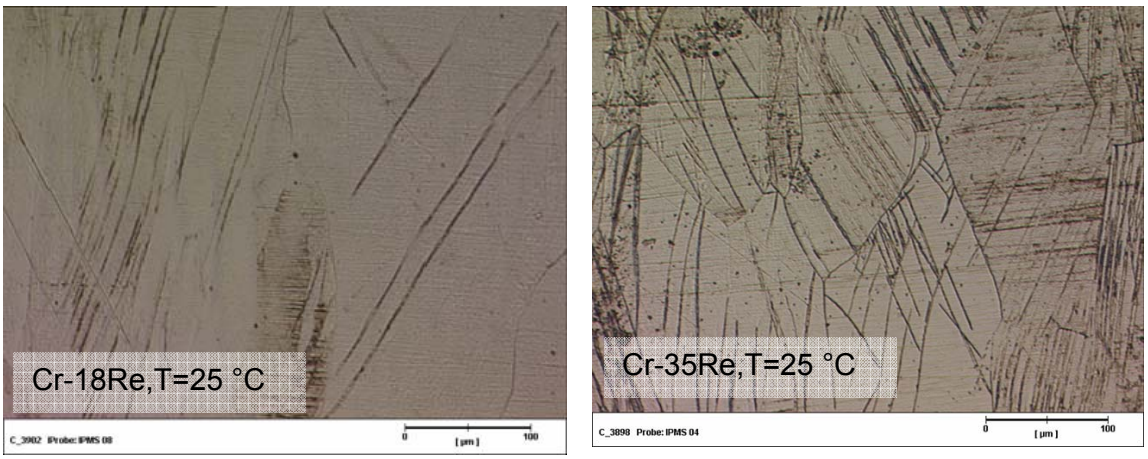

Figures 5.9a and 5.9b: Microstructure observed by optical microscopy of Cr-18Re and Cr-35Re alloys after 70% deformation under compression at room temperature.

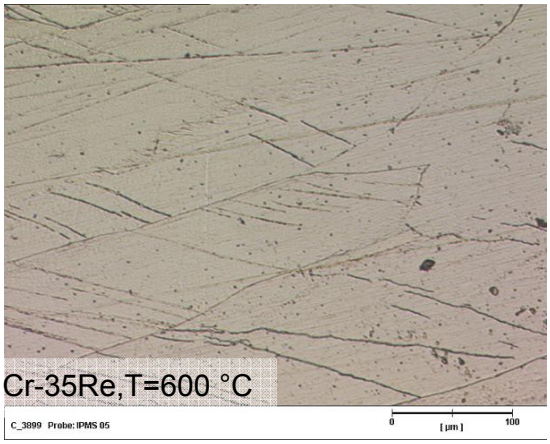

Figures 5.9c: Microstructure observed by means of optical microscopy of Cr-35Re alloy after 70% deformation at room temperature under compression and at 600 °C.

A cellular dislocation structure can be observed in the twin bands in figure 5.9. The diffraction spectrum of this area with elongated points reflects a high degree of disorientation in between the cells indicating that in the twin bands, where planar orientation maximises the shear stress, dislocation motion at room temperature is possible in both Cr-18Re and Cr-35Re alloys.

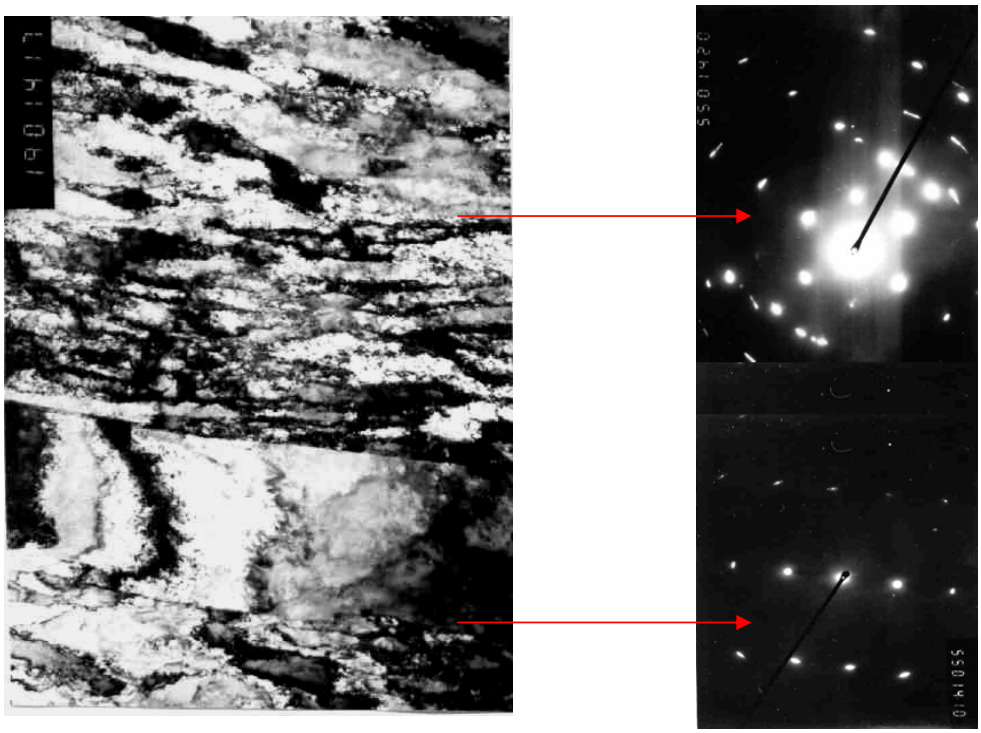

Figure 5.10: Structure of matrix and twin band in a Cr-35Re alloy deformed 70% under compression. The diffraction clichés show the matrix, below, where deformation has taken place by slip, observed in the strong contrast bands and the twin bands where a cellular dislocation structure has been created and observed in the elongated diffraction points of the cliché.

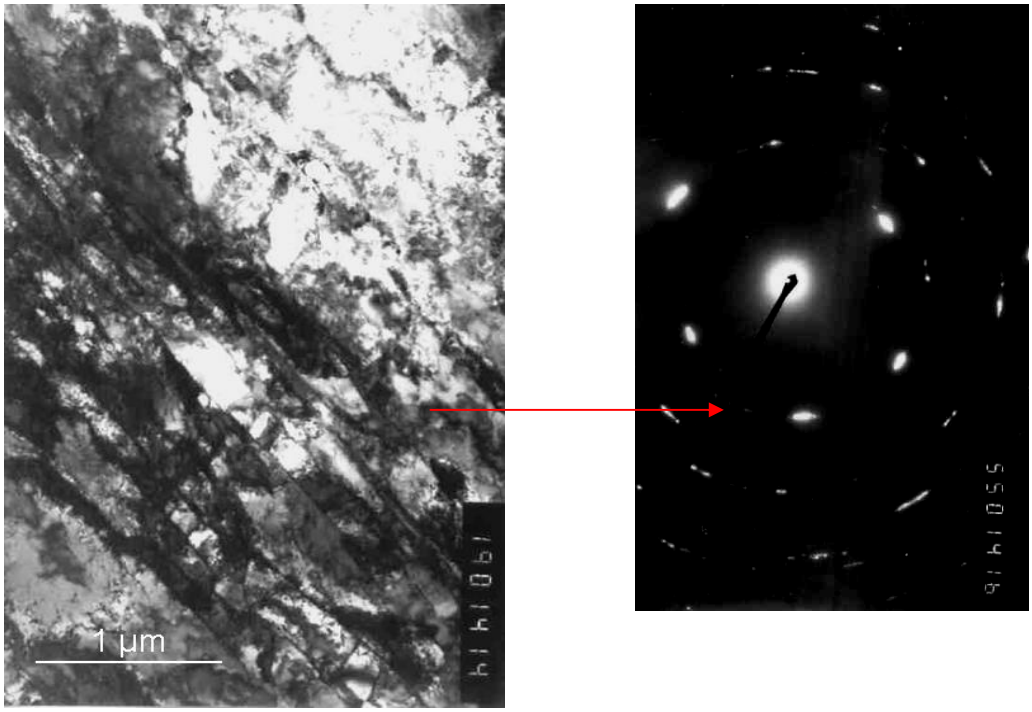

Figure 5.11: TEM image of a Cr-35Re alloy deformed 70% under compression at 600°C. There is a generalised cellular microstructure in the alloy. The elongated diffraction points in the diffraction cliché show the strong degree of disorientation between cells.

High temperature compression tests

Mechanical properties of Cr, Cr-18Re and Cr-35Re were investigated at 1100°C and at 1400 °C under compression. Figure 5.9 shows the stress-strain plots 1100°C. The influence of Re on the mechanical properties of Cr is very strong at this temperature. The addition of 18%Re to Cr increases compression elastic limit from 80 MPa to 300 MPa. Increasing the Re content to 35% has a limited effect on the elastic limit of the alloy, which increases to 310 MPa.

The serrations observed in the plot are related to the interaction of moving dislocations with diffusing atoms in the alloy. This phenomenon will be discussed after evaluation of the stress-strain plots of the alloys at 1400 °C where the serrations are more pronounced.

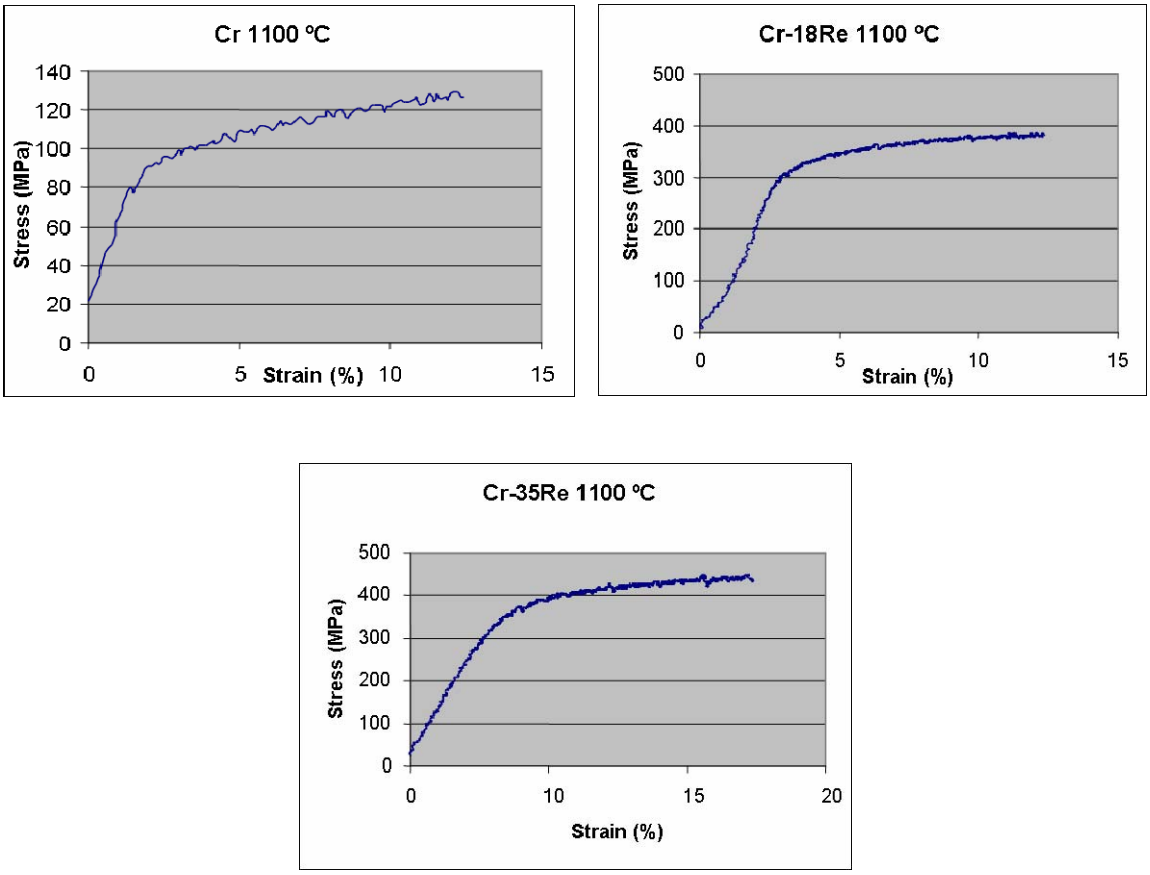

Figure 5.12: Stress Strain plots under compression of Cr and Cr-Re arc-melt alloys at 1100°C.

At 1400 °C the compressive elastic limit of Cr is well below 30 MPa, addition of 18%Re in the alloy increases the elastic limit at this temperature to 140 MPa, further additions of Re do not increase the elastic limit of the alloy at this temperature. The relatively small effect of Re additions above 18% on the compressive strength of Cr-Re alloys has been observed at all other temperatures and at 1400°C the effect is negligible. Actually, Cr-18Re presents a slightly higher compressive elastic limit than Cr-35Re, as shown in the detail plot in figure 5.14. The plots present serrations, observed already at 1100°C.

The serrations can be originated by either the interaction of the diffusing solute atoms, in this case Re, with the moving dislocations in the alloy or by the interaction between impurities in the alloy, mainly light elements, and the moving dislocations or by a mixture of both phenomena. This phenomenon is known as dynamic strain ageing and has been observed in several alloys, it is characteristic of solid solutions of elements with different atomic radius and in alloys with diffused impurities. The

serrations are of a different nature in Cr than in Cr-Re alloys. The serrations in Cr have a large amplitude and appear with a lower frequency, these serrations can only be originated by the interaction of dissolved light elements in the alloy with the moving dislocations. In the case of Cr-18Re and Cr-35Re alloys the serrations have a much higher frequency, indicating that these are mainly originated by the interaction between the Re atoms and the moving dislocations. Additionally, there may be an interaction between impurities dissolved in the alloy and dislocations which is not visible in the plot due to the preponderance of the solute-dislocation serrations.

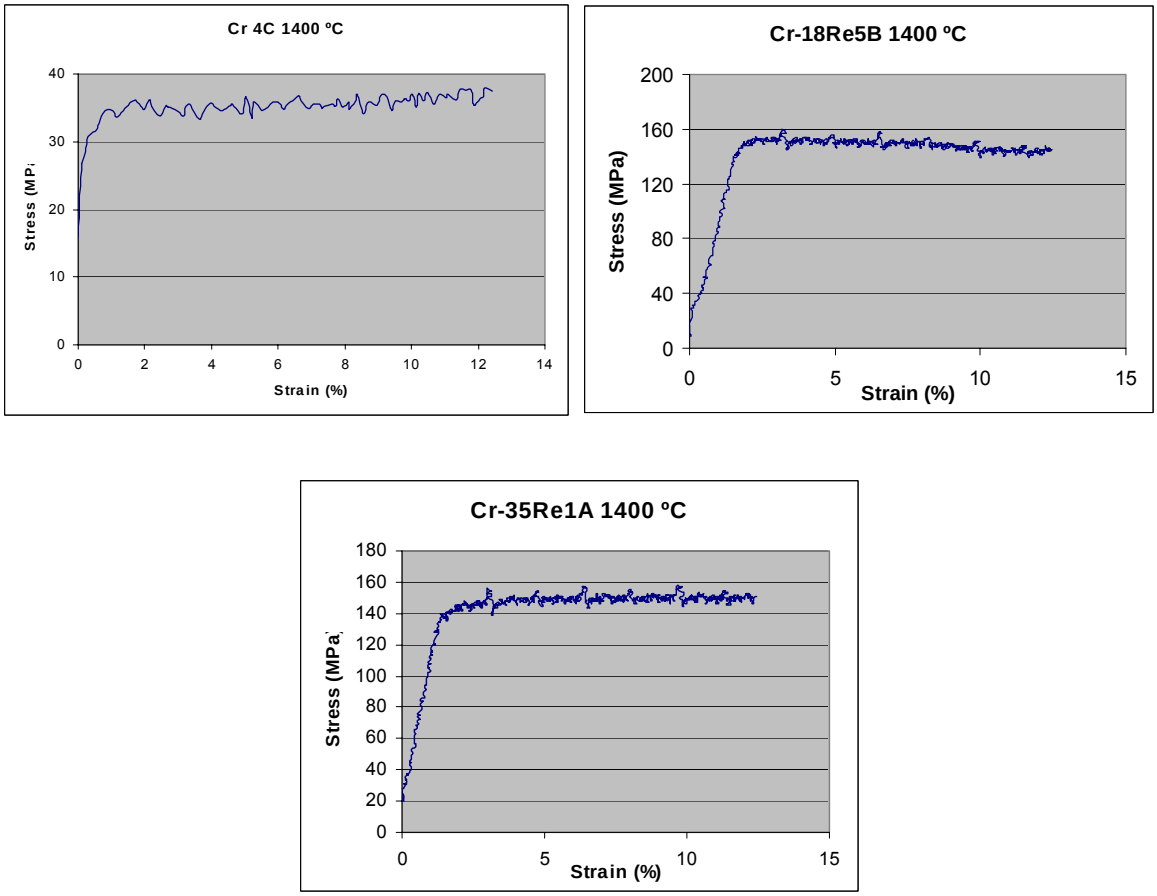

Figure 5.13: Stress strain plots of Cr and Cr-Re arc-melt alloys under compression at 1400 °C.

At 1400 °C the serrations are more pronounced. In the plot represented in figure 5.14, elaborated with a precision of 0.012% in the X axis, it can be observed that the serrations are more pronounced in Cr-18Re and Cr-35Re than in pure Cr. This indicates that the serrations are mainly related to dislocation-Re interactions, with light element impurities playing a minor role visible only in the serrations of the Cr

plot. Serrations in plastic flow may indicate the presence of the Portevin- Le Chatelier dynamic strain ageing effect in the alloys.

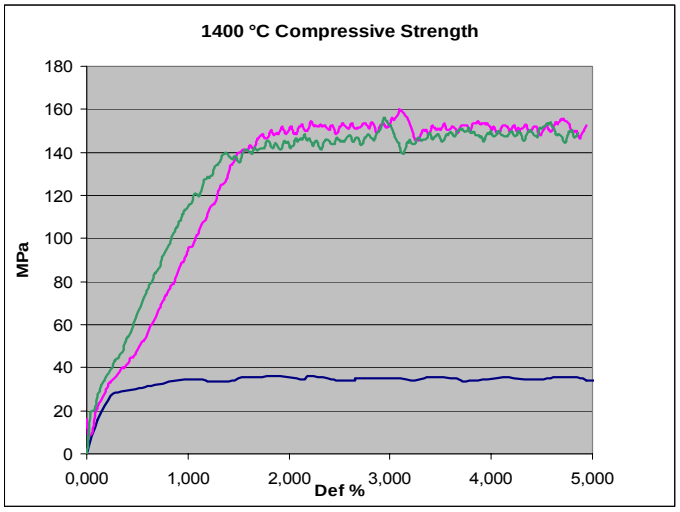

Figure 5.14: Stress Strain plot of Cr, Cr-18Re and Cr-35Re alloys under compression at 1400°C.
Blue: Cr
Pink: Cr-18Re
Green: Cr-35Re

To determine the existence of this effect in Cr-Re alloys, a further test was carried out in which the elastic limit of the alloys is measured under compression at an intermediate temperature at different strain rates. To obtain an elastic limit with a high enough value to measure any significant difference between the alloys, a temperature of 450°C was selected. Strain rates of 0.01 and 0.001 mm/s were imposed to the probes.

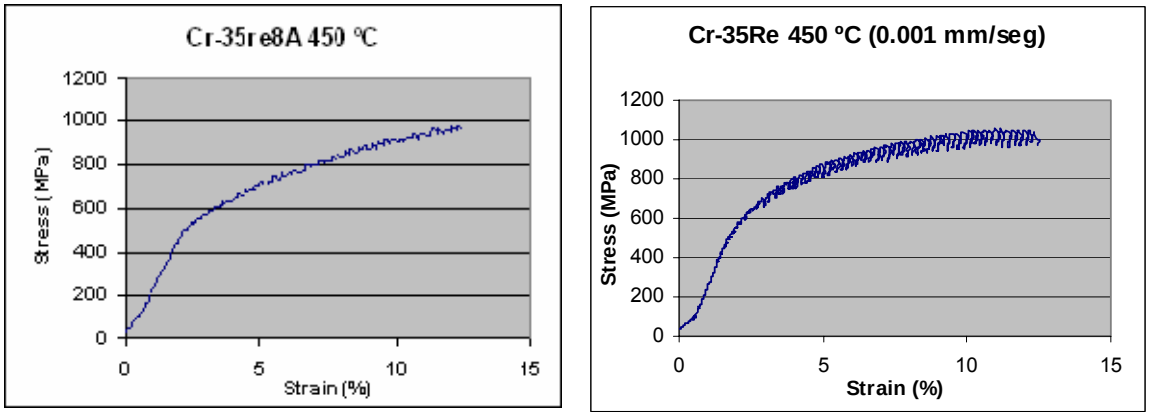

Figure 5.14: Stress Strain plot of Cr-35Re at 450°C under compression and a strain rate of 0.01mm/s and of 0.001mm/s

Figures 5.14 and 515 show that the strain rate- dependence in Cr-Re alloys is inverted. The yield stress for Cr-18Re at 450 °C is around 500 MPa at a strain rate of 0.01mm/s and around 600 MPa at 0.001 mm/s. Compressive stress at a deformation of 10% is 900 MPa at 0.01 mm/ and over 1000 MPa at 0.001 mm/s. The amplitude of the serrations also increases with decreasing strain rates, a further characteristic of alloys presenting the Portevin- Le Chatelier effect.

5.3.2 Fracture behaviour of Cr-Re alloys under tension

Figure 5.19 shows that the behaviour under tension of Cr-Re alloys is quite different than under compression. The difference between the strength values measured under tension or under compression can be explained by the appearance of local fracture under tension which decreases the effective charge section, a phenomenon not present under compression until very high deformation where internal sample cracking takes place.

Cr-18Re alloys do not show any plastic deformation under tension. This behaviour is due to intergranular fracture of the alloys due to the very high segregation of Cr to the grain boundaries. Inoculated alloys presented plastic deformation under tension in the whole temperature range.

Cr-35Re alloys show a ductile behaviour until 1200°C. Ductility of Cr-35Re is linked to the transgranular fracture component, the intergranular being responsible for brittleness. The fracture behaviour of Cr-35Re alloys was investigated in detail since parallel chemical stability tests carried out in parallel had demonstrated that the alloys were best suited for the application.

Table 5.2: Mechanical properties of Cr-35Re alloys under tension and under compression

Temperature ^{o}C	$\sigma_{0,2}$, MPa	σ, MPa	Def to rup, %
20	461 / 775	580	2,9
600	535 / 710	746	8,3
1000	345 / 330	460	10,8
1200	178 / 248	178	0,0

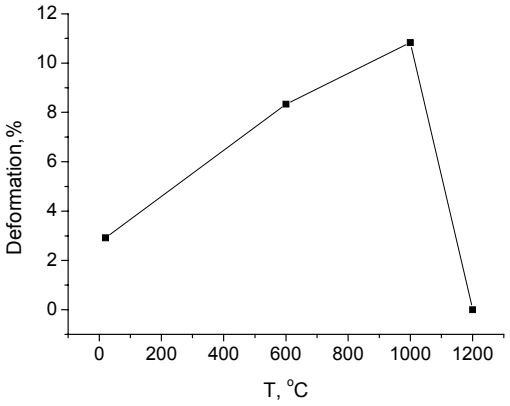

Fig.5.18a: Deformation to fracture of Cr-35Re at different temperatures

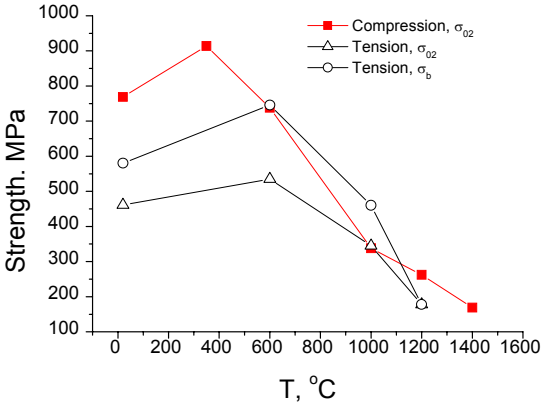

Figure 5.19b: Maximum strength of Cr-35Re alloy under tension and compressions at different temperatures

Figure 5.19 shows that at room temperature, fracture has transgranular and intergranular components. The transgranular components are responsible for the few percents of ductility that the material shows and are characterized by the presence of ductile dimples on the fracture surface. The intergranular component is dominant and is probably originated by the presence of impurities segregated at grain boundaries during alloy manufacture that embrittle this area.

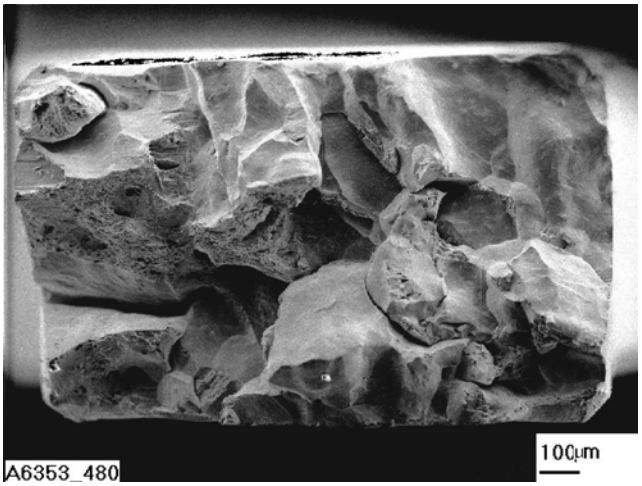

Figure 5.19: Fracture surface of Cr-35Re arc melt alloy deformed under tension at room temperature.

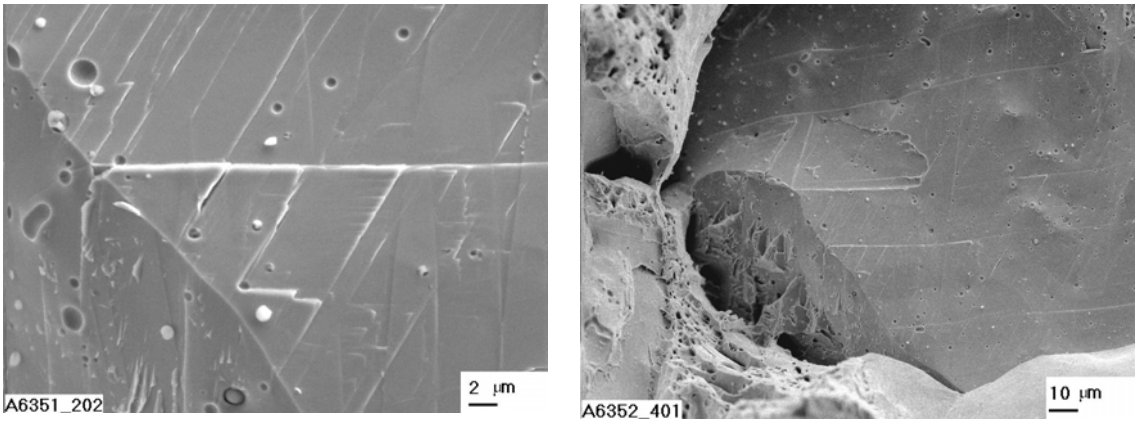

Figure 5.20: Detail images of intergranular fracture component, left, and transgranular fracture component, right, showing ductile fracture dimples.

Fracture behaviour at 600°C is basically ductile, with a generalized transgranular fracture showing ductile dimples. Figure 5.22 shows the fracture zone of a Cr-35Re alloy after 10% deformation under tension at 600°C. The generalized ductile transgranular fracture behaviour can be observed in particular in the detail image.

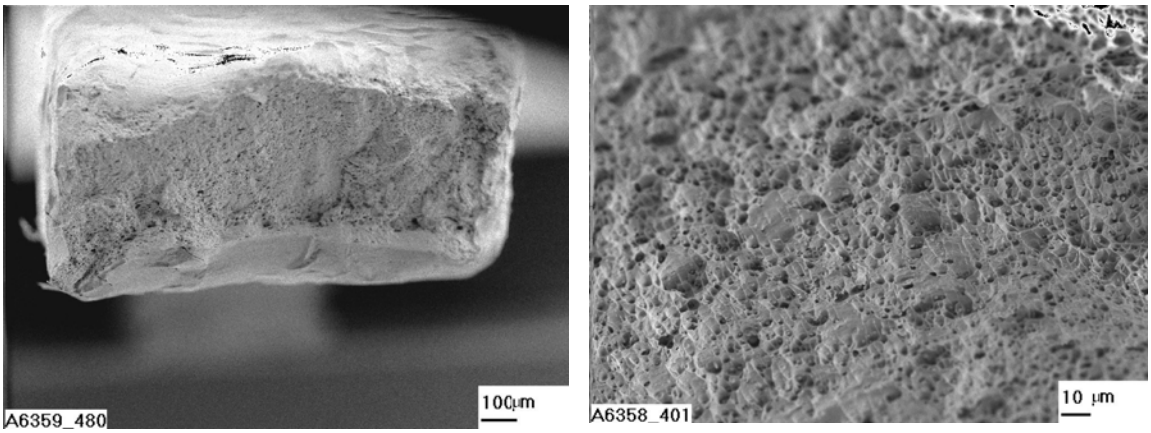

Figure 5.21: Left, fracture surface of a Cr-35Re alloy deformed under tension at 600 °C. Right, detail image of the fracture sample with ductile dimples

Increasing temperature to 1000°C changes again the fracture mode to a combination intergranular and transgranular with ductile dimples appearing on the transgranular component of the fracture surface observed also at room temperature. The transgranular component is dominant at 1000°C, this can be observed in figure 5.22, accounting for the increased ductility of the material.

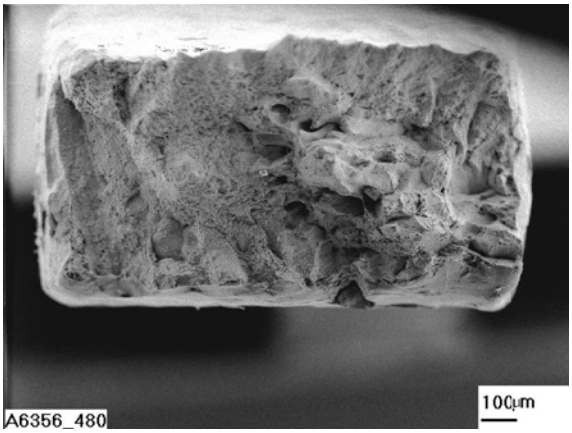

Figure 5.22a: Fracture surface of Cr-35Re after rupture under tension at 1000°C.

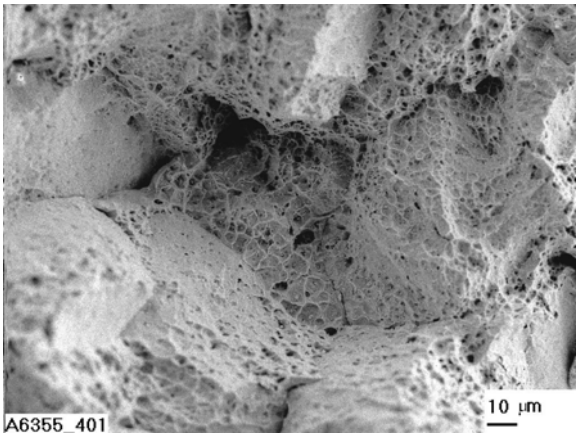

Figure 5.22b: Detail image of the fracture surface showing the transgranular component and the intergranular component. Observe the general presence of ductile dimples.

Fracture at 1200°C is basically intergranular with the alloy showing no ductility. Figure 5.22 shows that there is no transgranular component on the fracture and no ductile dimples.

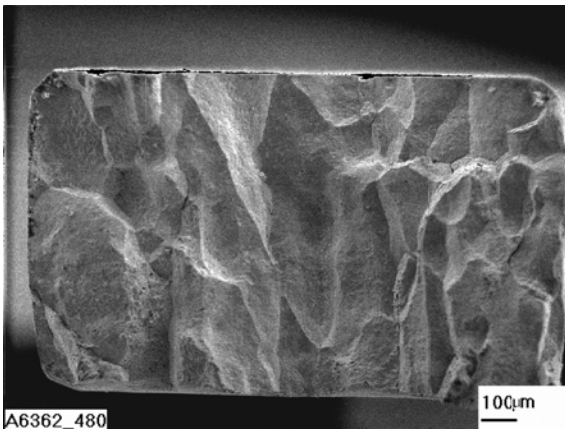

Figure 5.22a: Fracture surface of a Cr-35Re alloy after tension rupture at 1200 °C showing the intergranular fracture behaviour.

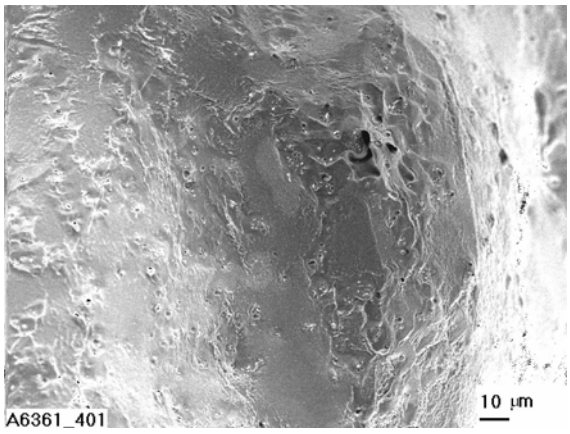

Figure 5.22b: Detail image of 5.22a.

5.4 Elastic modulus and coefficient of Poisson

The average value of Young's module on volume of sample was determined with the help of ultrasonic method. The ultrasonic method allows determining also shear modulus and Poisson's constant. Results are shown in table 5.3.

Table 5.3: Modulus of elasticity and coefficient of Poisson of Cr, Re and Cr-35Re alloys

	Cr	Cr-18Re	Cr-35Re	Re
Young modulus E	279 GPa	292 GPa	319 GPa,	469
Shear modulus G	115 GPa	118 GPa	123 GPa,	176 GPa
Coefficient of Poisson v	0,210	0,241	0.293	0,296

5.5 Discussion

Cr and solid solution Cr-Re alloys are BCC refractory metals. This type of materials presents in any case very limited room temperature ductility. The main feature related to the addition of Re in the alloy is the activation of twinning at room temperature. In Cr-Re alloys twinning is responsible for at least part of the increase in plasticity. This can be observed by the absence of cracks at the interfaces between twin bands and grain boundaries.

Powder metallurgical alloys have been used to prove qualitatively the effect of Re and it was not intended to use them for production purposes. Arc melt alloys showed much higher mechanical strength, in particular at high temperature where dissolved impurities play a major role in deformation. Compressive plasticity of Cr 35Re alloys is very high. Arc melt alloys have been deformed by up to 70% at room temperature without showing any internal fracture.

Trefilov in his discussion on the grain boundary strength of BCC refractory metals, states that it has a strong dependence on temperature [Trefilov, 1975]. Grain boundary strength decreases slightly up to 1000 °C where the decrease is much sharper. This behaviour is responsible for the fracture characteristics of the alloys. At room temperature fracture takes place in mixed inter and transgranular mode. At

intermediate temperature, up to 1000°C the fracture mode is basically transgranular, it is in this temperature domain that the alloy shows a higher ductility, reaching 10% elongation to fracture at 1000 °C. Plasticity rapidly decreases above this temperature, as fracture mode becomes again transgranular.

A further parameter that may have an influence on the fracture behaviour on Cr-Re alloys is the segregations of Cr and other impurities to the grain boundaries [Matsuda, 1994]. It has been observed that Cr-35Re does not have a particular tendency to segregations of Cr to the boundary region, which is the case of Cr-18Re, however, chapter 6 and 7 shows that there are indications that the grain boundaries have an increased concentration of Cr. EDX could not detect this since the area with a higher concentration of Cr may be of just a few nanometers, vacuum tests at high temperature described in chapter 7 show that Cr-35Re grain boundaries have a tendency to evaporation at very high temperatures, indicating that there might be pure Cr present in this area or that it may diffuse at high temperature.

Independently of the lack of plasticity at 1200°C, the ultimate tensile strength of Cr-35Re alloys is extremely high, with a value of 140 MPa at 1400°C that is considered to be sufficient for the application.

6. Chemical Stability of Cr-Re alloys in air and nitrogen

In chapter 2 and 5 it has been shown that the mechanical properties of BCC refractory metals are very much dependent on the contamination of the alloys by interstitial impurities. Therefore, the study of the chemical stability of Cr-Re alloys for application in satellite thruster engines must focus on three main directions:

- The determination of the mass change during exposure to aggressive media
- The study of the microstructure changes in the material
- The determination of the impact on ductility of the diffused impurities

Taking this into account, a series of tests were defined to determine the chemical stability of Cr-Re alloys in atmospheres representing the conditions found in combustion chambers. The effect of high temperature exposure to aggressive media has been quantified by microscopic observation of the alloys and by mechanical testing.

6.1 Experimental techniques

High temperature exposure: atmospheres and test procedure

In chapter 2 the chemical solicitations of a combustion chamber have been described. The atmosphere changes locally from reducing, basically nitrogen-rich, to oxidising. This is due to turbulences and to heterogeneous mixing of fuel and oxidiser. Therefore two main characteristics of Cr-Re alloys must be evaluated: first the resistance of the alloy to oxidation and in particular the stability of the surface oxide layer characteristic of Cr-alloys and its ability to protect the base material from nitrogen diffusion and second the ability of the base material in unprotected condition to withstand nitrogen diffusion, in case that the oxide layer breaks.

Therefore two test atmospheres have been selected:

- Nitrogen containing atmosphere
- Nitrogen and oxygen containing atmosphere

In chapter 2 it has been shown that the combustion chamber atmosphere has an average concentration of nitrogen of a bout 40 mol%. Therefore a mixture consisting of argon and nitrogen was used for study of behaviour in nitrogen. Room temperature partial pressure of argon was set at 0,2 kg/m^2 and nitrogen partial pressure at 0.5 kg/m^2. At 1500 °C the partial pressure of nitrogen was 1,30 kg/m^2, and for argon it was 3,25 kg/m^2.

Air was selected to study the resistance of the material to a nitrogen and oxygen containing atmosphere. Air has a mixture of 20 mol% oxygen and 80 mol% nitrogen; this is similar to the atmosphere composition in the most oxidising areas of the combustion chamber.

In both cases the test temperature was 1500 °C, the exposition times were set at 30 minutes and 1 hour.

After high temperature exposure, the samples were investigated by means of SEM. Their ductility before and after exposure was determined by three-point bending.

Measurement of ductility and sample geometry

Test samples were machined from ingots of the relevant alloys by electro-spark cutting. Specimen dimensions were 29x4x1,2 mm and placement of samples in 3 point bending rig is shown in figure 6.2. A layer of 0.1mm was removed from surface of each side by polishing with abrasive paper. After this the samples were polished by means of Cr_2O_3 powder with a grain diameter of 1-5 microns and finally electropolished. This polishing procedure was carried out to reduce the influence of surface condition on the chemical properties of the alloys. The selected geometry

was adequate to use the samples used to study the chemical stability for the ductility measurement tests by three point bending.

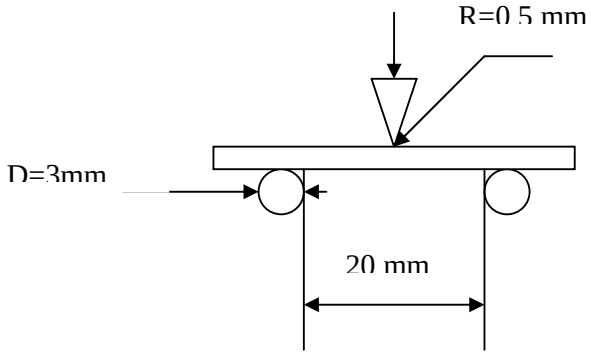

Fig. 6.1: Schematic representation of the bending test used to investigate material ductility before and after high temperature exposure

Investigated parameters

Mass change, microstructure and ductile to brittle transition temperature of the alloys were investigated before and after high temperature exposure. The mechanical properties of the layers formed on the samples during exposure were investigated by means of micro indentation.

6.2 Results

Figure 8.2 shows the appearance of the samples after the test. Cr and Cr-18Re samples exposed to air at 1500°C for 30' and 1h formed unstable layers that peeled off during the test as seen in figure 6.2, Cr-35Re formed a dark layer that did not peel off. Samples exposed to nitrogen formed dark, stable layers.

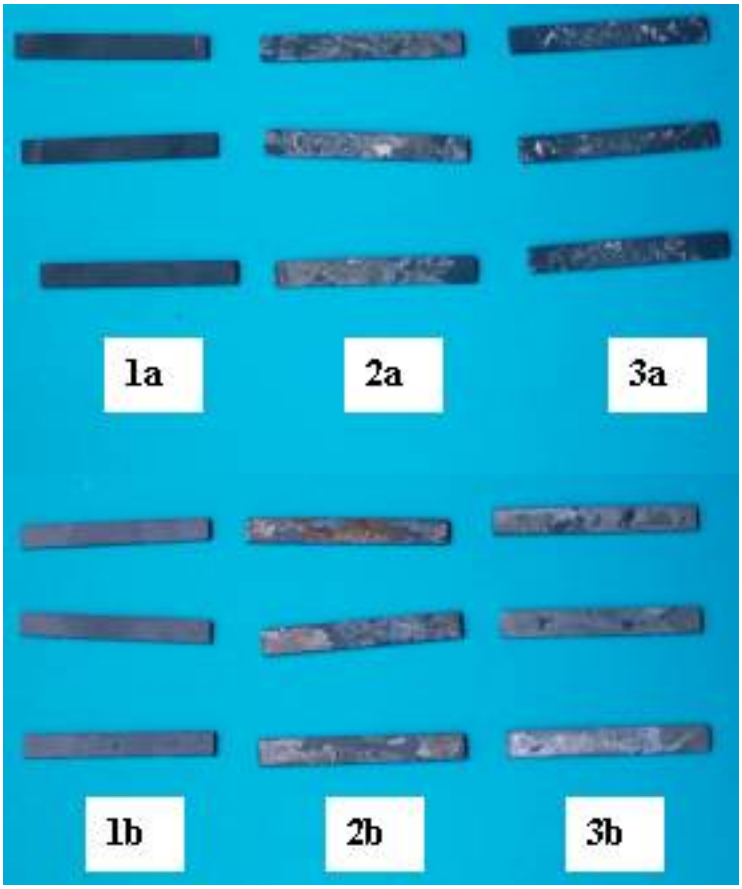

Figure 6.2: appearance of Cr and Cr-Re after exposure to air and nitrogen after 1500°C during 1h.

a) 1- Cr-35 at. % Re: 1h, 1500 °C, N_2; 2- Cr-18Re: 1h, 1500 °C, N_2; 3- Cr: 1h, 1500 °C, N_2
b) 1- Cr-35 at. % Re: 1h, 1500 °C, air; 2- Cr-18Re: 1h, 1500 °C, air; 3- Cr: 1h, 1500 °C, air

6.2.1 Microstructure of Cr-18Re samples exposed to air at 1500 °C

Cr-18Re samples exposed to air at 1500 °C during 30' and 1 h. were investigated by SEM. The examination showed the alloy is not capable to form a protective layer and that the grain boundaries of the material were very sensitive to high temperature exposure. During the exposure no film was formed of the surface of samples, in contrast with the behaviour of pure Cr, which forms a protective layer that delaminates at 1200 °C.

Figure 6.3 shows that fracture paths appeared along grain boundaries. No mechanical constraint was applied to the sample during the test. This may indicate that the instability of grain boundaries is due to evaporation of Cr segregated in the

grain boundaries or to its chemical reaction with atmospheric elements diffusing through grain boundaries. Diffusion was facilitated by the impossibility of the alloy to form a protective layer on the sample surface.

In chapter 7, Cr-18Re alloys exposed to high temperature in vacuum show a very similar behaviour this indicates that evaporation of Cr may play a major role in the instability of the grain boundaries of Cr-18Re at high temperature.

The cracks shown in figure 6.3 seem to follow a diffusion path into the grains, depending of crystallographic orientation of the grain; unfortunately, it was not possible to carry out texture studies to verify this. The tests carried out in chapter 7 indicate that evaporation Cr in a BCC matrix is sensitive to crystallographic orientation, a phenomenon known as thermal etching, resulting in similar patterns to the ones seen in the grain boundaries of alloys exposed to high temperature air and nitrogen.

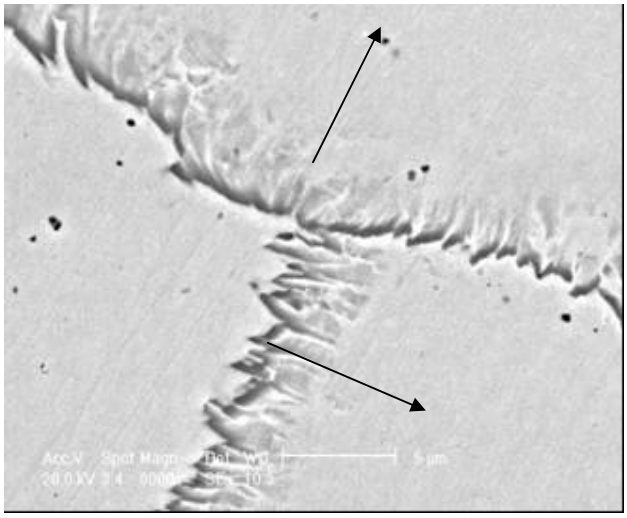

Fig. 6.3: Grain boundary fracture of Cr-18Re alloy exposed to air at 1500°C during 30'

The instability of grain boundaries makes Cr-18Re clearly unsuitable for application in high temperature aggressive atmospheres, in particular since the homogenisation of the material, which would probably correct the problem, is a complex process for cast Cr-Re alloys, as discussed in chapter 4.

6.2.2 Characterization of Cr-35Re after HT exposure to air and nitrogen

The exposure of Cr-35Re to either nitrogen or air at 1500°C results in the rapid formation of a dense dark layer on the surface indicating the reaction of the material with both atmospheres.

Microstructure of Cr-35Re after exposure to air

Observation of the transversal section of the material shows the formation of a multi layered structure below the surface up to a thickness of approximately 50µm for samples exposed to air 1 h. at 1500°C. This structure is constituted of a surface layer of about 15µm and a porous layer with a mean thickness of about 20 µm. Samples exposed to air for 30' present a similar structure with layers of 12 and 15 µm thickness respectively. Figure 6.4 shows this structure in Cr-35Re exposed to air at 1500 °C where the exposure time was increased to 4 hours to produce layers thick enough to be analysed by means of EDX.

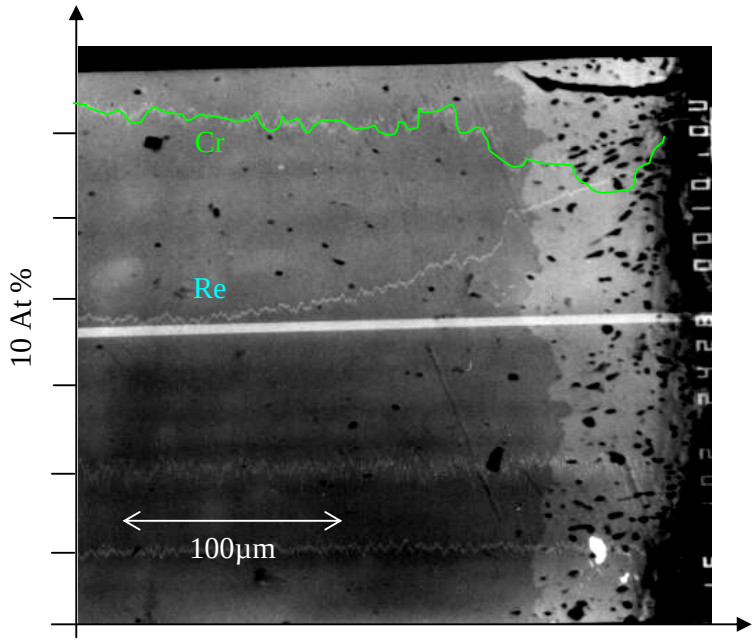

Fig. 6.4: Cross-section of Cr-35Re sample after annealing at 1500 °C – 4h, air and at% of obtained by EDX of surface layer composition.

EDX line-scan analysis of the multi-layered structure shows important differences of concentration between the layers. Qualitatively, the measurements show that the surface layer consists basically of a Cr oxide. The binary phase diagram of Cr-O corroborates the qualitative EDX analysis of the surface layer, since Cr_2O_3 is the only stable Cr oxide at the exposure temperature.

The second layer has an increased concentration of Re, indicating that Cr migration has taken place to the surface where it is oxidised. This phenomenon is characteristic of all materials protected by Cr oxides.

Surface images of the Cr-35Re alloys after high temperature exposure were taken by means of SEM to characterize the density of the layer. Figure 6.4 shows that after 30' of exposure to air at 1500 °C, the surface oxide layer formed on Cr-35Re still shows some porosity in particular in the grain boundaries. After 1 hour of exposure to air at 1500°C the surface layer is fully dense, figure 6.5 shows a grain boundary detail image, where it can be observed that there is no porosity present.

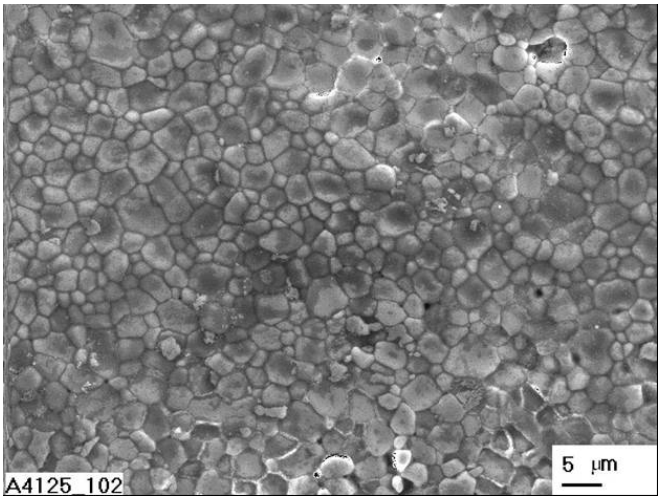

Fig. 6.4. Appearance of surface of Cr-35Re samples after exposure to air at 1500 °C in air during 0.5 hours

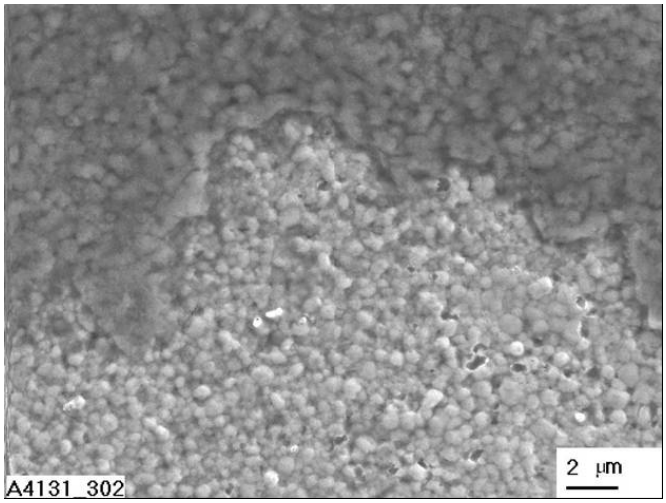

Figure 6.5: Grain boundary in Cr-35Re alloy after 1h exposure to air at 1500°C

Figure 6.6 shows that precipitation is present under the surface layer of the samples after exposure to air at 1500°C to 4h. Later in this chapter, it is shown that exposure to pure nitrogen does not result in any precipitation, this indicates that the precipitates in the samples exposed to air are oxides. Since Re oxides are volatile, the only possibility is that the precipitates are Cr_2O_3 originated by the diffusion of oxygen though micro cracks in the surface layer. The surface layer thickness does not increase practically with exposure time indicating that it is inert at the test temperature in air once a critical thickness of about 40 µm has been formed.

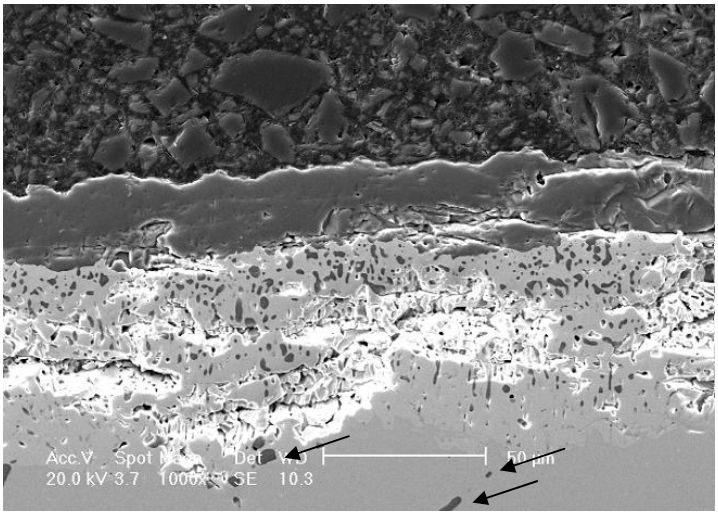

Figure 6.6: Cross section of Cr-35Re after exposure to air at 1500 °C during 4h. Arrows indicate isolated precipitation of oxides in the substrate.

Microstructure of Cr-35Re samples after exposure to nitrogen

Samples exposed to pure nitrogen at 1500°C form a dense surface layer in less than 1h. Figure 6.7 shows the surface of Cr-35Re exposed to nitrogen at 1500 °C during 1h in a grain boundary region. The morphology of the surface layer differs from that observed on alloys exposed to air and shown in figure 6.5.

The exposure to nitrogen at 1500 °C during 1h produces a double layer with a dense structure, of about 25µm in thickness and no evidence of Kirkendall porosity, indicating the diffusion of N into the substrate rather than the migration of one alloy component to the surface to react with the atmosphere. Figure 6.8 shows the cross section of the material obtained by cryogenic fracture. The double layer structure is obvious at the bottom of the picture.

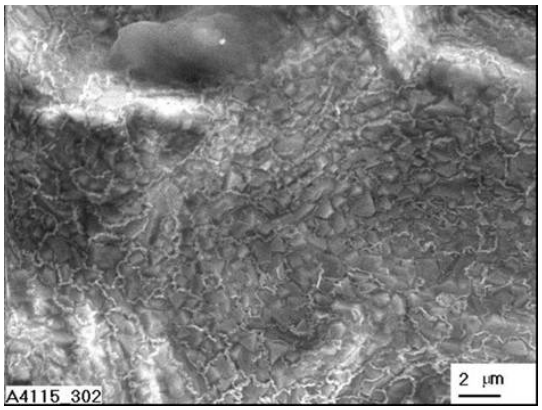

Figure 6.7: Surface of Cr-35Re alloy exposed to nitrogen at 1500 °C during 1h.

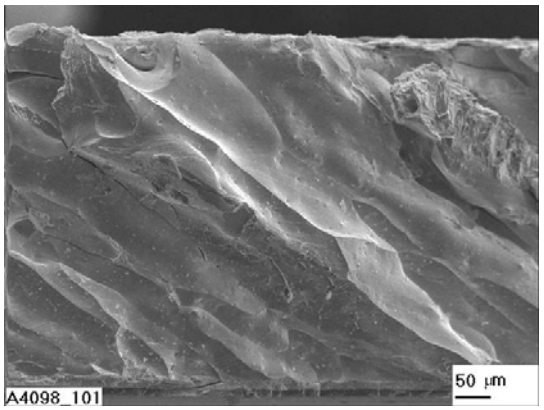

Figure 6.8: Cross section of Cr-35Re exposed to nitrogen at 1500 °C during 1h.

There is no precipitation of second phases in the substrate of the alloy, indicating either the perfect isolation of the surface layer or a very high solubility of nitrogen in the substrate, resulting in the impossibility to form nitrides.

The study of the mechanical properties of the different layers formed during exposure to air and nitrogen revealed an increase of substrate hardness. The mechanical properties of the layers formed during exposure to nitrogen and air at 1500° were determined by micro indentation with a pyramidal indentor and are presented in table 6.1.

The hardness of the surface oxide layer of the Cr-35Re samples exposed to air at 1500° is close to that of Cr oxide. It is interesting to note that the diffusion layer on these samples, which is mainly composed of Re, presents a very elevated hardness, indicating a high concentration light elements in solution in this layer since there is no evidence of precipitation. The increase of substrate hardness after high temperature exposure to air is in the order of 3 GPa.

The E-modulus of the of the nitride layer formed on Cr-35Re samples exposed to nitrogen at 1500°C has a value of 400-500 GPa, which is typical of ceramic materials, basically Cr nitride. The increase of substrate hardness is between 5 to 7 GPa.

The increase of substrate hardness during nitrogen exposure indicates that nitrogen diffuses into the substrate through the layer formed on the alloy surface; therefore, that this layer is not protective against light element diffusion. The multi-layer structure formed in samples exposed to air, presents better protective properties, translated into a smaller increase in substrate hardness during high temperature exposure. The oxygen reacts on the alloy surface to form a dense Cr oxide layer. This layer allows diffusion of some light elements into the substrate, nitrogen that diffuses through, is trapped in the Re layer immediately below, which shows a very elevated hardness value.

Table 6.1 Some characteristics of layers formed on the Cr-35Re alloy after annealing during 1 hour at 1500 °C in nitrogen and air

Atmosphere of annealing	Number of layers formed	Layer number from surface	Thickness, µm	Hardness, GPa	Modulus of elasticity GPa	Hardness of substrate	Hardness of Cr-35Re alloy, GPa
Air	2	1	0.3	34-36	600	8-9	5.0-6.0
		2	2	20-22	500		
Nitrogen	1	1	2	22-24	420	10-12	

The hardness increase of the substrate may be used to measure the level of light element diffusion during the exposure to high temperature. Hardness of the sample

exposed to air is in the region of 8-9 GPa while hardness of the samples exposed to nitrogen is in the region of 10-12 GPa. This indicates that the multi-layer structure formed during high temperature exposure to air is more protective than the single layer structure formed during exposure to nitrogen.

Despite the higher protection, some light elements diffuse into the substrate, preferentially through the grain boundaries; this is translated into an increase of the substrate hardness and the presence of some oxides at grain boundaries. The reaction at the grain boundaries is differentiated from that observed in Cr-18Re, since there is no grain boundary fracture and the oxides are isolated. The influence of these on the macroscopic mechanical properties of the material is discussed in section 8.2.4. This also renders evident that the solubility of nitrogen in Cr-Re is higher than the solubility of oxygen, since in samples exposed to air there is precipitation of oxides at grain boundaries, which are preferential diffusion paths for light elements, while in samples exposed to nitrogen, despite the diffusion of the element into the sample, there is no precipitation of second phases.

6.3 Influence of the HT exposure on the ductility of Cr-Re alloys

Three point bending tests were used to characterize the ductility of Cr-35Re samples exposed to air and nitrogen at 1500°C during 30’ and 1h. Supports with a tip diameter of 500 µm were employed for the test. The ductile to brittle transition temperature of the alloys after exposure is defined as the minimum temperature at which the samples can be bent to an angle to 90° by means of this device. The test was also used to determine the adherence of the protective layer to the substrate and the fracture mechanisms of the alloys after high temperature exposure to air and nitrogen.

6.3.1 Adherence of the surface layer

Surface layer adherence was tested by means of three point bending. Layers formed on samples during high temperature exposure to air and nitrogen show a strong adherence to the substrate, independently of the exposure time and atmosphere. In

some samples delamination of the surface layers occurs in the area where deformation attains its highest value in three point bending.

6.3.2 Material ductility

The exposure to high temperature air and nitrogen has a strong influence on the ductility of the Cr and Cr-35Re alloys. BCC refractory metals have a strong tendency to high temperature embrittlement. In chapters 4,5 and 6, it has been stated that Re is though to increase the resistance to embrittlement of Cr based alloys by increasing the solubility of light elements in the material, although there is little literature data on this phenomenon.

To determine the effect of Re on the solubility of light elements in the material at high temperature and on the resistance to embrittlement of the alloys, the DBTT of the samples exposed to air and nitrogen at high temperature was measured by three point bending. The lowest temperature at which the samples can be bent up to 90° without fracture is considered the DBTT of the material. The microstructure of the alloys and the fracture surfaces were also investigated. Cr-18Re alloys were not tested due to the spontaneous intergranular fracture behaviour that they present and that rendered them not useful for the application within the schedule of this work..

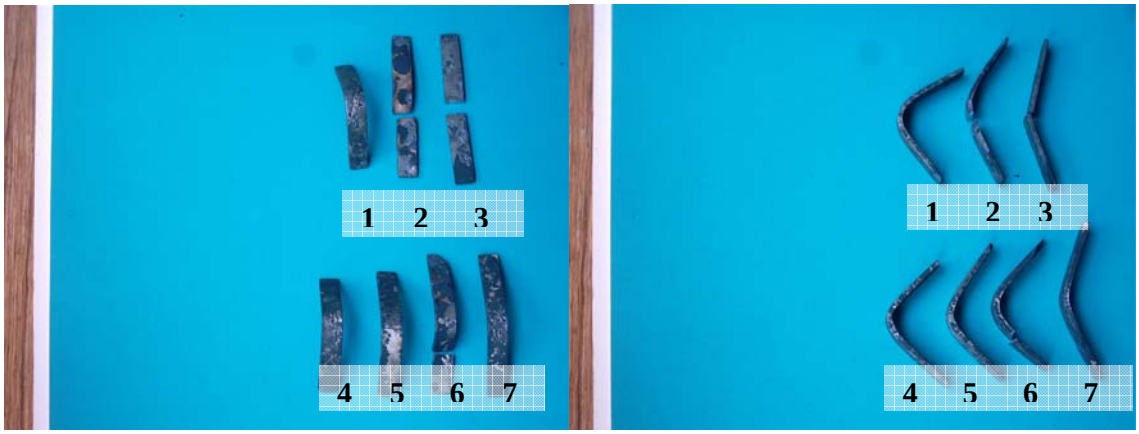

Figure 6.9: Influence of the exposure to nitrogen at high temperature on the ductility of pure Cr.

1 h 1500 °C, N_2: 1-T_{test}=200°C; 2-T_{test}=100°C; 3-T_{test}=300°C
30' 1500 °C, N_2: 4-T_{test}=400°C; 5-T_{test}=200°C; 6-T_{test}=100°C; 7-T_{test}=350°C

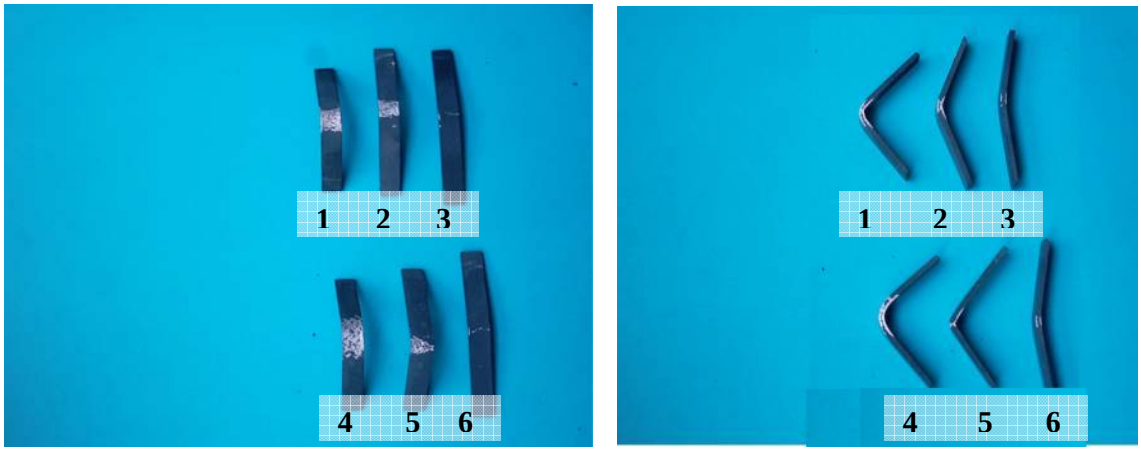

Figure 6.10: Influence of the exposure to nitrogen at 1500°C on the ductility of Cr-35Re

1 h, 1-T_{test}=300°C; 2-T_{test}=100°C; 3-T_{test}=200°C
30' 4-T_{test}=200°C; 5-T_{test}=300°C; 6-T_{test}=100°C

The deflection necessary to obtain a 90° angle in this test was 9,5 mm, which was attained by all Cr-35Re samples tested at room temperature before exposure. Table 6.2 shows the maximum deflections obtained from Cr-35Re after exposure to air and to nitrogen. Table 6.3 shows the results obtained on pure Cr for reference purposes. Samples bent at different temperatures are shown in figures 6.9 to 6.11.

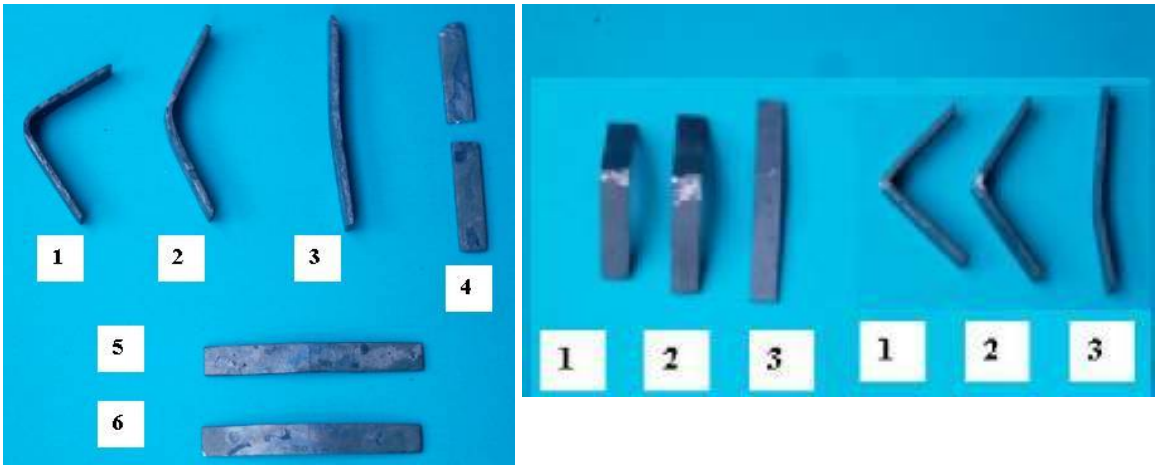

Figure 6.11: Influence of the exposure to air at 1500°C air on the ductility of Cr and Cr-35Re

Left: Pure Cr,
Exposure time 1h: 1-T_{test}=600°C; 2-T_{test}=500°C; 3-T_{test}=400°C; 4 -T_{test}=100°C
Exposure time 30': 5-T_{test}=500°C; 6-T_{test}=300°C

Right: Cr-35Re
Exposure time 1h: 1-T_{test}=400°C; 2-T_{test}=300°C; 3-T_{test}=200°C

The increase in the resistance to embrittlement observed in Cr-35Re samples is related to the lower content of intergranular oxides in the grain boundaries in these alloys after exposure to high temperature. Literature indicates that the solubility of oxygen and nitrogen in the Cr-Re alloys increases with the concentration of Re. Figures 6.12 and 6.13 show that the there is very little internal precipitation in Cr-35Re alloys, in particular in the grain boundary region.

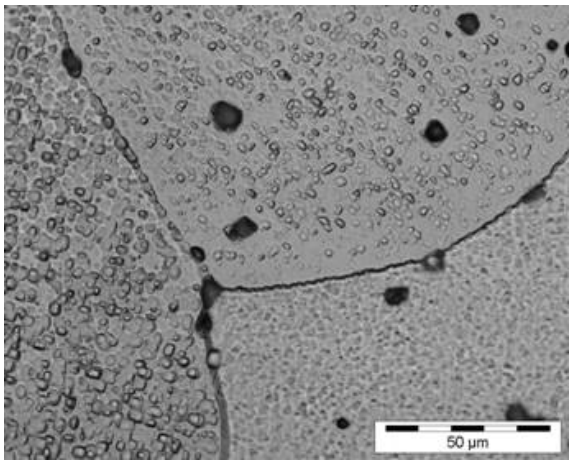

Figure 6.12: Grain grain boundaries of pure Cr after 1h. exposure to air at 1500°C.

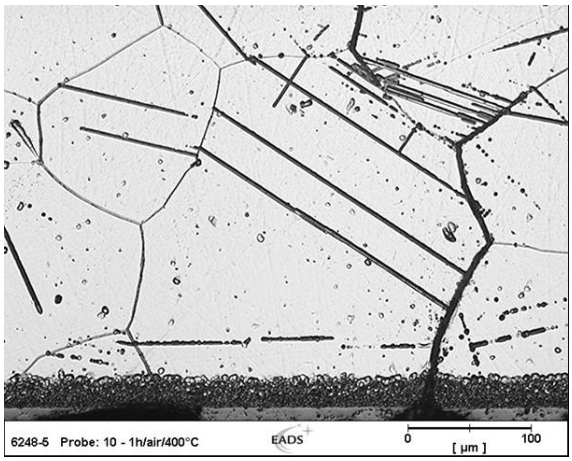

Figure 6.13: Microstructure of Cr-35 Re sample #14 after 1h. exposure to air at 1500°C and 3 point bending which cause the twinning.

Table 6.2: Control of size, weight and bending deflection change of Cr-35Re samples after annealing

			#	Initial dimensions		Initial mass, g	Sizes after annealing		Mass after exposure , g	Test temperature, oC	Deflection mm
				h, mm	b, mm		h, mm	b, mm			
Cr - 35 at. % Re	Annealing in air	1500 °C; 0,5 h	4	0,91	3,43	1,0654	1,11	3,52	1,0661	300	2,7
			5	0,91	3,52	1,0826	0,96	3,53	1,0841	400	9,5
			6	0,9	3,41	1,013	0,93	3,43	1,0146	500	4,4
			7	0,89	3,44	1,0123	0,94	3,47	1,0112	600	3,9
			8	0,89	3,44	1,035	1	3,44	1,0347	500	1
			9	0,89	3,43	1,0139	0,98	3,45	1,0111	200	0,9
		1500 °C; 1 h	10	0,89	3,44	1,0282	0,95	3,44	1,0302	400	0,9
			11	0,89	3,44	1,0538	0,92	3,46	1,05	600	2
			12	0,88	3,42	0,9376	0,9	3,44	0,9387	500	5,3
			13	0,98	3,65	1,2127	1	3,68	1,2142	200	6,5
			14	0,99	3,65	1,2519	1,03	3,67	1,244	300	9,5
			15	0,99	3,7	1,2131	1,08	3,75	1,211	100	1,1
	Annealing in nitrogen	1500 °C; 0,5 h	16	1,01	3,51	1,2592	1,03	3,53	1,2665	400	9,5
			17	0,99	3,68	1,2601	1,01	3,71	1,2661	300	6,9
			18	0,97	3,52	1,2206	0,99	3,55	1,2265	350	9,5
			19	1	3,51	1,2285	1,02	3,53	1,2343	200	9,5
			20	0,95	3,73	1,1587	0,97	3,75	1,1661	100	1,2
											0
		1500 °C; 1 h	21	1,02	3,51	1,2738	1,05	3,55	1,2843	350	9,5
			22	0,95	3,57	1,0933	0,98	3,6	1,1047	300	9,5
			23	0,99	3,64	1,2263	1,01	3,67	1,2362	200	1,1
			24	1,01	3,53	1,2485	1,05	3,55	1,2596	100	3,2
											0

The results indicate that the ductility of Cr-35Re alloys is more dependent on the presence of oxides in the grain boundaries than to the interstitial contamination by the diffusion of nitrogen into the substrate, which does not result in the precipitation of nitrides. The influence of Re on the resistance of the alloys to embrittlement by light elements is particularly noticeable on the samples exposed to air, ductile behaviour is observed even at 300 °C while on pure Cr the DBTT after exposure to air at 1500°C for 1 h. is 600 °C. The scattering of the results is due to the relative

large grain size of the samples, which covered sometimes the whole transversal section of the samples.

Table 6.3: Control of size, weight and bending deflection change of Cr samples after annealing

Cr			#	Initial dimensions		Initial mass, g	Final dimensions		Final mass, g	Test temperature, °C	Deflection, mm
				h, mm	b, mm		h, mm	b, mm			
Chromium	Annealing in air	1500 °C; 0,5 hour	1	0,97	4,04	0,7546	1	4,02	0,7344	200	3,4
			2	1,02	4	0,7838	1,07	4,01	0,7598	300	2,4
			3	1,09	3,97	0,8741	1,15	3,95	0,849	400	1
			4	1,04	3,95	0,8073	1,1	3,97	0,7874	500	0,9
			5	1,09	3,97	0,8687	1,15	3,98	0,847	600	0,8
			6	1,06	4,01	0,8309	1,1	3,99	0,801	300	0,5
		1500 °C; 1 hour	7	1,06	3,99	0,846	1,17	4,01	0,8253	400	0,4
			8	1,07	4,05	0,8489	1,08	4,08	0,8177	500	3,6
			9	1,06	3,89	0,7915	1,08	3,83	0,7519	600	9,5
			10	0,98	3,86	0,7537	1	3,83	0,7155	100	0,4
			11	1,03	3,98	0,7997	1,01	3,96	0,7672	200	0,3
			12	0,96	4	0,7307	0,97	4,05	0,7031		
	Annealing in nitrogen	1500 °C; 0,5 h	13	1,09	3,96	0,6485	1,13	3,99	0,6468		
			14	1,04	3,97	0,8005	1,06	3,99	0,8005	400	9,5
			15	1,05	3,94	0,8133	1,07	3,96	0,8156	300	2,9
			16	1,05	4	0,8243	1,07	4,01	0,8176	350	3,6
			17	1,09	3,95	0,8484	1,11	3,97	0,8478	200	5,6
			18	1,1	3,99	0,8356	1,14	4,02	0,8352	100	8,5
		1500 °C; 1 h	19	0,99	3,95	0,7282	1,02	3,97	0,7213	300	0,7
			20	1,04	3,95	0,7847	1,06	3,98	0,777	350	9,5
			21	1,02	3,93	0,782	1,05	3,96	0,7745	200	9,5
			22	1,03	4,03	0,8029	1,06	4,03	0,7942	300	9,5
			23	1,03	4,01	0,7761	1,05	4,05	0,7719	100	5,1

6.4 Discussion

Re has a positive effect on the high temperature chemical stability of Cr. Exposure to air at 1500°C indicates that the stability of the protective surface oxide layer is increased with Re contents approaching the solid solution limit. Delamination of the layer is typical for pure Cr exposed to oxygen at temperatures above 1100°C. On samples containing 35% Re, the layer does not delaminate nor peel off even after quenching. Samples produced from cast Cr-18Re alloys presented strong intergranular corrosion, leading to grain boundary fracture. This is due to the high concentration of Cr in the grain boundaries of Cr-18Re alloys, an issue that has been discussed in chapter 5.

The ductile to brittle transition temperature of near solid solution limit Cr-35Re alloys is influenced by the high temperature exposure to air, basically because of precipitation of oxides in the grain boundaries. DBTT attains 300 °C after 1,5h at 1500 °C in air. The increase of the DBTT in pure Cr is more pronounced than in near solution limit Cr-Re alloys, reaching 600°C after 1.5h at 1500 °C in air. This is related to the higher concentration of oxides in grain boundaries after exposure due to the lower protection offered by the surface oxide layer formed on pure Cr and to the lower solubility of oxygen in the pure Cr matrix which favours precipitation in crystal lattice defects.

High temperature exposure to nitrogen does not produce a significant increase in the DBTT of near solid solution limit Cr-Re alloys. This is due to the higher solubility of nitrogen in the Cr-Re matrix, with no visible precipitation of oxides at grain boundaries. Pure Cr presents the same behaviour. This is not typical of BCC refractory metals that exhibit a strong tendency to nitrogen embrittlement. All the samples that were tested presented surface originated fracture, with little trace of grain boundary failure. It is possible that the high solubility of nitrogen in the matrix at 1500 ^{o}C handicaps the precipitation of nitride on grain borders. Nitrogen in solution in the grains has a much lesser influence than nitrogen present in grain boundaries in precipitate form, which is usually observed after exposure to nitrogen at 1100-

1400°C. This leads to the conclusion that at temperatures over 1400 °C, the difference of nitrogen solubility in the grains and the grain boundaries is low.

The high dispersion of the results is related to the large grain size of the material that meant that between 1 to 6 grains supported the load on the transverse section of the samples. Reducing the grain size may improve the stability of the ductility of the material and allow produce more precise measurements.

7. Behaviour in vacuum

7.1 Introduction

The external surface of the combustion chamber structure is exposed to absolute vacuum conditions during operation. Metal loss in this area during high temperature operation due to the high vapour pressure of Cr could be an additional failure mechanism of the combustion chamber, in particular in case that preferential evaporation takes place in grain boundaries, which could act as a crack initiator during thermal cycling. In Cr-Re alloys Cr vaporization could produce significant composition changes on the surface layers of the alloy leading to embrittlement of the material.

A series of tests on Cr, Cr-18Re and Cr-35Re was defined to characterize the structural and chemical changes that take place on the external surface of the combustion chamber in service conditions and to determine:

- Applicability of the alloys in vacuum
- Contribution of evaporation to the degradation mechanisms
- Influence of thermal etching on the properties of the material

7.2 Experimental technique

Cr, Cr-18Re and Cr35Re samples polished to1µm surface roughness were annealed at 1400°C and 10^{-3} Pa during 30', 1h and 2h. Cr-18Re and Cr-35Re alloys samples were also annealed at 1600 °C and 1700°C and 10^{-3} Pa during 30', 1h and 2h. Cr was not tested at this temperature due to the high evaporation rate observed at 1400°C. Samples were weighted before and after annealing and their size measured with a precision of 1µm. After annealing the surface of the samples was characterized by means of SEM.

7.3 Results

Pure Cr

An experimental evaporation rate of approximately 125 μg cm^{-2} h^{-1} was obtained for pure Cr at 1400°C, this is equivalent to a metal recession rate of 0,17 mm/h. This value corresponds well with literature data and has been used to determine the precision of further results. Values at higher temperatures were not found in the literature. Increasing the temperature to 1600 and 1700°C further increases the evaporation rate of Cr up to levels corresponding to a metal recession rate of 0.5 mm/h at 1600 °C.

Cr-18Re

Increasing the content of Re in the alloy increases its vapour pressure. The mass loss of Cr-18Re alloys exposed at 1400 °C and 10^{-3} Pa during 0,5, 1 and 2 hours is negligible. However, the phenomenon of spontaneous grain fracture observed in chapter 6 can also be observed after exposure to vacuum. This indicates that Cr-18Re grain boundaries evaporate from 1400°C. Grain boundaries of Cr-18Re alloys are particularly rich in Cr, due to the tendency of Cr to segregate Cr to the grain boundaries during fabrication and high temperature exposure.

Cr-35Re

Cr-35Re presents a negligible metal loss at 1400°C. Microscopically it can be observed that Cr-35Re shows some thermal etching on the surface of the samples. This phenomenon is known in BCC metals; where the crystallographic orientation of each particular grain is linked to a specific vapour pressure. Generally, highest density planes evaporate at a faster rate because of their higher surface energy [Trefilov, 1975], but in BCC refractory metals, it is not the highest density plane, {110} but the plane {100} that has the highest surface energy and the highest evaporation rate. Figure 7.1 shows how crystallographic orientation influences the various thermal etching patters. Grains cutting the surface in orientations close to the plane {100} evaporate perpendicularly to the surface, and leave flat patterns observed in figure 7.1a and grains cutting the surface in oblique orientations are patterned with

pyramidal geometries seen in figure 7.1b. The remarkable metal loss in Cr-18Re is shown in figure 7.1c.

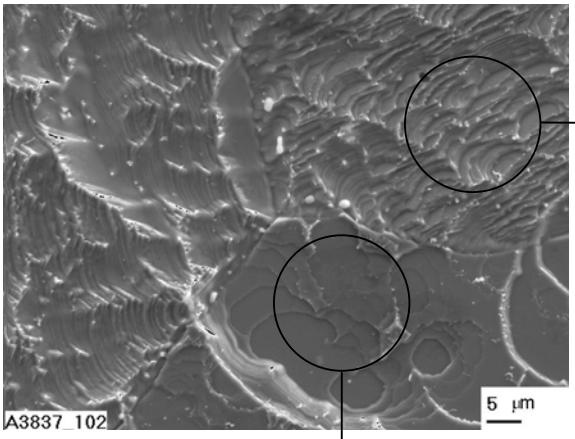

Figure 7.1: Thermal etching in a Cr-35 Re alloy exposed at 1400 °C during 1 h.

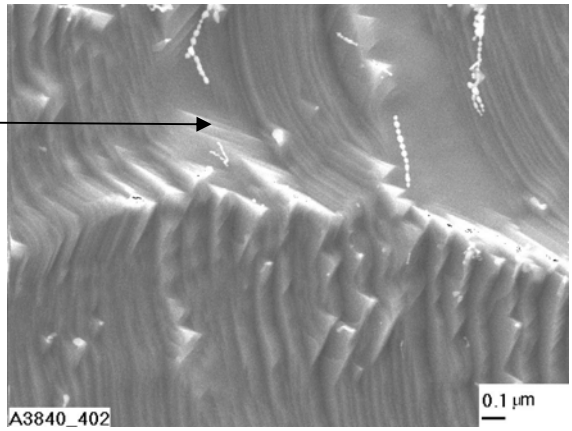

Figure 7.1a: Thermal etching in an area where {001} planes are oblique to the grain surface.

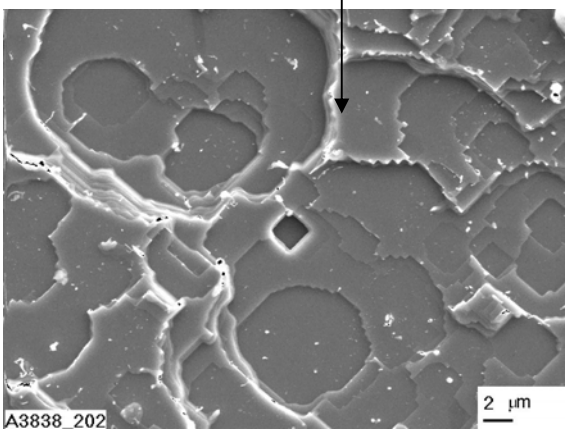

Figure 7.1b: Thermal etching in an area where {001} planes are parallel to the grain surface**.**

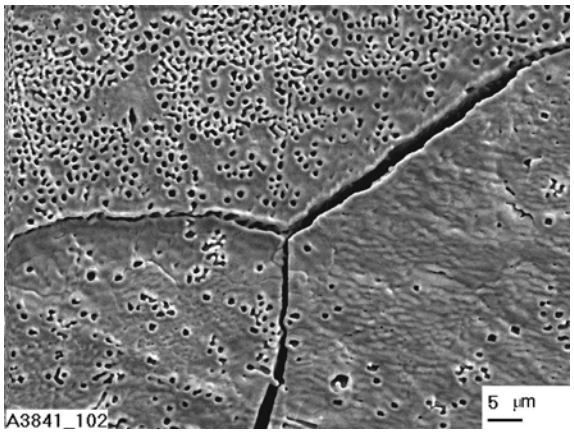

Figure 7.1c: Metal loss in grain boundaries and bulk grain in Cr-18Re alloy exposed at 1400°C and 10^{-3} MPa during 1h.

Increasing the temperature to 1600 and 1700°C accelerates evaporation in both Cr-18Re and Cr-35Re. Figure 7.2 shows that the spontaneous fracture behaviour observed in Cr-18Re alloys can be observed macroscopically 1700°C. Surface porosity in Cr-35Re alloys is evident after 2h exposure at 1600°C, this does not result into a selective evaporation of Cr at the grain boundaries, which is the case of Cr-18Re alloys, but in a homogeneous loss of Cr on the sample surface.

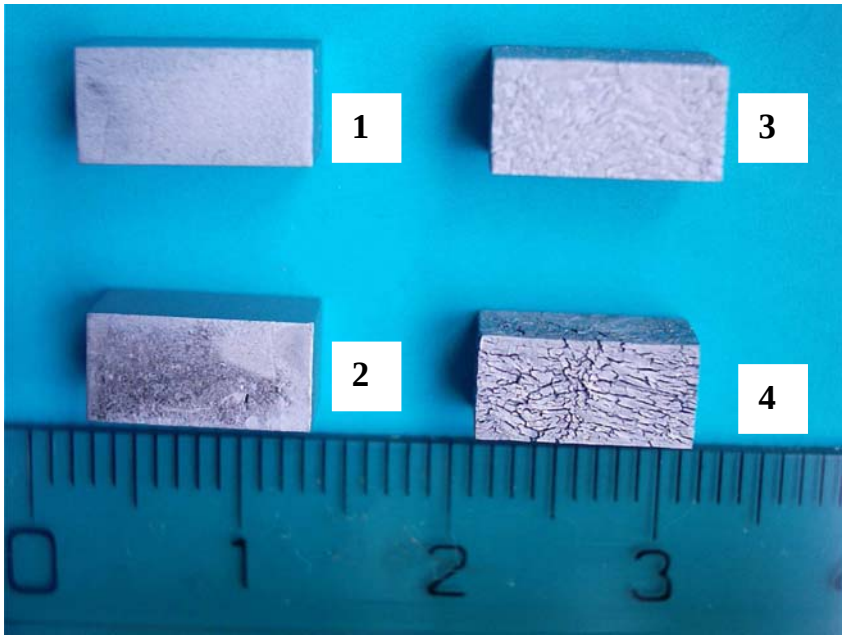

Figure 7.2: Cr-35Re and Cr-18Re samples after exposure to 1600°C and 1700°C during 1h at 10^{-3} Pa

- Sample 1: Cr-35Re exposed 1h at 1600 °C
- Sample 2: Cr-35Re exposed 1h at 1700 °C
- Sample 3: Cr-18Re exposed 1h at 1600 °C
- Sample 4: Cr-18Re exposed 1h at 1700 °C

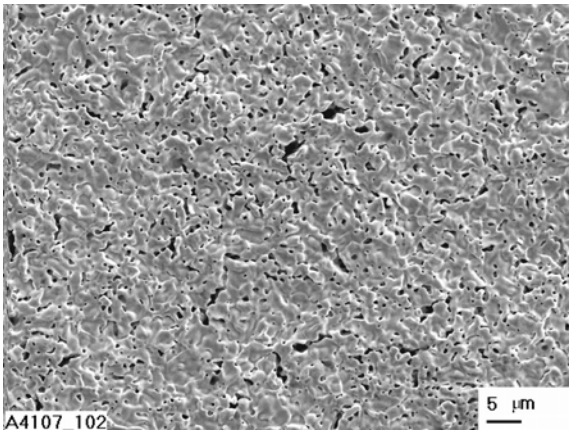

Figure 7.3a: Surface of Cr-35Re alloy after exposure to 1600°C at 10^{-3}Pa during 2h

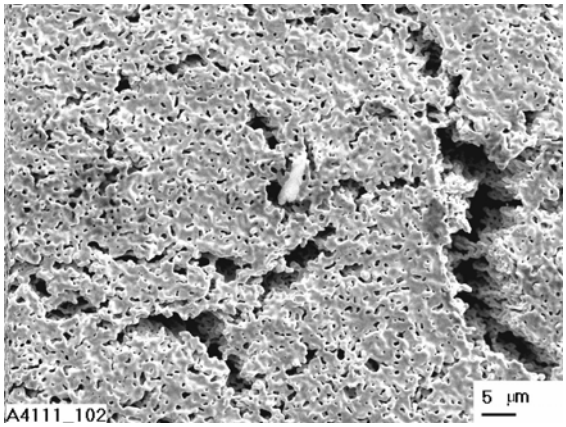

Figure 7.3b: Surface of Cr-18Re alloy after exposure to 1600°C at 10^{-3}Pa during 2h

Increasing the annealing temperature from 1600°C to 1700°C changes the etching behaviour of the material. Figures 7.4a and 7.4b show the surface structure of Cr-18Re and Cr-35Re samples annealed at 1700°C. Sample disintegration is evident in Cr-18Re alloys (figure 7.5), which do not show an important mass loss. Cr-35Re alloys also present some metal loss in the form of surface porosity and grain boundary cracks near the sample surface. Metal loss is very low in both Cr-18Re and

Cr-35Re alloys, but this parameter is not enough to measure the high temperature alloy stability in vacuum since selective Cr metal loss can fracture the alloy or weaken grain boundaries. A further element contributing to alloy degradation due to Cr loss is the increase of surface hardness, particularly remarkable in Cr-35Re alloys exposed to 1700°C at 10^{-3}Pa during 2h. The surface hardness of the alloy is increased on the surface layer to a value of 16-18GPa. Considering the base alloy hardness of 8 GPa and the absence of a chemical reaction, the increase in hardness may only be related to the precipitation of a new phase. Cr loss may have displaced the alloy composition into the σ phase domain. The fact that surface hardness of Cr-18Re alloys Cr-18Re does not show an increase in surface does not increase backs up this hypothesis.

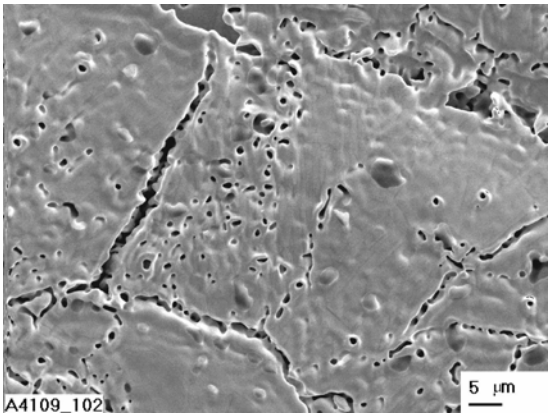

Figure 7.4a: Surface layer of a Cr-35Re alloy exposed at 1700°C and 10^{-3} Pa during 2h.

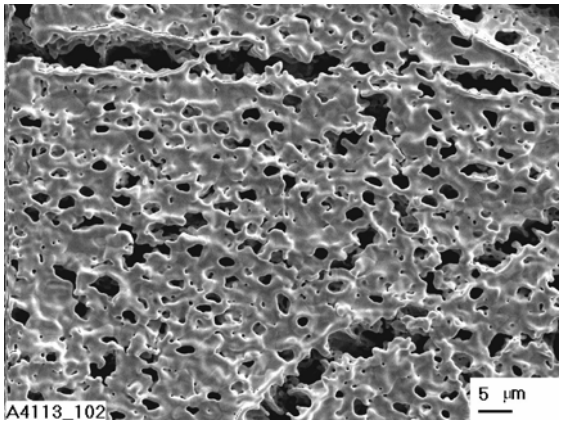

Figure 7.4b Surface layer of Cr-18Re alloy exposed at 1700°C and 10^{-3}Pa during 2h.

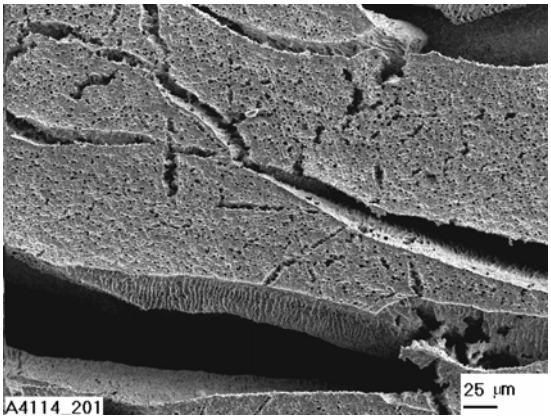

Figure 7.5: Sample disintegration in Cr-18Re alloys after exposure to 1700°C at 10^{-3} Pa during 2h

Table 7.1: Mass change of Cr, Cr-18Re and Cr-35Re exposed at 1400°C and 10^{-3} Pa during 0.5, 1 and 2 h

		1400°C at 10^{-5} Bar, exposition time, [h]			
		0	0.5	1.	2
Cr	Size of sample, mm	5.00x4.98x10.15	4.98x4.72x9.88	4.77x4.42x9.68	4.56x3.91x9.34
	Weight of sample, g	1.785	1.602	1.475	1.085
Cr-18Re	Size of sample, mm	5.06x5.04x10.17	5.05x5.03x10.16	5.05x5.03x10.16	5.04x5.03x10.16
	Weight of ample, g	2.5960	2.5864	2.5800	2.5785
Cr-35Re	Size of sample, mm	4.99x5.05x10.14	4.98x5.05x10.13	4.98x5.05x10.13	4.98x5.05x10.13
	Weight of ample, g	3.271	3.270	3.2704	3.2704

Table 7.2: Mass change of Cr, Cr-18Re and Cr-35Re exposed at 1600°C and 10^{-3} Pa during 0.5, 1 and 2 h

		1600°C at 10^{-5} Bar, exposition time, [h]			
		0	0.5	1.	2
Cr-18Re	Size of sample, mm	5.03x5.02x10.10	5.02x5.04x10.16	5.05x5.03x10.16	5.04x5.03x10.16
	Weight of ample, g	2.590	2.571	2.552	2.548
Cr-35Re	Size of sample, mm	4.99x5.05x10.14	4.98x5.05x10.09	4.98x5.05x10.11	4.98x5.02x10.10
	Weight of ample, g	3.271	3.2706	3.2704	3.269

7.4 Discussion

The addition of Re increases the resistance to sublimation of Cr. Mass change during high temperature exposure in vacuum decreases with increasing Re content. Mass change of Cr-35Re alloys is not measurable after 2h at 1400°C and is very low at higher temperatures. However it has been found that this parameter alone does not

guarantee high temperature stability, since grain boundaries can become unstable after minor loss of Cr, as has been observed in Cr-18Re alloys in the alloy bulk and in Cr-35Re alloys on the surface layer of the alloy.

Grain boundaries of Cr-18Re alloys are unstable at high temperature and present a similar behaviour to the one seen during high temperature exposure to air and nitrogen. This indicates that segregation of Cr to the grain boundaries and its evaporation during high temperature exposure plays a major role in the high temperature stability of Cr-18Re and limits its high temperature applicability.

The increase of vapour pressure in the alloy has not been quantified. Quanlitatively it is related to the higher melting point and vapour pressure of Re, which in solid solution with Cr increases the resistance to evaporation of the alloy. This behaviour is characteristic of solid solutions where the melting point of the solute is much higher than that of the solvent. Near solid solution alloying of Cr with Re improves significantly the resistance of the alloy to vaporization. Considering the objective service temperature of the external surface of the combustion chamber, the applicability of the alloy referred to vacuum has been demonstrated.

8 Determination of the thermal and electric properties of Cr-Re alloys

8.1 Introduction

A further set of parameters that needed to be investigated for the application was the influence of the Re content on the thermal conductivity, thermal capacity and coefficient of thermal expansion in Cr-Re alloys. Electrical conductivity was also measured in this work to verify the results.

The influence of the Rhenium content on the thermal and electrical properties of Cr-Re alloys was investigated in samples of the following compositions:

1. Pure Chromium
2. Chromium with 18 atomic % of Rhenium
3. Chromium with 35 atomic % of Rhenium

The materials used to perform the tests and their main characteristics are shown in table 8.1.

Table 8.1: Samples used to determine thermal and electric properties of Cr-Re alloys

Material	Microstructure	Oxygen content
Pure Cr	Recrystallised	Unknown
Cr 18 at % Re	As cast	1200 ppm
Cr 35 at % Re	Recrystallised	600 ppm
Cr 35 at % Re	As cast	95 ppm

The samples were machined with the geometry required for the thermal conductivity tests represented in figure 8.1. The same geometry was also used to carry out the thermal capacity investigations, which do not request a specific geometry. The two

millimetre diameter hole observed in the figure was drilled to allow the introduction of a thermocouple in the sample.

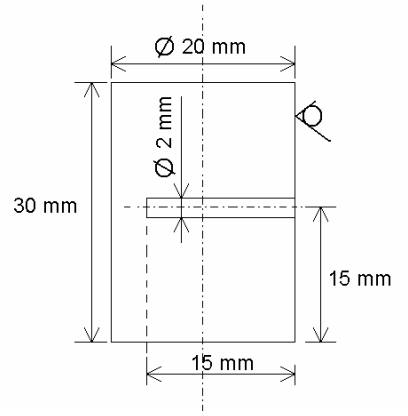

Figure 8.1: Geometry of the samples used for the thermal properties tests carried out in EADS

The four samples already machined and ready for testing are shown in figure 8.2. Their identification numbers correspond to the materials on table 8.1.

Figure 8.2: Samples used for the measurement of the thermal properties

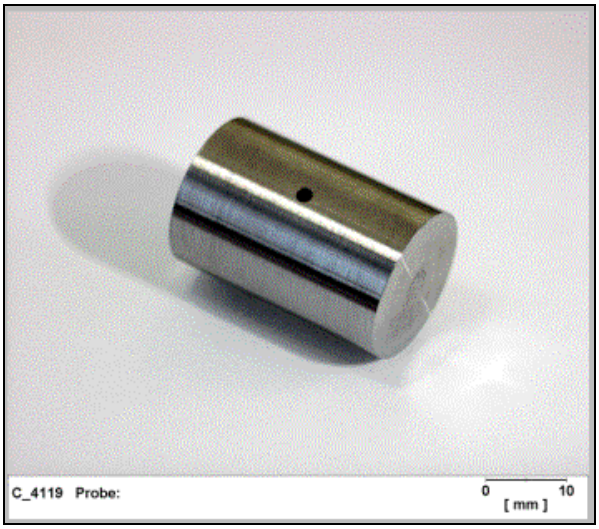

Figure 8.6: Detailed image of sample 4. Chromium 35 at% Rhenium

Additionally, representative samples of Cr, Cr-18Re and Cr-35Re alloys were sent to Netzsch for the determination of the heat capacity and thermal conductivity by laser flash based DSC. The samples which were sent to the Netzsch[1] laboratory where machined into the disc geometry required for the Laser equipment used.

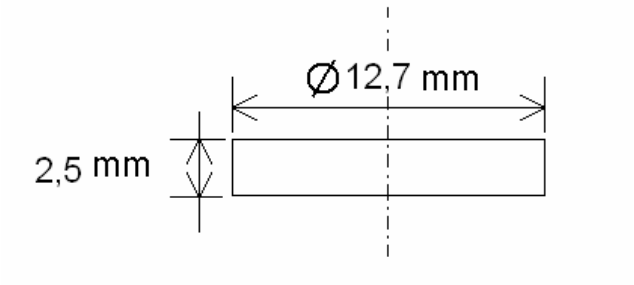

Figure 8.8 > Geometry of the samples mechanized for the temperature conductivity tests carried out by Netzsch

For the measurement of the thermal capacity in the DSC equipment, the requested geometry is a disc with a diameter of 5,5 mm and 1 mm height.

[1] Netzsch-Applikationslabor Sektion Thermophysikalische Eigenschaften
NETZSCH Gerätebau GmbH, Wittelsbacherstraße 42, D-95100 Selb/Bayern,

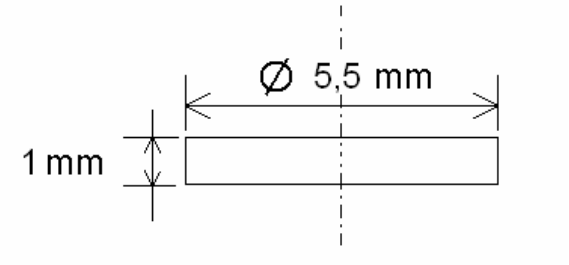

Figure 8.9 > Geometry of the samples mechanized for the thermal capacity tests carried out by Netzsch

8.2 Experimental techniques

8.2.1 Determination of the thermal capacity of Cr-Re alloys

Two procedures were used to determine the thermal capacity, the classic method of heat exchange in an adiabatic container and the differential scanning calorimetry, DSC, method based on a laser flash. Plain calorimeter tests in adiabatic container are standard in EADS and have the inconvenient of requiring relatively large sample geometries. The results shown in this work have been obtained by DSC which has the advantage of needing much smaller samples. Plain calorimeter tests have been used to determine the deviation of DSC from the standard method, which did not exceed 3%. Below the experimental procedure to obtain thermal capacity is discussed. The measurement by adiabatic container is just discussed for reference purposes.

Measurement by adiabatic container

The procedure to measure the thermal capacity by the method of heat exchange with water in an adiabatic container was carried out in the following steps:

1. The sample is heated to a temperature about 100 °C
2. It is introduced into a identified amount of water at a known temperature
3. All the system stays isolated until the equilibrium temperature is reached

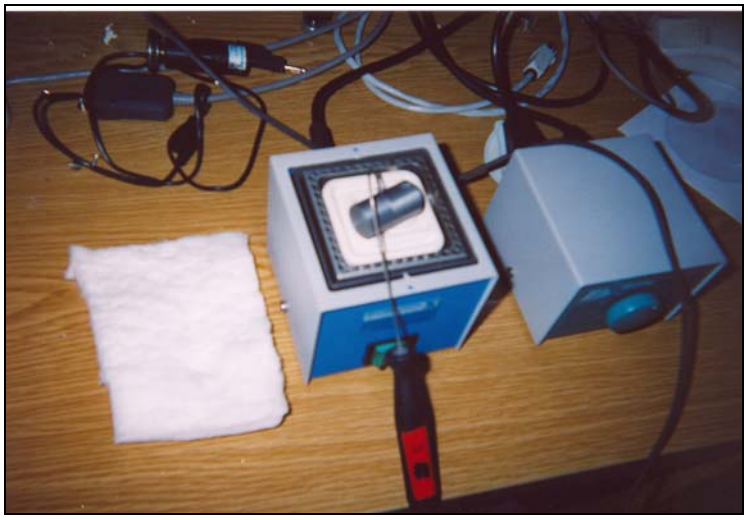

Figure 8.10: Heating of the sample up to T_m

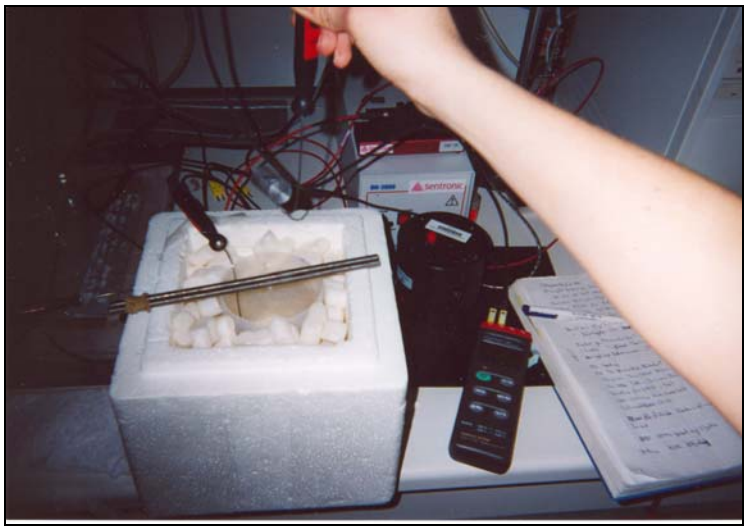

Figure 8.11: Introduction of the sample in the isolated water container

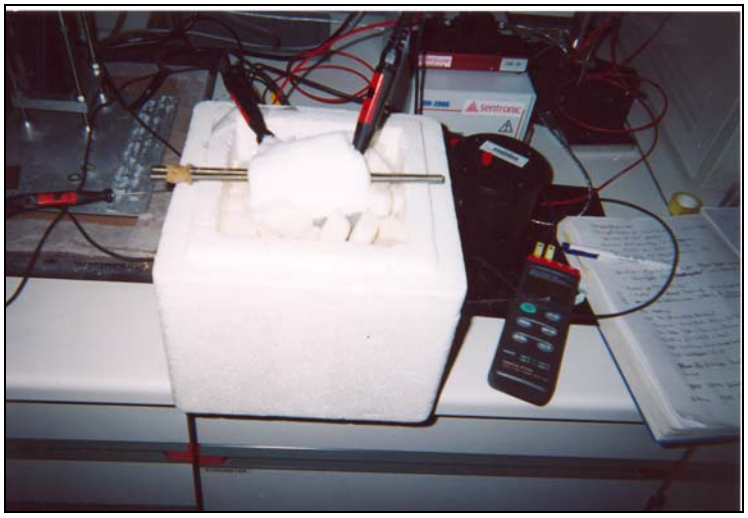

Figure 8.12: Temperature recording to measure the equilibrium temperature

The quantity of heat released by the metal may be calculated by the following, where T_s is the temperature of the heated sample, m_s its weight and c_s its thermal capacity:

$$Q_s = m_s\, c_s\, (T_s - T_f)$$

The heat amount that the water needs to increase its initial temperature, T_w, to the equilibrium temperature, T_f, is:

$$Q_w = m_w\, c_w\, (T_f - T_w)$$

Supposing that the system is perfectly isolated, the heat liberated by the sample is used completely to rise the temperature of the water. So the interchanged heat is:

$$Q = m_s\, c_s\, (T_s - T_f) = m_w\, c_w\, (T_f - T_w)$$

And the thermal capacity of the sample can be calculated:

$$c_s = \frac{m_w\, c_w\, (T_f - T_w)}{m_s\, (T_s - T_f)}$$

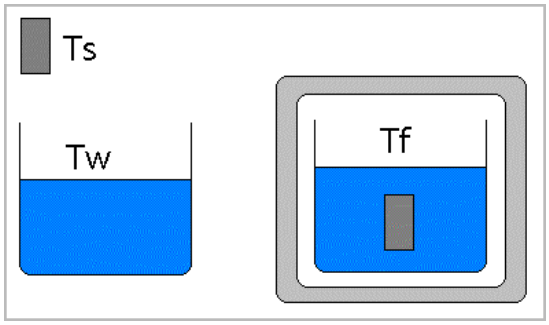

Figure 8.13: Schematic representation of the experimental set-up

Considering that the system is not 100% adiabatic, some part of the heat, Q_L, released by the sample, will be lost though the walls.

$$Q_s = Q_w + Q_L$$

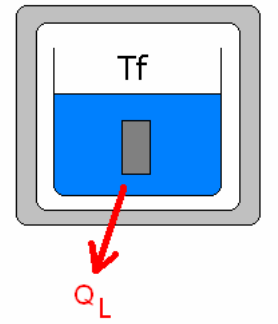

Figure 8.14: Heat loss through the walls

To obtain the thermal capacity of the sample the heat evacuation though the walls should be taken into account:

$$c_{s\,real} = \frac{m_w\, c_w\, (T_f - T_w) + Q_L}{m_s\, (T_s - T_f)}$$

So the measured and the real thermal capacity are related as follows:

$$c_{s\,real} = c_s + \frac{Q_L}{m_s\, (T_s - T_f)}$$

Measurement of the heat capacity by the laser flash DSC method

The measurement of the heat capacity by means of laser flash DSC was carried out with a Differential Scanning Calorimeter DSC 404 C Pegasus®, the characteristics of which are listed bellow:

- Temperature range: -120°C to 1650°C
- Quantitative measurement of the specific heat from -120°C to 1500°C
- Evacuation and operation with purge gas possible

Figure 8.20: Laser flash DSC apparatus 404 C Pegasus used in the study

The equipment used can be operated with three furnace systems, allowing measurements to be conducted over the temperature range of -120 to 1650°C. The heating element design and the furnace placement via a motor-driven furnace hoist yield very stable and reproducible baselines, allowing an accurate measurement of the quantitative specific heat.

8.2.2 Heat conductivity

The measure of the heat conductivity of the alloys was carried out by two methods, by infra-red imaging of the thermal flow in an alloy sample, which is of standard use in EADS and by laser flash apparatus, which was carried out externally. Infrared

imaging is the standard method in EADS and has the inconvenient of requiring relatively large sample geometries. The results shown in this work have been obtained by DSC which has the advantage of needing much smaller samples. Infrared imaging has been used to determine the deviation of DSC. Deviation was insignificant from the standard method. The measurement by means of direct infrared imaging is just discussed for reference purposes.

Measurement by means of infrared imaging

The heat flow was produced in the equipment illustrated in figure 8.15.

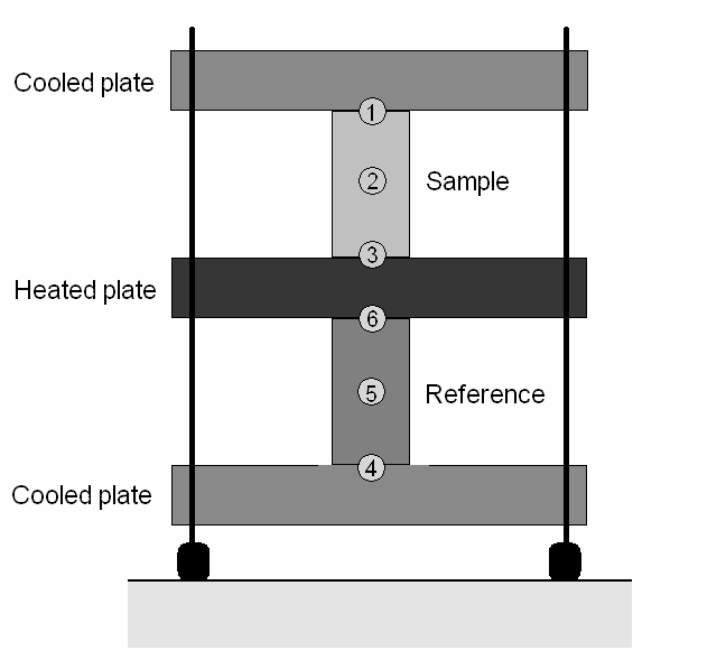

Figure 8.15: Schema of the equipment used to measure heat conductivity by infrared imaging in EADS. Numbers 1 to 6 represent measurement points

The performance of the tests has to get through two phases:

a) Placing two reference samples of known conductivity λ_{REF}, calculus of the power (Watt) necessary at the heated plate to get the measuring temperature T_m.

$$U\,I = \frac{\Delta Q}{\Delta t} = 2\,\lambda_{REF}\,A\frac{\Delta T}{\Delta x}$$

Where λ is the conductivity coefficient and A is the area of the cross section of the samples.

b) Maintaining one of the reference samples, the tested sample is placed and the hot plate is heated up to T_m. When the surface of the sample gets to this temperature, the power of the heater is turned off. The experiment runs until the temperature equilibrium between both surfaces of the samples is established.

$$U\,I = \lambda_{REF}\,A\frac{\Delta T_{REF}}{\Delta x} + \lambda_s\,A\frac{\Delta T_s}{\Delta x}$$

The thermocouples (numbers 1,2,3 for the sample and 4,5,6, see figure 8.15) for the reference provide the temperature of both surfaces as well as the centre of each sample, so the temperature gradient is known every time. The thermal conductivity of the sample can be calculated as:

$$\lambda_s = \frac{U\,I - \lambda_{REF}\,A\dfrac{\Delta T_{REF}}{\Delta x}}{A}\left(\frac{\Delta x}{\Delta T_s}\right)$$

The material used as reference is Inconel 600, Ref:36455 (Alfa Aesar), with a composition Ni:Cr:Fe 72:14-17:6-10 in weight percent.

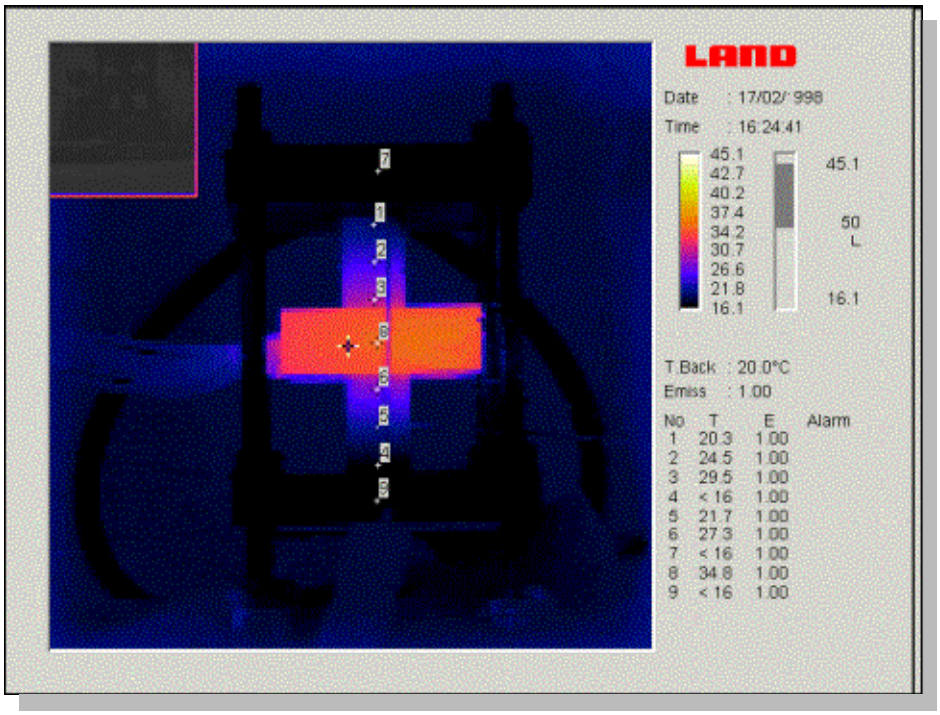

Figure 8.16: Infrared image taken during one test

The tests were carried out in an inert Argon atmosphere, with a gas flux between 50 and 100 ml/min. Measurements were taken from room temperature up to 1200 °C, with a heating rate of 20 K/min.

Atmosphere	Ar
Gas flux	50 - 100 ml/min
Temperature range	RT – 1200 °C
Heating rate	20 K/min

Table 8.2: Parameters used in the determination of the thermal conductivity by infra red imaging.

Measurement by means of DSC based on laser flash

The measurement of the heat conductivity was carried out by a LFA - Laser Flash Apparatus 427. The Laser Flash Method is a thermophysical measuring method which measures the thermal diffusivity of a sample (solid, liquid or powder) at constant temperatures, while monitoring its temperature increase caused by the absorbed energy of laser flash. In principle it is similar to the method used in EADS but it has the advantage of a high precision and a higher temperature range.

The main characteristics of the LFA 427 are:

- Temperature range: -40°C to 2000°C
- Laser with variable power and pulse width
- Vertical system
- Vacuum tight, various atmospheres
- Special sample holders available for powder, liquid (molten metals), slag, fiber and sandwich samples
- Software with 15 separate data evaluation models including finite pulse and heat loss correction

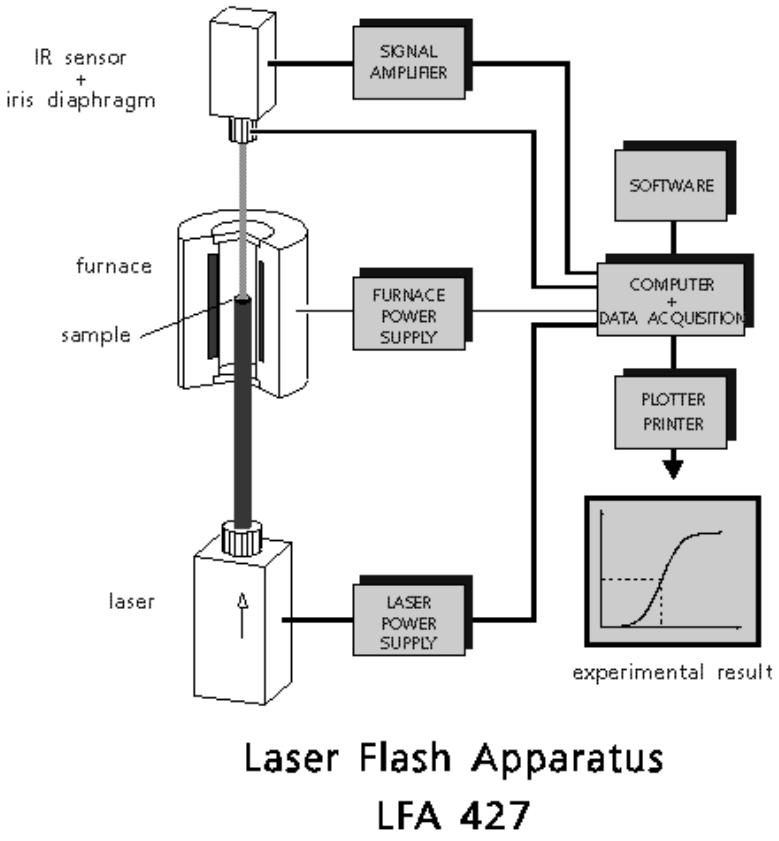

Figure 8.19: Schematic representation of the LFA 427 apparatus

The tests were carried out in identical flow conditions as the infra red imaging measurements. Argon atmosphere, with a gas flux between 50 and 100 ml/min was used. Data were taken in a temperature range from room temperature up to 1200 °C, with a heating rate of 20 K/min.

Atmosphere	Ar
Gas flux	50 - 100 ml/min
Temperature range	RT – 1200 °C
Heating rate	20 K/min

Table 8.2: Parameters used for the determination of the thermal conductivity by laser flash infrared imaging.

The thermal diffusivity can be measured with the NETZSCH LFA 427 over the temperature range of -40 to 2000°C. The thermal diffusivity values can be converted to thermal conductivity using the specific heat and bulk density. A high degree of reproducibility and accuracy, along with fast measurement times, simple sample geometries and small sample sizes, are some of the advantages of thermal diffusivity measurements over the so-called direct thermal conductivity measurement methods. The fact that materials with thermal diffusivity values ranging from 0.001 to 10 cm^2/s can be accurately measured is an additional advantage.

Calculation of heat conductivity

Independently of the method used, thermal conductivity of the tested materials has been calculated by means of the following equation:

$$\lambda(T) = \rho \cdot c_p(T) \cdot a(T).$$

Where

- λ: Thermal conductivity
- ρ: Density
- c_p: Thermal capacity
- a: Temperature conductivity
- T: Temperature

8.2.3 Measurement of electric conductivity in Cr-Re alloys

To perform the electric conductivity measurements, a Sigmascope SMP10 has been used. The SMP10 is a hand-held instrument which provides rapid measurements. It can also operate contact free. The corresponding measurement probe ES40 operates at the measurement frequencies of 60 kHz, 120 kHz, 240 kHz and 480 kHz. For automatic temperature compensation of the conductivity measurement the current temperature of the specimen can be measured using either the temperature sensor integrated in the probe ES40 or an optional external sensor.

Figure 8.17: Equipment used to measure the electrical conductivity, SIGMASCOPE® SMP10

The Measurement range of this equipment is 0.5 – 65 MS/m (Mega Siemens/m) or 1 – 112 % IACS (International Copper Standard). Copper reference material has been used to determine the electric conductivity of the different Chromium-Rhenium alloys using international recognized Boeing standards.

The electric conductivity was measured on the surface of four pieces of the as cast alloys, one face was cut and polished with paper with a grain of 800 to allow contact with the head of the electrical conductivity measurement device.

Figure 8.7 > Samples used for the measurement of the electrical conductivity

1) Cr, 2) Cr-18Re, 3) Cr-35Re, 4) Cr-35Re

8.3 Results

2 types of Cr-35Re alloys were used to determine to which degree the thermal properties of the alloy were sensitive to changes in microstructure. The alloys labelled IND had a recrystallised microstructure with equiaxed polygonal grains and were contaminated by 600ppm of oxygen in solution. The samples labelled ARC have a microstructure corresponding to the alloys described in chapter 5 and can be considered technically pure, with 60 ppm oxygen in solution.

8.3.1 Thermal capacity obtained by means of Laser Flash DSC

Pure Chromium

The evolution of the thermal capacity of pure Chromium as a function of temperature is shown in figure 8.21. The plot shows three distinct zones, below, around and above room temperature. The data below room temperature has been obtained from Trefilov, (1975). The match between measured room temperature heat capacity and bibliographic data showed a deviation of less than 2%.

The contribution of the lattice vibrations (phonons) is proportional to T^3 below room temperature, but in metals, the contribution of the electrons has to be added, resulting in a relationship C-T. Below room temperature the contribution of the electrons to the specific heat is not very significant, as it is proportional to the temperature by a factor of $(\pi^2/3)(k_BT/E_F)$, and even at room temperature this factor is only of order 10^{-2}.

As expected, around room temperature the thermal capacity shows a linear behaviour versus temperature. The prediction of this behaviour is one of the most important consequences of Fermi-Dirac statistics. The linear equation that links the thermal capacity expressed in [J/g K] with the temperature in [K] is: C [J/gK]= 0,0002 T [K] + 0,3756 At room temperature, the thermal capacity of pure Chromium is 0,50 J/gK, value that corresponds well to the classical Dulong-Petit Law, which predicts $3Nk_B$=25 J/molK, for Chromium 0,48 J/gK.

Cr-18Re and Cr-35Re alloys

The thermal capacity of the CrRe alloys has been measured in a temperature range that goes from 25 °C to 1200 °C by means of DSC. Figures 8.24 and 8.25 show the results obtained. No measurements below room temperature were possible due to technical reasons.

The thermal capacity of the alloy is lowered with Rhenium additions. The possible explanation lays in the alteration of the electronic structure of Chromium by the Rhenium addition, as introduced in chapter 3. The density of states at the Fermi level

increases with the addition of Re, so more states are available for the electrons to jump as they get thermally excited. The thermal capacity is defined as the amount of heat that has to be given to a gram of substance to elevate its temperature one Celsius degree. If more electrons are able to contribute to the process, the thermal capacity will be consequently lowered, as the results confirm.

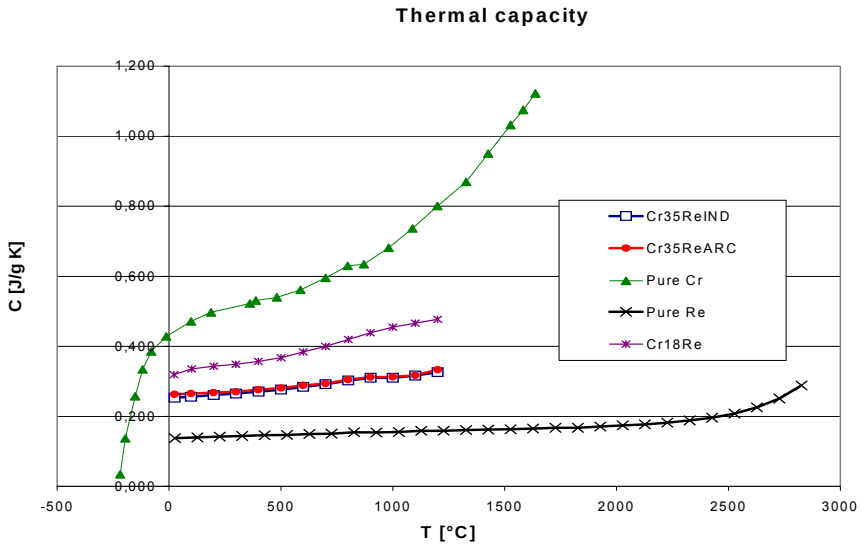

Figure 8.26: Thermal capacity of Cr, Re and Cr-Re alloys.

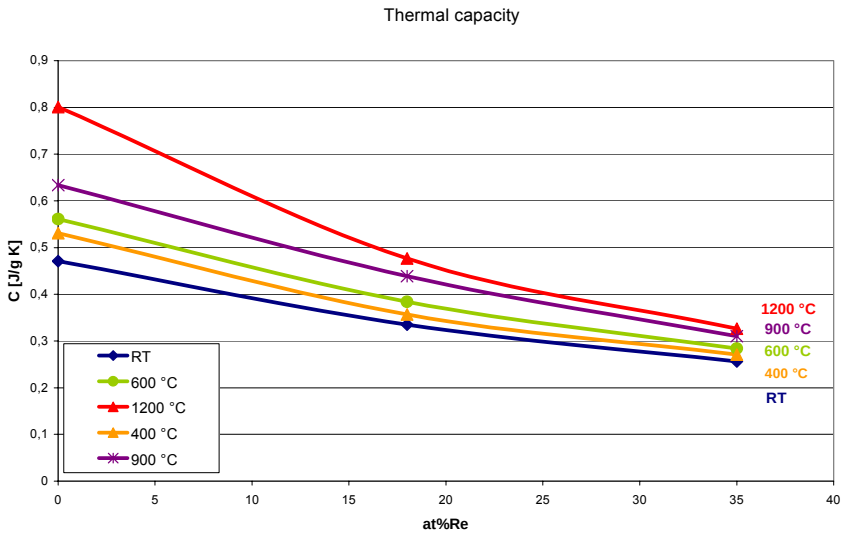

Figure 8.27: Thermal capacity of Cr-Re alloys as a function of Re content at different temperatures

The relationship between the thermal capacity and the Rhenium content can be well expressed through a linear equation, with good correlation for all the temperatures.

Table 8.4: Linear approximation to the relationship C-at%Re expressed as aX+b=Y

20 °C	C = - 0,0062 [at%Re] + 0,4629
	R^2 = 0,9817
400 °C	C = - 0,0075 [at%Re] + 0,518
	R^2 = 0,9691
600 °C	C = - 0,0079 [at%Re] + 0,5499
	R^2 = 0,9798
900 °C	C = - 0,0093 [at%Re] + 0,6247
	R^2 = 0,99
1200 °C	C = - 0,0136 [at%Re] + 0,7751
	R^2 = 0,9641

8.3.2 Thermal conductivity obtained by means of Laser Flash DSC

Thermal conductivity is a probability controlled phenomena, as the thermal energy gets distributed along the sample from the cold zones to the hot ones, suffering along this path frequent collisions. Thus the thermal conductivity is dependant of the electron mean free path, which is limited by the grain size and the lattice imperfections.

Figure 8.29 shows the thermal conductivity results obtained through Laser Flash DSC for Cr-18Re and Cr-35Re alloys, as well as the data for pure Chromium taken from the Handbook of thermophysical properties of solid materials.

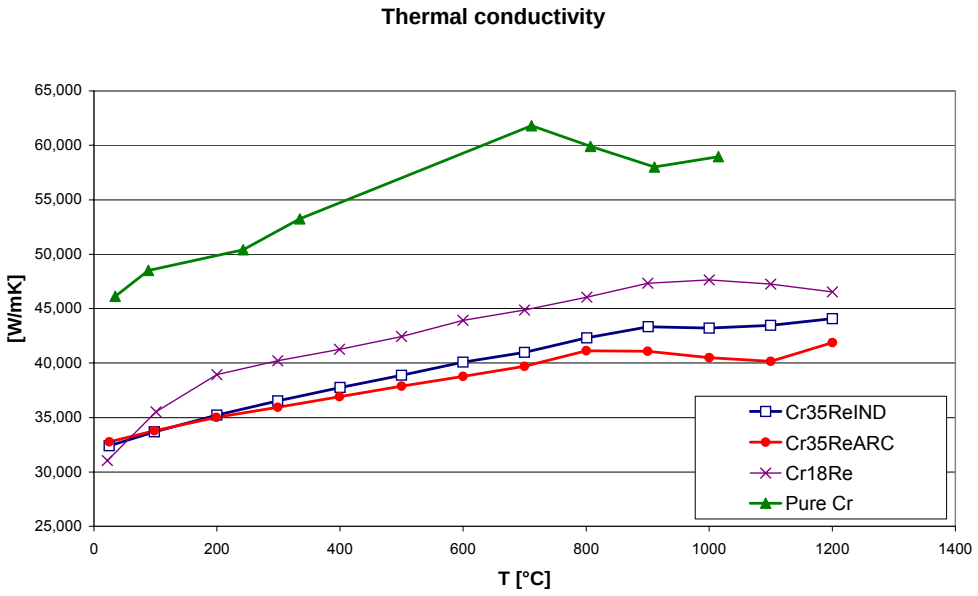

Figure 8.29: Thermal conductivity of different Cr-Re alloys as a function of temperature

The lower thermal conductivity of the Chromium-Rhenium alloys compared to pure Chromium can be understood by the presence of Rhenium atoms in the chromium matrix which reduce the lattice symmetry and increase the number of scatter centres for phonons and electrons, thus reducing the thermal conductivity. The slight difference between the properties of Cr-35Re alloys is discussed in section 8.3.3.

8.3.3 Electric conductivity

The electric conductivity of the sample was measured to get additional information about the properties of the material and make a qualitative study of the electronic structure of the alloy. The electric conductivity of the samples has been determined at 20 °C. Three measurements have been made for each material and average values from 10 measurements have been calculated and shown in figure 8.34. Evolution of electric conductivity is similar to evolution of thermal conductivity. They are strongly lowered as Rhenium is added to the pure Chromium, but do not change much as the Rhenium content increases from 18 at% to 35 at%.

The electric conductivity of Re and room temperature is 5.16 MS/m. Like the thermal conductivity, the electric conductivity is a probability controlled phenomena [6,7] and therefore dependant on the mean free path of the electrons. That explains why the Rhenium addition lowers the electric conductivity, as it disturbs the lattice symmetry.

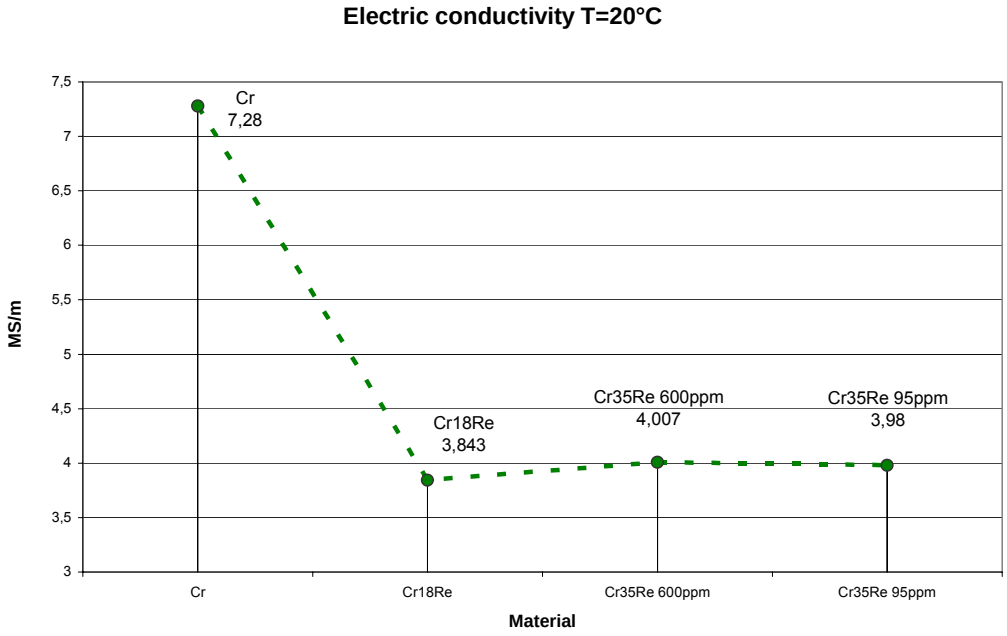

Figure 8.34: Electric conductivity at 20 °C

The fact that the electric conductivity is slightly increased when increasing the Re content from 18 to 35 a% Re is an indication that the Fermi energy of the alloy is increased when increasing Re content. The initial strong decrease due to distortion of lattice symmetry is compensated by the increase of available sites for the electrons to jump, therefore allowing more of them to contribute to the transport of electric current.

8.4 Coefficient of Thermal Expansion

8.4.1 Experimental procedure

Coefficient of Thermal Expansion (CTE) of Cr-Re alloys were investigated between 20°C and 1500°C. The coefficient of thermal expansion was determined on a roller dilatometer with a scale of registration 1:6000. Heating velocity was 10^{o}C per minute. Tests were conducted in protective atmosphere. Cr was measured for reference purposes.

8.4.2 CTE results

Table 8.5.2 shows the CTE of Cr, Cr-18Re and Cr-35Re alloys at different temperatures. CTE of Cr-35Re has a linear dependence with temperature, indicating absence of phase transformations in the alloy. Cr-18Re alloys present the high temperature fracture mechanism discussed in chapters 6 and 7.

Table 8.5: CTE of Cr, Cr-18Re and Cr-35Re from 20 °C to 1500 °C

Temperature interval, [°C]	Coefficient of thermal expansion, [$\alpha x10^{-6}$ °C^{-1}]			
	Pure Cr	Cr-18Re	Cr-35Re	Pure Re
20 – 50	6,2	7,9	8,0	6,2
20 – 100		8	8,1	
20 – 150		8,1	8,2	
20 – 200		8,1	8,2	
20 – 250		8,2	8,3	
20 – 300		8,3	8,3	
20 – 350		8,4	8,4	
20 – 400		8,5	8,5	
20 –4 50		8,6	8,6	
20 – 500	9,8	8.4	8,7	6,1
20 – 550		8.8	8,8	
20 – 600		9	8,9	
20 – 650		9,5	9	
20 – 700		9,8	9	
20 – 750		9,9	9,1	
20 – 800		10	9,2	
20 – 850		10,2	9,3	
20 – 900		10,3	9,5	
20 – 950		11	9,6	
20 – 1000	12,1	Fracture	9,7	6,7
20 – 1050			9,8	
20 – 1100			9,9	
20 – 1150			10,0	
20 – 1200			10,2	
20 – 1250			10,3	
20 – 1300			10,4	
20 – 1350			10,6	
20 – 1400			10,8	
20 – 1450			11	
20 – 1500	14	Fracture	11,2	7,1

8.5 Discussion

It has been observed that Re additions strongly influence the thermal and electric properties of Chromium. The thermal conductivity, thermal capacity and electric conductivity values are significantly lowered.

The thermal capacity of Chromium is lowered as Rhenium is added. The possible explanation lays in the alteration of the electronic structure of Chromium by the Rhenium addition discussed in chapter 2. If the density of states at the Fermi level increases, more states are available for the electrons to jump as they get thermally excited. When more electrons are able to contribute to the process, the thermal capacity will be consequently lowered, as observed. The relationship between C and the Rhenium content can be well expressed through a linear equation, with good correlation for all the temperatures. The influence of the Rhenium content increases with temperature, which can be understood taking in account that as temperature increases, more electrons are thermally excited and can climb to the states, whose density has been enlarged by the addition of Rhenium.

The lower thermal conductivity of the Chromium-Rhenium alloys compared to pure Chromium can be understood by the presence of Rhenium atoms in the chromium matrix which reduces the lattice symmetry and increases the number of scatter centres for phonons and electrons, thus reducing the thermal conductivity.

The tests have shown that the thermal properties of the Cr-35Re samples with different microstructure differ slightly. The difference, of about 3-10% depending on the temperature, is not large, but significant enough not to be elapsed. A possible reason for the differences found in the thermal capacity values is that the segregation of Cr to the grain boundaries of the recrystalised material lowers its thermal capacity and increases its conductivity as the Cr segregations constitute a continuous network of material with a higher heat conductivity.

The electric conductivity is strongly lowered as Rhenium is added to the pure Chromium, but does not change much as the Rhenium content increases from 18

at% to 35 at%. Like the thermal conductivity, the electric conductivity is a probability controlled phenomena, and therefore it is dependant of the mean free path of the electrons. Re disturbs lattice symmetry and electric conductivity sinks. The slight increase of the conductivity observed in Cr-35Re over Cr-18Re may be due to the increase in the density of states which are available for the electrons to jump, therefore allowing more of them to contribute to the transport of the electric current.

Concerning the applicability of the alloy for satellite thruster combustion chambers, the decrease in thermal capacity and the decrease of thermal conductivity cannot be considered as positive effects of Re additions to the alloy, since both contribute to a theoretically lower thermal shock resistance. The fact that the CTE of the alloy decreases at high temperature with Re content is a positive contribution to the thermal shock resistance of the alloy.

The combination of the parameters investigated in this chapter does not allow making a clear estimation on how the thermal shock resistance of the alloy, critical for the application will evolve by increasing Re content. Therefore a non standard and application specific thermal shock test had to be made to test the behaviour of the alloy under solicitation. This test, combining all solicitations on the material is defined in chapter 9.

9 Thermal shock and thermal gradient resistance of Cr and Cr-Re alloys

9.1 Introduction

During operation the combustion chamber structure is exposed to linear thermal gradients of 500 K/mm and thermal shocks of 500K/min during 100cycles. The most widely used test to measure thermal shock resistance of materials is quenching in a liquid media. This type of test does not allow measuring the resistance of the alloy to thermal gradients, a solicitation that resulted in the formation of cracks in the combustion chamber tested in chapter 1. Resistance to thermal shock is a parameter dependent on several variables, basically the Coefficient of Thermal Expansion (CTE) of the alloy, its mechanical properties and its thermal conductivity. Cr-Re alloys have an increased mechanical resistance even at very high temperature and a low CTE. Their thermal conductivity is however decreased, the experimental investigation of the mechanical properties of the alloy is therefore necessary.

There is no single standard test to reproduce these solicitations so a special rig was constructed in the framework of this work on the basis of an arc melt furnace. This rig reproduces qualitatively the thermal shock on the alloy surface and the thermal gradient in the cooling film breaking point on the structure.

9.2 Experimental techniques

An arc melt furnace with a tungsten electrode was used to produce the high energy spark necessary to heat up the sample. A water cooled copper crucible was adapted with a top plate with 4 cavities which were machined to fit 4 samples of 20x5x5 mm.

Samples were cooled to -20°C to contract them and then clamped on its base on the copper water cooled crucible shown in figure 9.1 by means of a screw. Electric arc power was set to guarantee that a pure Cr sample was melt on the surface in approximately 4 seconds, the equivalent of a heating rate of approximately 500K/s. Electric arc was held on the sample for 20 s.

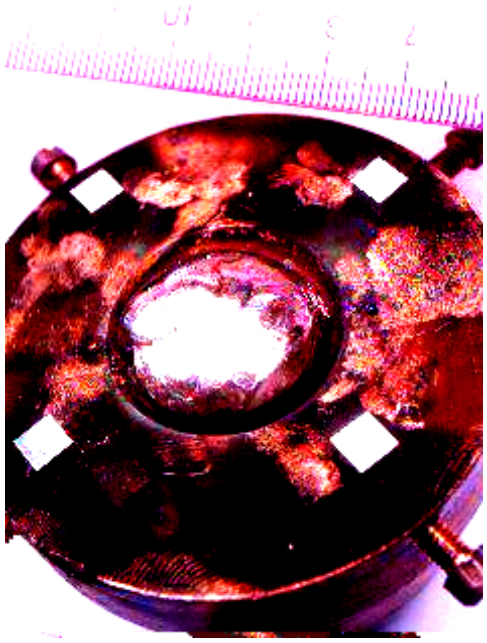

Figure 9.1: Water cooled copper crucible with Cr-Re alloy samples inserted in cavities

The tight clamping in the water cooled copper crucible guaranteed that a strong thermal gradient was present in the clamping area, reproducing the temperature gradient of point C in figure 1.14, corresponding to the cooling film breaking point in the real application in addition to the electric arc-induced thermal shock of about 500°C/s on the surface.

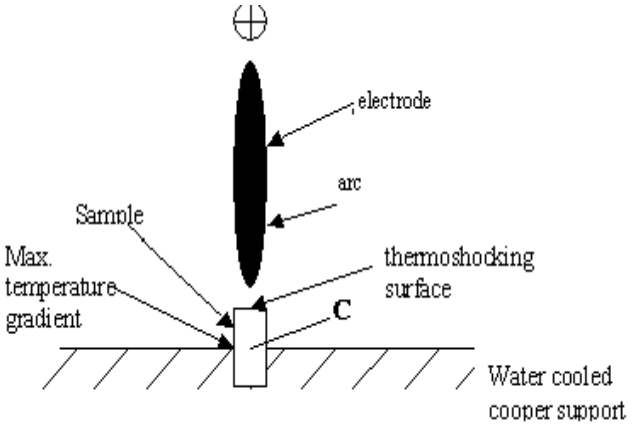

Figure 9.2: Schematic representation of the experimental device used to test the thermal shock resistance. Conditions in point C correspond to the cooling film braking point in the application.

The exact temperature gradient could not be measured but can be considered as the technically highest attainable with the available equipment and is highly linear due to the geometry of the rig. After exposure to heat during 20 s, samples cooled down attaining room temperature at the centre of the unclamped area after approximately 2 minutes. Figure 9.2 shows a representation of the rig.

A maximum cooling rate of 200°C/s was obtained during the first 2 to 4 seconds directly after electric arc removal. Samples were cycled 100 times and characterised for microstructure and micro cracking after the test.

9.3 Results

Thermal stress was sufficient to warp pure Cr but could not permanently deform Cr–Re samples. Figure 9.3 shows that Cr-18Re did not present any internal cracks in the high thermal gradient area, twinning is evident around the interface area between the heated and cooled areas of the sample. The surface of the sample did not withstand the cyclic thermal shock. Figure 9.3 shows that Cr-18Re samples presented grain boundary cracks on the heating surfaces up a depth of approximately 1mm. This may be related to segregation of Cr to grain boundaries that may have melt during heating of cracked during cooling. Pure chromium samples used to set the test parameters presents no micro cracking at grain boundaries of the thermally shocked surface. The presence of porosity indicated that localised melting has occurred.

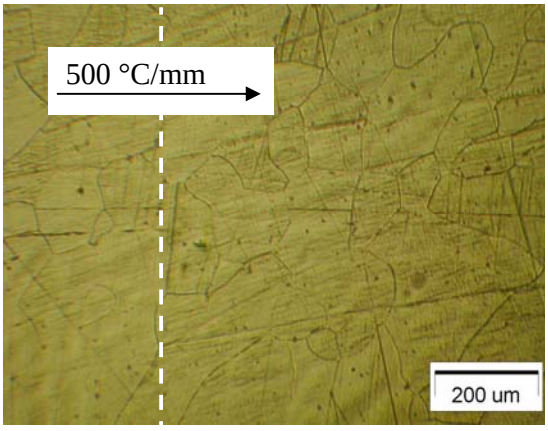

Figure 9.3a: Interface area in Cr-18Re alloy after exposure to 500K/mm temperature gradient during 100 cycles.

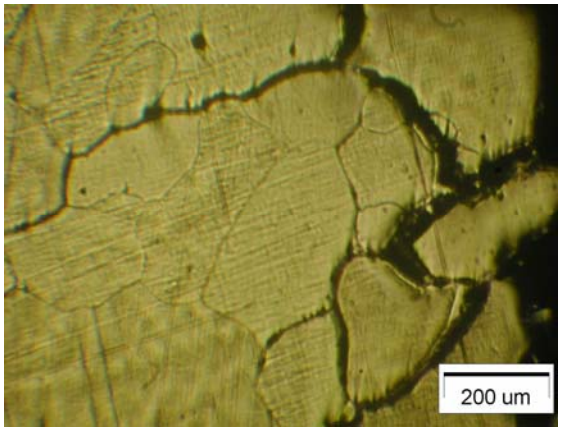

Figure 9.3b: Surface of Cr-18Re alloy after exposure to 500K/s thermal shock during 100 cycles.

The tendency to accommodate deformation by twinning of Cr-35Re alloys plays a major role on their resistance to thermal gradients. Figure 9.4a shows that twinning is present in the interface area between the cooled and heated zones of the sample in particular in the cooled side and that no cracks can be observed in the vicinity of the crack tips and the interfaces between twins and grain boundaries, a phenomenon observed in chapter 5 relating increased twinning capability of the alloy and the increase in ductility observed. Figure 9.4b shows that microcracks are not present on the thermo shocked surface indicating the higher strength of Cr-35Re grain boundaries, observed in the other chapters of this work.

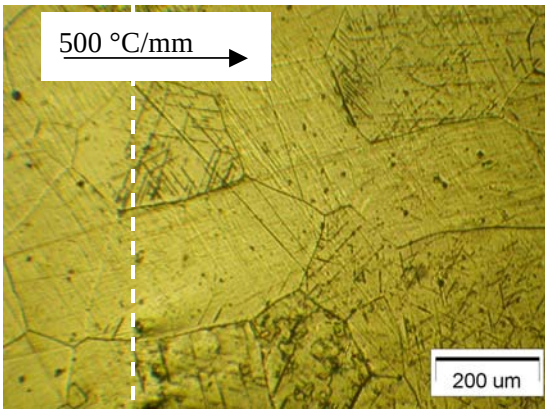

Figure 9.4a: Interface in Cr-35Re alloy after exposure to 500K/mm temperature gradient during 100 cycles

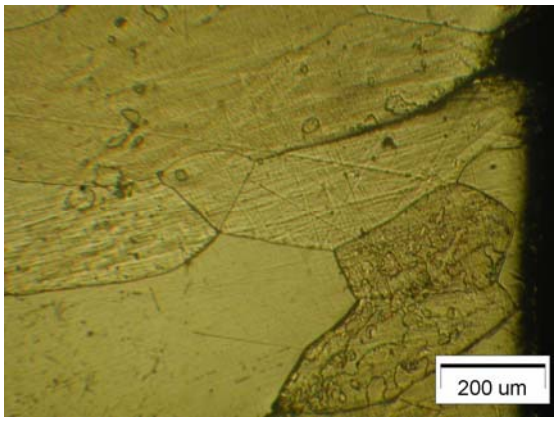

Figure 9.4b: Surface of Cr-35Re alloy after exposure to 500K/s thermal shock during 100 cycles

9.4 Discussion

The installation which was manufactured to perform the tests reproduced approximately the thermal shock and thermal gradient conditions present in the combustion chamber of a satellite thruster. Heating with electric arc was appropriate to reproduce heating kinetics, but this can only give a qualitative indication of the alloy resistance to thermal shock since the chemical solicitation present in the real application is not present. The samples were tested under slight compression due to the thermal dilatation inside the sockets, this may have improved slightly the measured resistance to constraints induced by thermal gradient but it should have no influence on the thermal shock measurements since the thermally shocked surface is free of clamping induced constraints.

As real-time measurements of temperature were not possible maximum temperature was tabulated by means of reaching the melting point of the alloy on the sample surface in a given time. The thermal gradient obtained in the interface area could not be quantified it is however the highest possible that could be technically produced.

There are 2 main properties considered to contribute to the thermal shock and thermal gradient behaviour of materials: the coefficient of thermal expansion and the thermal conductivity of the alloys. The results obtained in chapter 8 do not give a clear indication of how the lower CTE will combine with the lowered thermal conductivity of the Cr-Re alloys to influence the thermal shock and thermal gradient behaviour. CTE of Cr-18Re and of Cr-35Re, measured in chapter 9 is much lower than that of Cr, reducing the level of thermo mechanical stress generated in the alloy during cycling. The lower thermal conductivity of the alloys has an inverse effect, as temperature gradients in the sample are larger; hence increase the thermo-mechanical constraints. Improved mechanical properties of Cr-re alloys should also contribute to an improvement of the thermal shock resistance.

Results obtained indicate that the improvement of mechanical properties and reduced thermal expansion coefficient of Cr-Re alloys have a positive effect on the thermal shock and thermal gradient resistance of the materials.

The low grain boundary strength of Cr-18Re alloys discussed in chapters 6 and 7 and related to the instability of segregated Cr is also responsible for the surface cracks present on the thermo shocked surface. This behaviour has already been observed in Cr-18Re alloys exposed to high temperature in vacuum and air and nitrogen. The thermal gradient resistance of Cr-18Re is remarkably good, but this may be related to the fact that the samples were clamped under compression decreasing tendency to grain boundary facture. The temperature level on the interface area did not probably attain a value at which Cr is capable of segregating to the grain boundaries.

Cr-35Re alloys show an excellent resistance to thermal shocks and thermal gradients with no presence of cracks on the thermally shocked surface and on the area with maximum thermal gradient. Their capability to accommodate deformation by twinning

and the increased strength of their grain boundaries is basically responsible for the good thermal shock and thermal gradient behaviour. The lower CTE of Cr-35Re and its improved mechanical properties compensate its lower heat conductivity and ultimately lead to a good thermal shock and thermal gradient behaviour of the alloys.

9. General discussion

The need to find cost effective substitutes to the Pt-alloys used at present for the manufacture of satellite thrusters motivated this work, which resulted in a partnership between the EADS Corporate Research Center and the Technical University of Catalonia on the field of alloy design and characterization. As an industrial research work, a number of topics related to the applicability of the alloys had to be investigated in addition to the properties of the alloys, particularly their manufacturability.

The number of alloy systems to be investigated was opened from the beginning, however preliminary studies on the applicability of Cr as a combustion chamber material showed that it might have potential for the application provided that its room temperature mechanical properties, it's recrystallisation temperature and it chemical resistance were improved.

Prior studies had shown that the Re effect W and Mo alloys is also present in Cr alloys. This effect had been previously observed basically on the mechanical properties of the alloys, on the increase of the material ductility and by the apparition of twinning as a deformation mechanism at room temperature, usually absent or very localised in BCC refractory metals.

Manufacturing of the alloys has been investigated by means of powder metallurgy, based on a process described by Povarova [Povarova, 1997,2] for W-Re alloys and by means of arc melting and casting in a cold crucible, based on the indications of [Trefilov, 1975].

Powder metallurgical manufacturing presents problems related to the affinity of Cr to oxygen. High purity samples could not be obtained, but the effect of Re on the mechanical properties of the alloys was clear enough to justify proceeding with this investigating manufacturing methods by which high purity samples could be produced. The compression strength and limit of elasticity of Cr-Re alloys improved with increasing Re contents. As foreseen by the literature generalised twinning of a

was present in Cr-35Re samples. The presence of twinning in samples containing 18at% Re was observed and is not explicitly mentioned in existing literature. Contribution of twinning to ductility was evident, as twin bands did not initiate any cracks at grain boundary interfaces even at high deformation percentages.

Arc melting and casting was used to produce high purity samples. The tendency of Cr-18Re to dendritization, related to the large spacing between the liquidus and solidus, was the main problem that had to be faced. Eventually segregation was reduced by active metal additions to the alloy and homogenisation treatments at 1700°C.

The study of the properties of the high-purity alloys comprised their mechanical behaviour under compression and tension, their chemical resistance to air and nitrogen at high temperature and its influence on ductility, their evaporation behaviour and their thermal properties. The study of the thermal shock and thermal gradient resistance of the alloy was also carried out.

Mechanical properties of melt and cast Cr-Re alloys improve greatly with Re content. Ductility of Cr-35Re is remarkable for a BCC refractory metal, attaining 5% under tension at room temperature. Ductility on industrial alloys may be higher, as limited alloy supply required that very small samples were used for the tests, making the results very sensitive to sample defects, such as micro-porosity. Compressive mechanical properties of cast alloys at room temperature were similar to those of PM samples, high temperature mechanical properties of cast alloys were much higher that those of PM samples, mainly because PM samples precipitated and intergranular phase which had a viscous behaviour above 1400°C. The phase was generated by dissolved impurities in the PM alloys that segregated to grain boundaries were they precipitated.

High temperature chemical resistance of Cr-Re alloys is very much dependent on the concentration of Re in the alloy. The study revealed that Cr-18Re alloys are not stable to sustained high temperature exposure, as Cr segregates to grain boundaries and there it evaporates or melts, producing intergranular high temperature fracture.

This phenomenon is equally observed in exposure to vacuum and to air above 1500 °C and renders the alloy unsuitable for the application.

The behaviour of Cr-35Re alloys exposed to air at high temperature is characterized by the formation of a protective double layer structure formed of a dense Cr oxide layer, and a Re rich layer showing some porosity. This layer has good adhesion on the sample surface. The influence of high temperature exposure to air on ductility in Cr-35Re alloys is limited, with some samples showing a DBTT around room temperature after exposure to air at 1600°C during 4 hours. The results on ductility present some scatter in samples exposed and not exposed to air at high temperature due to the large grain size of the alloys relative to the cross section of sample.

Exposure of Cr-35Re alloys to nitrogen at high temperature produces a surface layer with good adherence and no porosity. This layer is not protective against diffusion of nitrogen during exposure as dissolved nitrogen can be detected in the substrate after exposure. Nitrogen does not form precipitates in the substrate, the increased solubility of light elements in the Cr-Re matrix with increasing Re contents is indicated in some references [Milman, 1995]. The nitrogen in solution increases the hardness of the substrate by 3 GPa up to a depth of over 1mm, whilst little influence could be detected on the ductility of the samples, but this may be due to the large scatter of the results.

Behaviour of Cr-Re alloys under exposure to vacuum at high temperature depends on Re content. As mentioned before, Cr-18Re alloys show a grain boundary instability that causes their fracture during exposure. Cr-35Re alloys did not present any significant sublimation during exposure and did not show any grain growth until the highest test temperature of 1700 °C, meaning that the recrystallisation temperature of the alloys is sufficiently high for the application.

The combination of improved mechanical properties, lower Coefficient of Thermal Expansion and decreased thermal conductivity observed particularly in Cr-35Re alloys makes it difficult to make a prevision on the influence on Re additions on thermal shock resistance. It is for this reason that an experimental set-up was

developed in the framework of this work to test Cr-Re alloys under extreme thermal shock and gradient solicitations.

The grain boundary instability of Cr-18Re alloys detected in all tests involving high temperature exposure is the main responsible for their insufficient thermal shock and thermal gradient resistance, which is critical for the application. The instability of grain boundaries of Cr-18Re alloys produces microcracks on the thermally shocked surface with a depth of over 200µm.

Cr-35Re alloys show an excellent thermal shock and thermal gradient behaviour, related partially to ability to accommodate deformation by twinning in the interface between the hot and cold areas and their excellent high temperature compressive mechanical properties. Microcracks on the thermally shocked surfaces could only be detected up to around 100µm.

All tests lead to the conclusion of a possible applicability of Cr-35Re alloys in satellite thruster combustion chambers operating at temperatures over 1500°C with hydrazine-based propellants. A prequalification of Cr-35Re alloys is taking place at present at EADS Astrium, figure 10.1 shows the first engine fully manufactured in Cr-35Re alloy ready for welding of the Nimonic injector head. Weldability tests were carried out in the Technical University of Catalonia outside the scope of this work.

Figure 10.1: First Cr-35Re satellite thruster engine for pre-qualification.

10. Bibliography

[Agev, 1962] „The Crystal Chemistry of the Compounds of Rhenium with Transistion Metals“ N.V. Agev and V. Shekhtman in: B.W. Gonser (ed), Rhenium, Elsevier Publishing and Co., New York, p. 45, 1962.

[Astrium, 2001] “Astrium Products 2001” Published by EADS Astrium, 2001.

[Buckmann 1997] Buckmann et al. Re as an alloy addition to VA metals. Re and Re alloys, 1997.

[DARA, 1991] DARA Vorhaben Internal report “Neue Materialien für Klein Triebwerke“. Report DARA-NM-ZB-0102. Public Funded Project Report, 1991. Available at EADS library in Ottubrunn site.

[DASA, 1999] DASA Technische Niederschrift. “Preliminary Analysis of XXN Thrusters” Report TN-RIA54-1999-00013-A. Available at EADS library Ottobrunn site for public consultation.

[German, 1996] “Sintering theory and practice” R.M. German. New York, Wiley-interscience, pp. 1-23, 1996.

[Gritsiv, 1999] „The Cr-Re Phase diagram“ A.V. Gritsiv, A.A. Bondar, T. Ya. Velikanova, and V. M. Vereshchak. Powder metallurgy and metal Ceramic, Vol. 38, Nos 3-4, 1999.

[Holzwarth, 2001] Uwe Holzwarth, “Mechanical and thermomechanical properties of commercially pure Cr and Cr alloys”, Journal of Nuclear Materials 300, pp. 161-167, 2002.

[Hopmann, 1999] Helmut Hopmann “Schuppkraft für die Raumfahrt, Entwicklung die Raketenantriebe in Deutschland” Stendiger Verlag, 1999.

[Huang, 1998] W. Huang and Y.A. Chang, “Thermodynamic analysis of the Cr-Re system and prediction of the Cr-Ni-Re system”, Journal of Alloys and Compounds, 274, pp. 209-216, 1998.

[Hughes, 1956] J.E. Hughes and G.A. Geach. The alloys of rhenium with Mo and W having good high temperature properties. 2nd Plansee Seminar, Proceedings 1956.

[Klopp, 1975] W.D. Klopp, “A review of Cr, Mo and W alloys”, J. Less Common Metals, 42, pp 261-278, 1975.

[Klopp, 1987] W.D. Klopp, “Technology Status of Mo and W Alloys”, Trans. of Fourth Symposium on Space Nuclear Systems”, Alburquerque, January 1987.

[Kremel 2002] Kremel, S; Danninger, H; Yu, Y. Effect of carbothermic reduction of surface oxide on the mechanical behaviour of sintered steels prepared from Cr pre-alloyed powders. Proceedings of the International Conference DF PM 2002.

[Laptev, 1994] A.M. Laptev et.al “Mathematical simulation of hot isostatic pressing: application in science and technology” Powder metallurgy science& technology, Vol.5 (3), pp. 8-16, 1994.

[Laptev, 2001] A.M. Laptev et.al “Investigation of input data for compaction modeling of hot isostatic pressing”. IOS Press, pp. 151-159, 2001.

[Matsuda, 1994] K. Matsuda Jindo “Computer Simulation Study on the Structure and Strength of Gain Boundaries in Metals: Effects of Impurity Segregation” Advanced Materials 1993 Composites, Grain

Boundaries and Nanophase Materials, Ed. Sakai, Volume 16B, pp. 1345-1349, 1993

[Medvedeva 2002] Medvedeva et al. Carbon stabilised A15 Cr_3Re precipitates and ductility enhancement of Cr based alloys. Acta Materialia 50, 2002.

[Milman 1995] Milman, The influence of directed alloying and thermomechanical treatment on the structure and mechanical properties of high purity chromium, molybdenum and tungsten, Journal de Physique IV Colloque C7, supplement au journal de Physique III, Volume 5, Nov 1995.

[Milman 1997] Milman Yu. V. and Kurdyumova. Rhenium effect of improving the mechanical properties of Mo, W and Cr and their alloys. Rhenium and Rhenium alloys, the Minerals and Metals Society 1997.

[Mounier, 1999] H. Mournier “Modellierung und Simulation des Mechanischen Legierens in einer Hochenergie-Kugelmühle“ Diplomarbeit, Universität Siegen, 1999.

[Mournier, 2000] H. Mournier “Modeling the mechanical alloying process”. 2nd Imacs symposium on mathematical modeling. Mathmod 2, Vienna, Feb.2-4, pp. 685-690, 2000.

[Neumann, 1987] Binary Alloy Phase Diagrams, M. Venkatraman and J.P. Neumann, 1987, Seite 1320.

[Nevittin, 1963] „Alloy Chemistry of Transition Elements“ M.V. Nevittin: P.A. Beck (ed), Electronic Structure and Alloy Chemistry of the Transition Elements, Interscience Publishers, New York, p. 101, 1963.

[Plansee, 1991] Metallwerke Plansee. DUCROPUR Technische Eigenschaften Datenblatt. Plansee, 1992.

[Povarova 1997,1] K. B. Povarova et al. “Physicochemical principles of the design of rhenium alloys” International symposium on rhenium and rhenium alloys. Orlando, Florida, February 10-13, pp. 647-659, 1997.

[Povarova 1997,2] K.B. Povarova et al. “Low and high-rhenium tungsten alloys: properties, production, and treatment”. International symposium on rhenium and rhenium alloys. Orlando, Florida, February 10-13, pp. 691-705, 1997.

[Rocflam, 1997] DASA Internal Report “Study note on Rocflam validation, Liquid Film Cooling, Droplet Wall Interaction, Thermal Balance of Wall Structure” Report number 68326-TR-27. DASA, 1997.

[Sully 1967] A. H. Sully, E.A. Brendes “Chromium” Butterwoth, London, 1967.

[Techniques, 1] G. Roblin, “Techniques de l’Ingenieur” Reference R6-710

[Techniques, 2] C. Legressus “Techniques de l’ingenieur” Reference PE-865

[Techniques, 3] M. Moncel “Techniques de l’ingenieur” Reference M-260

[Trefilov, 1969] I.V Gridneva Yu. V. Milman and V.I Trefilov, “On the Mechanical Properties of Crystals with Covalent Bond”, Phys. Stat. Sol 36, pp 59-57, 1969.

[Trefilov 1975] Trefilov V., Milman Yu.V., Firstov, S.. Physical Fundamentals of Strength of Refractory Metals. Nuakova Dumka, Kiev, 1975.

[Trefilov, 1981] V.I. Trefilov and Yu. V Milman, The influence of temperature and structural factors on mechanical properties of refractory metals. Proceedings on the 10 th Plansee Seminar, Ed. Hugo M. Ortner, 1981.

[Trefilov, 1984] V.I. Trefilov et al. “Characteristic Temperature of Deformation of Crystalline Materials”, Crystal Research and Technology 19, pp. 413-421, 1984.

[Tuffias 1991] R.H. Tuffias et al. Fabrication of advanced Chemical Rocket Combustion Chambers. Surface Modification Technologies IV. The Minerals and Materials Society 1991

[Tuffias 1999] R. H. Tuffias et al. Engineering Issues of Iridium/Rhenium Rocket Engines Revisited. Proceeedings of the Joint Propulsion Conference and Exhibit 20-24 June 1999

[Ultramet, 2001] Picture taken web-site of Ultramet. www.ultramet.com

[Wadsworth 1993] Wadsworth et al. Strengthning and toughening in refractory metal alloys, The Minerals and Materials Society (Critical issues in the development of high temperature Structural materials), 1993.

[Wukusik 1966] C.S. Wukusick, “The Rhenium Ductilizing Effect”, Refractory Metals and Alloys IV, R&D vol41 N° 1 Gordon and Breach, 1961.

[Yoshikazu, 2002] Ro Yoshikazu et al. “Deveopment of Cr-base alloys and their compressive properties”, Scripta Materialia 46 pp. 331-335, 2002.

11. Patents, publications and conference proceedings

- Patent application P611032/DE/1. “Oxidation resistant, ductile Cr-Re alloys high temperature applications. Patent granted.

- Patent application P610892/DE/1. “Coating process specially adapted for coating of hollow structures”. Patent granted.

- Patent application P610895/DE/1. “Process for internal coating of hollow structures” Patent granted

- Patent application P610939/DE/1. “Reduction process of surface oxides on metallic powder particles during sintering”

- L. Gimeno-Fabra “Equiaxed to epitaxed transition in thick noble metal CVD coatings”. Proceedings of the International Meeting on Space and Aerospace Materials Technology in Seibersdorf. Austria 11.2002.

- L. Gimeno-Fabra “Microstructure control in coatings for satellite thrusters obtained by metallorganic CVD” International Conference on Modern Problems of Aerospace Science and Technology. TsAGI, Moscow, Russia, 10.2002.

- L. Gimeno-Fabra “Development of Cr-Re alloys for high temperature application in missile structures”. Proceedings on the Military Science Symposium in Erding, March 2003.

- L. Gimeno-Fabra, N.P. Brodnikovskyy et al. “Development of ductile Cr-Re alloys for high temperature application in aggressive atmosphere” Proceedings of the NATO Advanced Research Workshop on Structural Materials in Kiev, 11. 2003.

- L. Gimeno-Fabra, N. P. Brodnikovskyy et al. “Development of ductile Cr-Re alloys for high temperature application in aggressive atmosphere”. NATO Science Series 2003, Mathematics Physics and Chemistry.

- L. Gimeno-Fabra, H. Nizard “Characterisation of equiaxed to epitaxed growth mode in thick noble metal CVD coatings produced from metal-organic precursors”. Materials Science and Engineering Technology 04-2002.

- I.K. Igumenov, L. Gimeno-Fabra. “MOCVD of Ir-Al_2O_3 protective coatings”. Proceedings of the European CVD conference. Paris, France, 03-2003.

- N. B. Morozova, L. Gimeno-Fabra Thermal properties of Ir(I) acetyacetonato1,5-cyclooctadiene) and Ir(I) methylcyclopentadienyl(1,5-cyclooctadiene) Proceedings of the European CVD conference. Paris, France, 03-2003.